FLEXURAL BEHAVIOUR OF CONCRETE SLABS REINFORCED WITH GFRP BARS AND HOLLOW COMPOSITE REINFORCING SYSTEMS

A Thesis submitted by

Mohammed Al-Rubaye

For the award of

Master of Engineering (Research)

2018

Abstract

Solid concrete slabs are very important structural members in building and construction because traditional slabs reinforced with steel carry the load and transfer it to the beam. However, steel reinforcement corrodes, which affects the integrity of concrete structures by reducing their strength and serviceability, thus leading to failure. For this reason, non-corrosive Glass Fibre Reinforced Polymer (GFRP) bars are an effective alternative reinforcement in concrete slabs. Moreover, concrete slabs are very heavy and make up a high percentage of the dead load in a building structure; this in turn means that more concrete is needed. There is therefore a crucial need for lighter slabs with a better structural performance and this can be provided by Hollow Core Slabs (HCS). However, HCS slabs contain internal voids which cause premature shear failure and the walls to collapse. In response, a hollow Composite Reinforcing System (CRS), with four flanges to improve their bond to concrete, has been developed to stabilise the voids in concrete members.

This study investigates the flexural behaviour of concrete slabs reinforced with FRP bars and CRS. Four slabs (a solid slab reinforced by GFRP, a hollow slab reinforced by GFRP, a slab reinforced by GFRP and CRS, and a slab reinforced by steel and CRS) were tested under four-point static bending to better understand the structural performance of this new construction system. The results proved that solid and hollow slabs behaved similarly due to the voids located in the areas under compressive stress, and that CRS enhanced the structural performance of hollow core concrete slabs by 85%, while the stiffness of GFRP reinforced hollow slabs and the load carrying capacity increased by 32%. CRS was found to be more compatible with GFRP bars than steel bars due to their similar modulus of elasticity. A theoretical evaluation of the behaviour of concrete slabs reinforced with GFRP bars and CRS using the Fibre Model Analysis was also carried out. This FMA considered the tensile strength of concrete and the flanges of CRS, and found that the predicted failure load was only 13% less than the failure load measured experimentally. Important parameters such as the number of voids, the compressive strength of concrete, and the reinforcement ratio were also analysed with regards to the overall behaviour of the slabs. The results of this study provide useful information for the construction industry on the structural performance of concrete slabs utilising CRS and for the effective and safe design of such a construction system.

Certification of Thesis

This Thesis is entirely the work of Mohammed Baqer Ahmed Al-Rubaye except where otherwise acknowledged. The work is original and has not previously been submitted for any other award, except where acknowledged.

Principal Supervisor: Allan Manalo

Associate Supervisor: Weena Lokuge

Associated publications

The below article has been submitted for review and publication from the research contained within this thesis.

Journal

Mohammed Al-Rubaye, Allan Manalo, Omar Alajarmeh, Weena Lokuge, Brahim Benmokrane, and Azam Edoo ‘The flexural behaviour of concrete slabs reinforced with GFRP bars and hollow composite reinforcing systems ’*Journal of Construction and Building Materials* (*under review*).

Acknowledgement

I would first like to thank Associate Professor Allan Manalo for his unfailing support and encouragement; his door was always open whenever I ran into trouble or had a question about my research or writing. He allowed this thesis to be my own work while consistently guiding me in the right the direction. I also want to thank my associate supervisor, Dr Weena Lokuge for her encouragement, insightful comments, and difficult questions.

I also want to thank Composite Reinforcement Solutions Pty Ltd for providing the hollow composite reinforcing systems. Acknowledgment is also given to the technical staff and postgraduate students at the Centre for Future Materials (CFM) at the University of Southern Queensland (USQ) for their assistance in preparing and testing specimens.

Many thanks also to Robert Clayton for proofreading my thesis.

Finally, I express my profound gratitude to my family, especially my parents and my wife Noor Abady, for their unfailing support and continuous encouragement throughout these years of study, research, and finally writing this thesis; it would not have been possible without them.

Thank you

Mohammed Al-Rubaye

Table of Contents

List of Figures

List of Tables

Chapter 1

Introduction

1.1 Background

Precast concrete solid slabs have been used extensively (NPCAA, 2002) in the building industry. These slabs are usually reinforced with steel to they can carry loads and transfer them to the beam (Yardim et al., 2013, Taylor et al., 1966). However, as the steel reinforcement corrodes the strength of the slabs is reduced and this can eventually lead to failure (Aravinthan and Manalo, 2012). This is a critical factor in structures built close to marine or industrial environments (Smith, 2016). For example, the million dollar 20-storey Iluka high-rise apartment complex at Surfers Paradise, was built in 1972 and then demolished in 2013 the steel reinforcement in concrete slabs and other structural elements had corroded so badly (Dalton, 2014). The Australian Corrosion Association (ACA) has reported that more than AU$10 billion is lost every year due to the corrosion of steel reinforcement (Goldston, 2016). This means there is a need to find an alternative reinforcing material that will minimise or eliminate corrosion in concrete structures.

One such alternative reinforcement is Glass Fibre Reinforced Polymer (GFRP) bar, this non-corrosive reinforcement can significantly reduce the cost of the maintenance and repair of concrete structures (Abdalla, 2002). GFRP bars also have a higher longitudinal tensile strength, and they are lighter and are non-magnetic (Manalo et al., 2014). Studies have shown that GFRP bars are successful as internal reinforcement to beams (Maranan et al., 2015), columns (Maranan et al., 2016), and slabs (Bouguerra et al., 2011), however, being lighter than steel, GFRP reinforcement compared to steel is not effectively realised in concrete slabs due to the huge amount of concrete because the reinforcement provided normally is just within the minimum requirement (Hag-Elsafi et al., 2001). Since a slab is part of the structure that consumed the largest amount of concrete in a building, it is a major contributor to the dead load (Sacks et al., 2004), so this structural component should be designed to significantly reduce the weight and the amount of the material. As a result, many researchers (de Castilho et al., 2005, Pajari, 2009) have created voids inside a slab to reduce the amount of the concrete and its overall weight.

A hollow core slab (HCS) is a common structural elements for precast concrete slabs, wall panels in industrial, commercial, residential and infrastructure construction, and in bridge decks (Mones and Breña, 2013). However, several researchers have found that voids can result in early shear failure and significantly reduced the slab capacity (Azad and Hakeem, 2016, Brunesi et al., 2015). Meng (2016) suggested that CFRP sheets saturated with epoxy resin and bonded

inside the voids can increase the shear capacity of HCS. This system is difficult to implement, especially for small diameter voids, so the strong bond between the CFRP sheets and the concrete cannot be guaranteed. Therefore, there is a need for a new type of FRP system which can create hollows inside the slab and yet fully interact with the concrete.

A new type of hollow composite reinforcing systems (CRS) has recently been designed and developed to create voids in reinforced concrete slabs. The CRS has four flanges that act as shear connectors, much like the rib shear connector in the stay-in-place FRP decks introduced by (Benayoune et al., 2008, Oguejiofor and Hosain, 1992, Honickman, 2008b, Hall and Mottram, 1998), to provide a fully composite action with the concrete. This paper investigates the flexural behaviour of one-way concrete slabs reinforced with GFRP bars and CRS. Four concrete slabs (a GFRP-reinforced solid slab, a GFRP-reinforced hollow slab, a GFRP-reinforced slab with CRS, and a steel-reinforced slab with CRS) were cast and tested under four-point loads to evaluate the hollow composite reinforcing system. The capacity of these slabs was predicted theoretically using Fibre Model Analysis (FMA) and then compared to the experimental results. Moreover, the FMA also evaluated important parameters of slab behaviour such as the number of voids, the compressive strength of concrete, and the reinforcement ratio. The results from this study will advance our understanding of the behaviour of hollow concrete slabs reinforced with GFRP bars and hollow composite systems, and also provide a solution for light weight slabs for civil engineering and construction.

1.2 Research objectives

The main objective of this study is to investigate the flexural behaviour of a one-way concrete slab reinforced with GFRP bars and hollow composite systems. The specific objectives of this research are as follows:

1. To determine how effective composite reinforcing systems are in concrete slabs;

2. To investigate the behaviour of hollow concrete slabs reinforced with GFRP bars and compare them to steel reinforced hollow slab; and

3. To theoretically evaluate the failure load of concrete slabs reinforced with GFRP bars and hollow composite reinforcement and analyse the effect that critical parameters such as (voids number, Concrete strength and reinforcement ratio) have on the failure load of slabs.

1.3 Research significance

This research offers an important opportunity to advance our understanding of the behaviour of hollow concrete slabs reinforced with GFRP bars and hollow composite systems. It seeks to develop a light weight slab by clarifying and solving several issues faced by hollow core slab systems. The new findings in this research project are summarised below:

1- Flexural behaviour of concrete slab reinforced with GFRP bars and hollow composite systems;

2- Effectiveness of hollow composite systems for concrete slabs; and

3- Simplified theoretical models for concrete slabs reinforced with GFPR bars and hollow composite systems.

1.4 Structure of the dissertation

The thesis is organised in the following format:

Chapter 1: The first chapter is an introduction and states the objectives of this study.

Chapter 2: This chapter is an intensive review of reinforced concrete slabs and their associated issues such as heavy weight and steel corrosion. It also reviews other studies related to hollow concrete slab, including their failure and the current methods used to enhance their structural performance. This provided enough background to identify the research gap in this area.

Chapter 3: This chapter presents the material properties and the experimental program, including specimen preparation, the test set-up, and the instrumentation used.

Chapter 4: This chapter presents the results and observations of the experimental work. The crack propagation and failure behaviour, load-deflection behaviour, and load-strain behaviour of the tested concrete slabs are presented in detail.

Chapter 5: This chapter discusses the results by analysing the influence of the design parameters considered in this study, including a comparison of hollow core and solid slabs, the effectiveness of CRS in reinforcing concrete slabs, and the effect of the type of reinforcement (GFRP or steel).

Chapter 6: This chapter presents a simplified theoretical evaluation of the failure load of concrete slabs with composite reinforcing system using the Fibre Model Analysis. Using the developed model, the effect of other important design parameters such as the number of voids, the compressive strength of concrete, and the reinforcement ratio on the failure load of the concrete slabs was analysed.

Chapter 7: This chapter provides a summary and conclusions of the study, and also highlights recommendations for future work in this field of research.

1.5 Summary

Hollow concrete slab systems are now being used to reduce the use of concrete materials and to minimise the self-weight of a structure, however, the voids in hollow core slabs makes them prone to shear failure and the walls to collapse. Hollow composite reinforcing systems have recently been developed to stabilise the voids in concrete members. At the same time the use of GFRP bars as internal reinforcement for concrete structures is increasing in an effort to eliminate the corrosion problem caused by steel bars. Therefore, this study investigated the performance of concrete slabs reinforced with GFRP bars and hollow composite reinforcing system to better understand the behaviour of this new construction system.

Chapter 2

Literature review

2.1 General

This chapter is an overview of the current state of solid reinforced concrete slabs with issues such as the corrosion of steel reinforcement and their heavy weight. This chapter also covers the issues that hollow core slabs have with the existence of voids. As a consequence, the literature includes methods that can enhance the behaviour of hollow core slabs, while this chapter also describes the hollow composite reinforced system needed to overcome these issues.

2.1 Solid concrete slab reinforced with steel bars

Concrete slabs reinforced by steel reinforcement are important structural members that are used as an essential part of a building structure, as shown in Figure 2.1 Reinforced concrete slabs generally transfer the load imposed onto the beams and column (Park and Gamble, 2000), but the major problem with a solid slab is the weight that contributes to the total dead load in the building structure. It has been found that a slab contributes between 40 to 60% of a building's self-weight (Yardim et al., 2013). In large projects, this results in complicated and expensive connections and joining systems, heavy lifting equipment to for transportation and installation, and additional formwork during construction (Elliott, 2016, Yee and Eng, 2001). Thus, any reduction in the slab weight is must be considered in the design, as should the corrosion of steel reinforcement in slabs (Apostolopoulos and Papadakis, 2008a).

Figure 2.1 Precast concrete slab (Wideslab.com).

2.2 Corrosion of steel in reinforced concrete

The problem of steel corrosion is common in concrete structures exposed to harsh environments such as industrial buildings, and in mining, and marine infrastructures (Smith, 2016, Maranan et al., 2014, Aravinthan and Manalo, 2012, Tawfik et al., 2012). In aggressive environments, steel corrosion can reduce the service life of reinforced concrete by 20 to 30 years from the 50 year general expectation (Mehta, 2002).

The rate of the steel corrosion impacts on the design service life of reinforced concrete structures (Manalo et al., 2014) as shown in Figure 2.2, while the financial losses due to corrosion is fast becoming a major economic concern. Around the world, hundreds of billions of dollars are spent repairing and strengthening structures experiencing steel corrosion. For example, the Australian economy spends AU$10 billion per year to repair damaged and deteriorated steel reinforced concrete structures (Goldston, 2016).

Figure 2.2 Steel corrosion in a structure (Manalo et al., 2014).

The durability of reinforced concrete is affected by many environment factors, but the most common are related to de-icing or sea water. The steel is affected when there is a loss alkalinity due to chloride or the concrete becomes carbonated; both actions actively increase the vulnerability

of steel to corrosion (Domone and Illston, 2010). In reinforced concrete, the steel reinforcement and surrounding concrete is affected by corrosion such that the corroded bars lose their original shape (Du et al., 2005), and the rust from steel increases the volume of the original steel. This causes cracking due to the splitting stress acting on the concrete. Moreover, this reduction in the cross-sectional area of the reinforcement bars also reduces the mechanical properties of the reinforcement bars. In fact, as the interaction between steel reinforcement and concrete increases (Lundgren, 2005). (Cairns and Millard, 1999) it results in the whole corrosion mechanism shown in Figure 2.3. Many studies such as (Coronelli and Gambarova, 2004, Chernin et al., 2010) have revealed the effect that corrosion has on ductility, stiffness, deflection, and the bond mechanism.

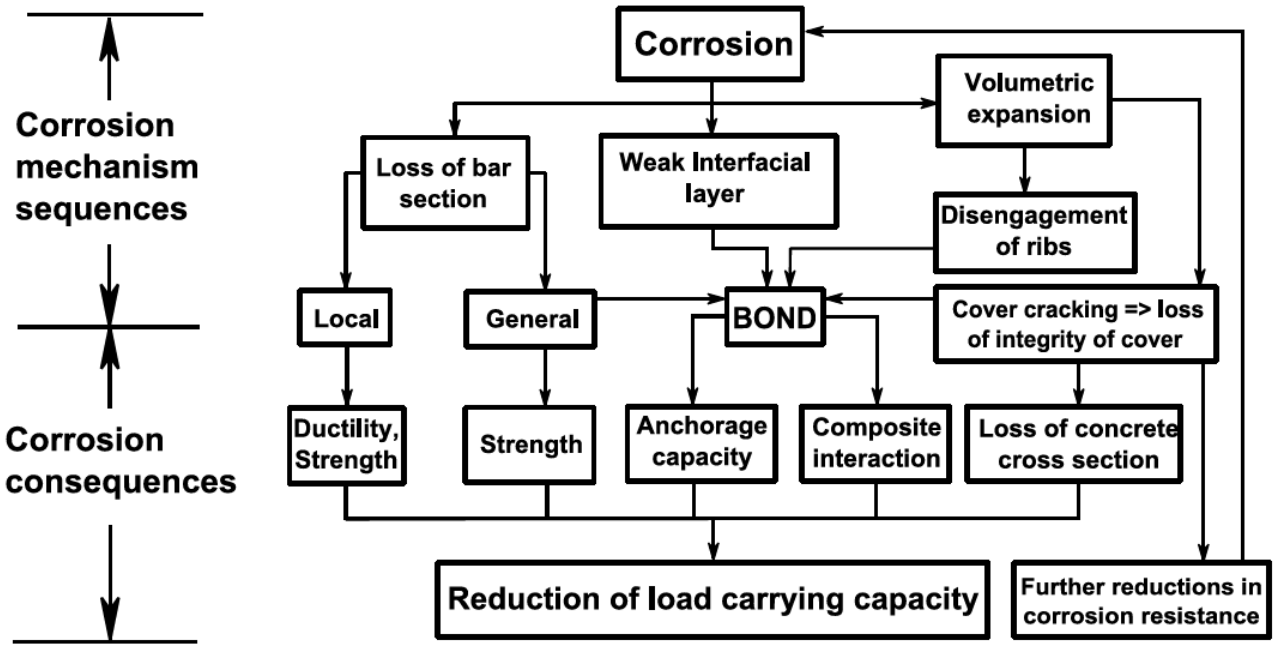

Figure 2.3 The effect of reinforcement corrosion reported by (Cairns and Millard, 1999).

There are two types of corrosion that affect the degradation of steel bars (Apostolopoulos and Papadakis, 2008b), general corrosion and local corrosion. (Tepfers and Concrete, 2000). General corrosion is caused by carbonation and is distributed uniformly along the reinforcement, whereas local or pitting corrosion also is where chloride contamination leads to local pits along the steel bar (Tahershamsi, 2016, Tepfers and Concrete, 2000). When the level of corrosion increases the stress-strain relationship shows a decrease in ductility (Almusallam, 2001). The other important

parameters affected by corrosion are yielding and ultimate stress (Apostolopoulos et al., 2006, Du et al., 2005, Tahershamsi, 2016, Fernandez et al., 2015). The composite action of reinforced concrete members formed as the concrete and reinforcement bonds is a very important parameter (Tahershamsi, 2016). The bonding mechanism for steel bars stems from the chemical adhesive, friction, and mechanical interaction between the concrete and steel (Lutz and Gergely, 1967). This means the radial micro cracks in concrete are the result of reduced chemical bond (Tahershamsi, 2016), as shown in Figure 2.4.

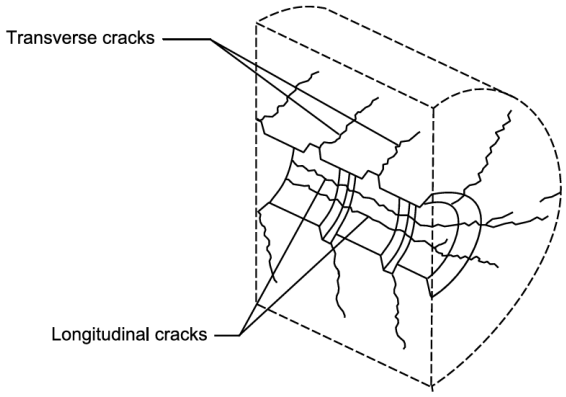

Figure 2.4 Longitudinal and transverse cracks due bond stress (Magnusson, 2000).

Figure 2.5 shows that the steel reinforcement corrosion affects the load carrying capacity, stiffness, and force redistribution of the mechanical behaviour of reinforced concrete. These reductions in in the steel cross section due to corrosion results in a decrease in the structure of shear, moment, and stiffness (Tahershamsi, 2016). Moreover, the ductility of the steel bars affects the force, moment, redistribution, and load carrying capacity of a statically indeterminate structure. As mentioned before, corrosion expands the volume of the bars which causes cracking in the surrounding concrete as well as spalling of (Tahershamsi, 2016, Apostolopoulos and Papadakis, 2008b). This has increased the interest on the use of FRP bars as an alternative reinforcement in concrete structures to minimise and eliminate corrosion due to steel reinforcements.

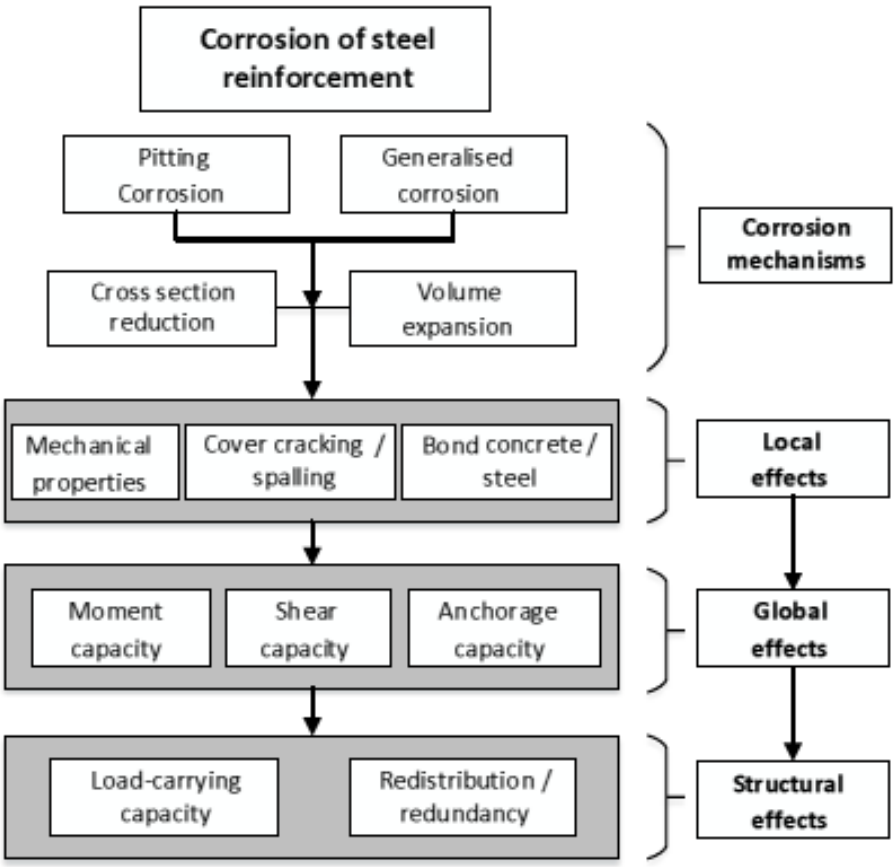

Figure 2.5 Effect of the corrosion on the load carrying capacity, stiffness, and force redistribution of a concrete element (Tahershamsi, 2016).

2.3 GFRP bars in reinforced concrete

Glass fibre reinforced polymer (GFRP) bars are commonly used in barrier walls, bridge deck slabs, parking garages, and other concrete structures because their low cost (Robert et al., 2009, Robert and Benmokrane, 2010). GFRP is manufactured by pultrusion to produce bars with a constant cross section; Figure 2.6 shows a typical configuration of a GFRP bar. The design of GFRP properties depends on the characteristics, amounts, and bonding interaction between the fibres and the matrices. GFRP bars produced by V-Rod Australia followed the FRP specification by (Association, 2002b). Professor Benmokrane has published information regarding the physical and mechanical properties of GFRP bars of different diameters, as shown in Table 2.1. GFRP consists of glass fibre strands bounded with thermosetting vinyl ester resin through the process of pultrusion. Recently, the manufacturing qualities of GFRP in alkali resistance enhanced the

fibre/matrix interphase which significantly improved the bars resistance to a harsh environment. (Maranan, 2016, Manalo et al., 2014).

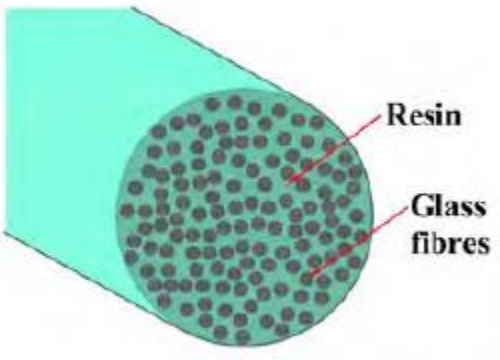

Figure 2.6 Typical configuration of a GFRP bar (Maranan et al., 2016).

Table 2.1 Physical and mechanical properties of GFRP bars manufactured by V-Rod ®.

Property	Unit	#3	#4	#5	#6
Bar diameter	Mm	9.5	12.7	15.9	19.0
Unit weight	kg/m	0.243	0.380	0.558	0.811
Cross-sectional area	mm^2	71.3	126.7	197.9	285.0
Tensile strength	MPa	1372	1312	1184	1105
Tensile modulus	GPa	65.1 $\pm$ 2.5	65.6 $\pm$ 2.5	62.6 $\pm$ 2.5	63.7 $\pm$ 2.5
Tensile strain	%	2.11	2.00	1.95	1.99
Poisson's ratio	-	0.25	0.26	0.25	0.25
Flexural strength	MPa	1734	1377	1239	1196
Flexural modulus	GPa	65.5	64.9	63.5	60.2
Flexural strain	%	2.65	2.12	1.95	1.99
Transverse shear capacity	kN	41	67	94	127
Nominal bond strength	MPa	14			
Glass content by volume	%	65			
Glass content by weight	%	83			
Longitudinal thermal expansion	$x10^{-6}/C$	6.2			
Transverse thermal expansion	$x10^{-6}/C$	23.8			
Glass type	-	E			
Resin type	-	Vinylester			

Note: The numbers reflected in the table represent the nominal values.

GFRP is a composite and anisotropic material containing fibre impregnated within a polymeric matrix. The non-corrosive property of GFRP is the main reason for using GFRP rather than steel as a reinforcement in concrete structures (Deepa et al., 2016, Manalo et al., 2014). GFRP also has a higher tensile strength-to-weight ratio, a higher fatigue resistance, and better thermal and electrical insulation (Robert et al., 2009). In 2012, (Chang and Seo, 2012) experimentally investigated the flexural behaviour of one-way solid slabs reinforced with GFRP bars and compared them to steel reinforced slabs. They showed that GFRP reinforced slabs performed better and had a longer fatigue than steel reinforced slabs because the modulus of elasticity of GFRP reinforcements is closer to the modulus of elasticity of concrete than steel. Furthermore, (Gu et al., 2016) concluded that a greater amount of GFRP reinforcement in a concrete beam will result in smaller deflection and narrower cracks. Moreover, (Chang and Seo, 2012) indicated that the slip of reinforcement in concrete was smaller in FRP bars than steel due to the lower modulus of elasticity of the former. The bond between GFRP bars and concrete is now better because many manufacturers are providing sand particles around the surface of the GFRP bars e (Okelo and Yuan, 2005); this developments has resulted in GFRP bars being widely used in structural designs (Robert et al., 2009).

With GFRP-reinforced concrete beams, because the mechanical and physical properties between GFRP and steel are different, beams reinforced with GFRP exhibit different behaviour than those reinforced with steel (Alsayed and Alhozaimy, 1999, Masmoudi et al., 2012, Matos et al., 2012, Maranan et al., 2015). The beams reinforced with GFRP bars have wider cracks and larger deflection, which affects its serviceability requirements, and because their elastic modulus is lower, GFRP bars slip more than steel bars (Davalos et al., 2008).

The main disadvantage with GFRP bars is their brittle behaviour up to failure. Overall, FRP reinforcement is a non-ductile material (it does not yield) unlike steel. GFRP bars are difficult to bend onsite due to their plasticity, but they can be bent with the correct machinery. Moreover, GFRP bars in the flexural members show excessive cracking and large deflection due to their low modulus of elasticity (Goldston, 2016). Table 2.2 summarises the advantages and disadvantages of GFRP bars.

Table 2.2 Advantages and disadvantages of GFRP bars (Goldston, 2016).

Advantages	Disadvantages
High longitudinal tensile strength	May be susceptible to fire depending on matrix type and concrete cover thickness
Lightweight	Low durability of glass fibres in a moist environment
Corrosion/Chemical resistant	Low shear and compressive strength
Non-magnetic	Low modulus of elasticity
High durability/Service life	Cannot be field bent
High fatigue endurance	No yielding before brittle rupture
Low maintenance	Degrade under UV radiation

2.4 Behaviour of concrete slabs reinforced with GFRP bars

The American Concrete Institute (Grothe and Park) developed a guide for designing concrete structures reinforced with FRP bars; it contains a design of an FRP reinforced concrete member where the flexural capacity of steel was similar to the FRP reinforced concrete member. The ACI determined the steps required for important characteristics such as shear, flexural, and serviceability requirements. This guide also provides other details related to FRP such as the historical development, material properties (physical, mechanical), construction practices, and shrinkage reinforcement, etc., (Grothe and Park, 2000).

When analysing the flexural strength of a cross section for beams or slabs, the ACI guide provided the assumptions (Goldston, 2016) as shown below:

- Maximum compressive strength for concrete was 0.003.
- The tensile strength for concrete was negligible.
- Linear elastic until failure was the tensile behaviour of FRP reinforcement.
- Strain in the FRP reinforcement and concrete was proportional to the distance from the neutral axis.

- There was perfect bonding between the FRP reinforcement and concrete.

The failure mode for concrete slabs reinforced with GFRP bars can be governed by concrete crashing, rupture of the FRP bars, balance failure (both FRP reinforcement and concrete crashed failure occurred at the same time) (Grothe and Park, 2000). The failure mode was completely dependent on the reinforcement ratio (ρ_f) and the balanced reinforcement ratio (ρ_{fb}). The failure mode was governed by concrete crashing when $\rho_f > \rho_{fb}$ as shown in Figure 2.7 (a) whereas, the failure governed by FRP rupture when $\rho_f < \rho_{fb}$ is shown in Figure 2.7 (b). When the concrete reached 0.003 (assumed ultimate strain) then at the same time reached the rupture strain of FRP bars, this means $\rho_f = \rho_{fb}$ as shown in Figure 2.7 (c). In the case of concrete crashing in over reinforced section, this was preferred more than the rupture of FRP in the under reinforced section. In the under reinforced section when FRP reached its maximum strain, failure suddenly occurred without prior waring. Moreover, the over reinforced section provided some ductile behaviour and some plastic response, unlike the under reinforced section. Equations (2-1) and (2-2) are for calculating the reinforcement ratio (ρ_f) and balanced reinforcement ratio (ρ_{fb}) respectively.

$$\rho f = \left(\frac{A_f}{bd}\right) \qquad (2-1)$$

$$\rho\, fb = 0.85\, \beta \frac{fc}{f_{fu}} \frac{E_f \varepsilon_{co}}{E_f \varepsilon_{co} + f_{fu}} \qquad (2-2)$$

A_f: area of FRP tensile reinforcement.

b: width of slab.

d: depth of slab.

fc: concrete compressive strength.

ε_{co}: concrete strain which equals 0.003.

f_{fu}: tensile strength of FRP reinforcement.

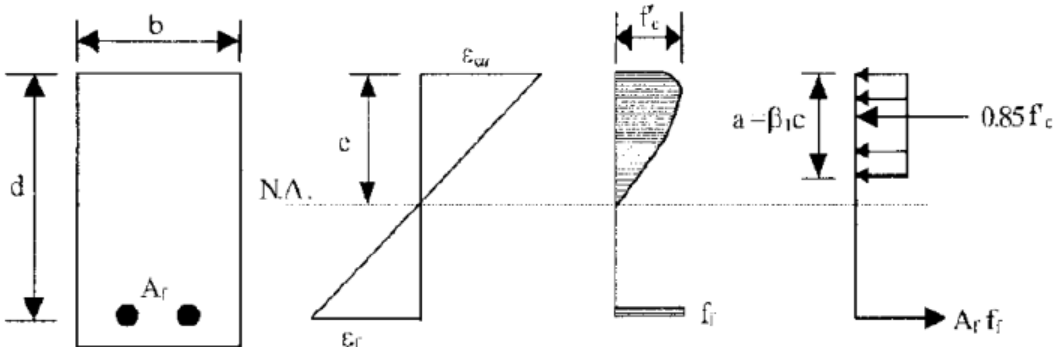

Figure 2.7.a Failure occurred by concrete crashing (Standard, 2011b).

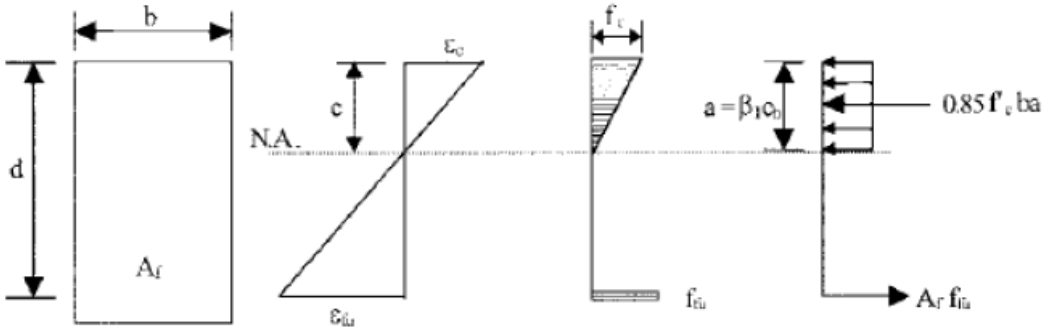

Figure 2.7.b Failure occurred by FRP rupture (Standard, 2011b).

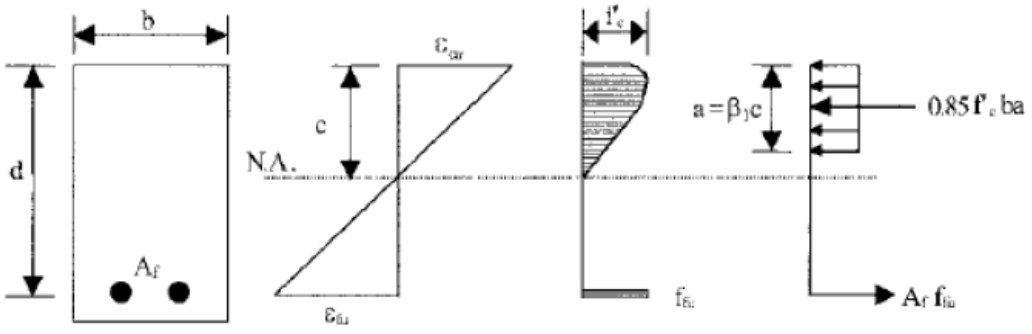

Figure 2.7.c Balance failure condition (Standard, 2011b).

(Chang and Seo, 2012) investigated the behaviour of slabs reinforced with GFRP bars in four point loads. The slabs were (4000 mm *1000 mm*150 mmu and had different reinforcement ratios. This study included the flexural and shear behaviour, cracking behaviour, failure modes, the load-deflection behaviour, and strain behaviour. Chang and Seo found that slabs reinforced with GFRP showed bilinear elastic until failure which is different to steel, as shown in Figure 2.8. Stiffness after the first cracking occurred decreased significantly compared to slabs reinforced with steel. Moreover, the deflection and strain of concrete slabs reinforced with GFRP bars was much higher than for slabs reinforced with steel. For failure mode, slabs reinforced with GFRP often experience concrete crashing, as shown in Figure 2.9.

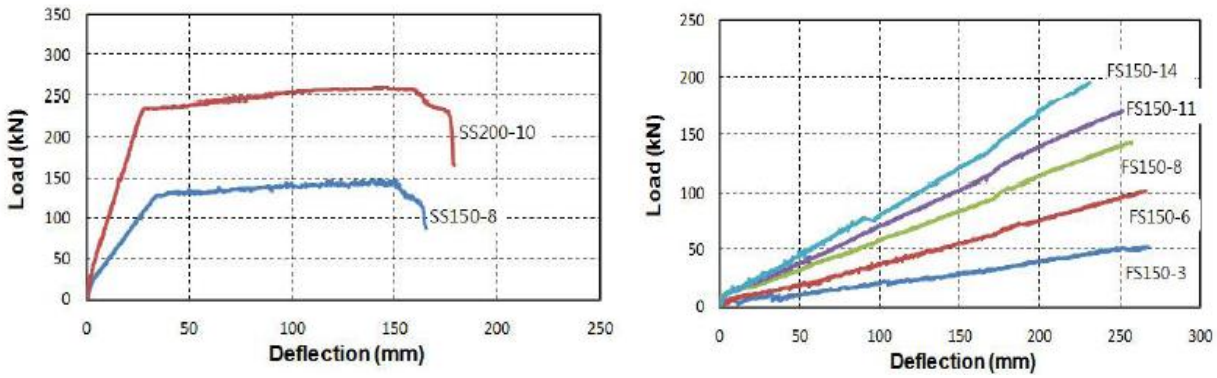

(a)/ Steel. (b)/ GFRP.

Figure 2.8 Load-deflection behaviour for slabs reinforced with steel and GFRP bars.

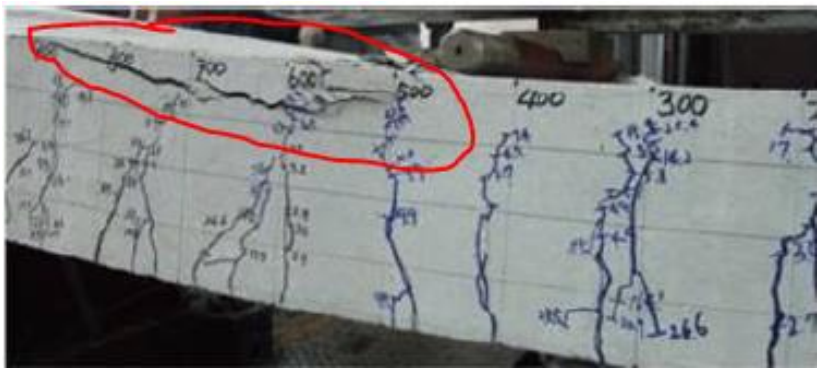

Figure 2.9 Concrete crushing failure for slab reinforced with GFRP bars.

In another study (Ombres et al., 2000), investigated the flexural behaviour of one way concrete slabs reinforced with GFRP bars. They tested three slabs reinforced with GFRP bars and one reinforced with steel up to failure. The results show that the slabs reinforced with steel failed by concrete crashing whereas the one with steel failed by steel yielding, followed by concrete crashing, while the slabs reinforced with GFRP bars had much larger deflections than the slab reinforced with steel, as shown in Table 2.3.

Table 2.3 Test result for slabs (Ombres et al., 2000).

SLABS	Experimental ultimate load (N)	Failure mode	Maximum deflection (mm)	Theoretical ultimate load (N)
SB3	16.79	Concrete crushing	132.33	17.19
SB4	21.90	Concrete crushing	128.27	20.18
SB5	29.98	Concret crushing	124.97	22.50
SSB2	22.16	Yielding steel-Concrete crushing	49.53	20.18

2.5 Hollow core concrete slabs

There is a strong need to design a slab system with a reduced self-weight. The result is a hollow core slab (HCS) with an internal void. HCS is a structural member that is used extensively in the floors and roof systems of buildings, parks, and other structures, to reduce the cost and the self-weight. These slabs offer easier handling and faster installation than solid slabs (Al-Jabri et al., 2005, Braxton, 1986), and the light weight and non-corrosive properties of GFRP bars means they can be used as the main reinforcement in HCS.

The creation of voids also reduces the shear and flexural capacities of hollow core slabs (Azad and Hakeem, 2016), while the voids help to reduce the moment of inertia of the structure due to the reduced cross-sectional area of concrete. (Yang, 1994) further indicated that the shear capacity of hollow slabs is influenced by the shape of the voids; they found that cylindrical voids have a higher shear capacity than non-cylindrical voids. However, the shear resistance of hollow core slabs is less than solid slabs.

To better understand the behaviour of hollow core slab systems, (Wariyatno et al., 2017) tested slabs with different hole configurations. Three different slabs were tested, i.e. solid slab, slab with PVC pipe to create a cylindrical hole, and a slab with Styrofoam to create a square hole, as shown in Figure 2.10. Their results showed that hollow slabs reduced the weight by 24% -25% compared to a solid slab, but hollow slabs were not as strong as solid slabs because shear cracks developed in the hollow core. However, the solid slab failed by flexural failure.

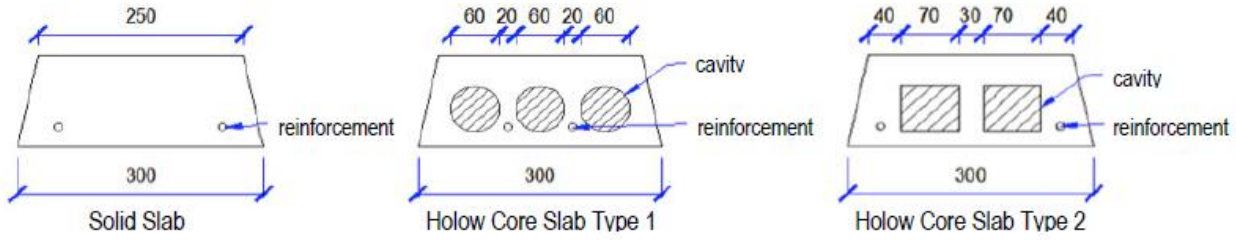

(a): Solid slab. (b): Hollow core slab type 1. (c): Hollow core slab type 2.

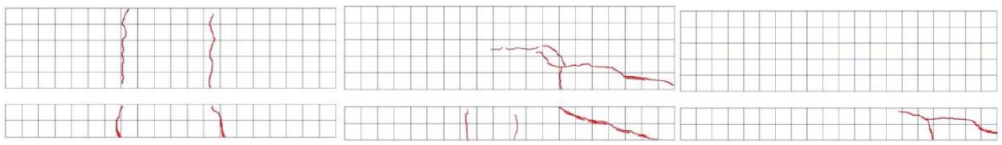

(a): Solid slab (b): Hollow core slab type 1 (c): Hollow core slab type 2

Figure 2.10 Specimens details and failure (Wariyatno et al., 2017)

In another study (Chung et al., 2015) analysed the shear behaviour of circular voided reinforced concrete floor slabs. They used FE analysis to investigate how the voids affected the shear strength of hollow slabs, and found that shear cracks wills probably develop around the voids, as shown in Figure 2.11. They therefore suggested using a material shaper to improve the hollow slabs. It is clear that hollow concrete slabs are affected by different design parameters, so in the next sub-sections, the parameters that affect the behaviour of hollow concrete slabs are reviewed.

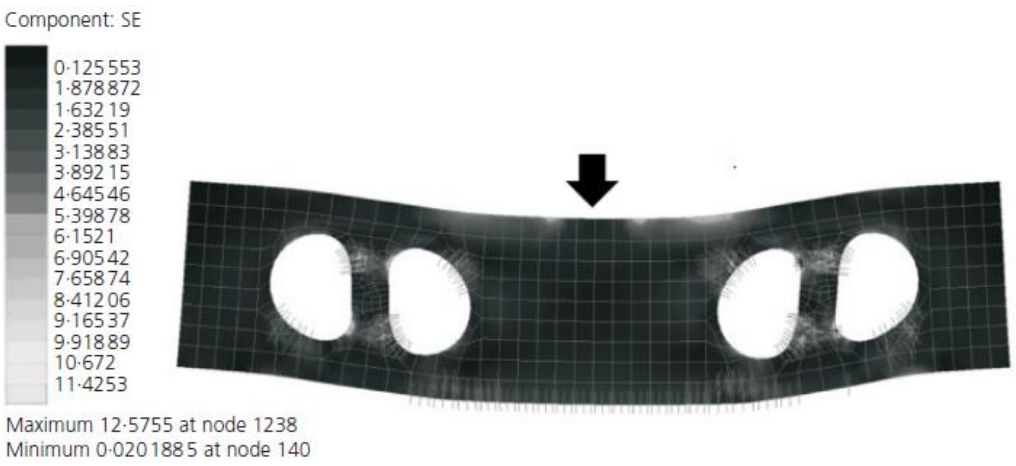

(a)

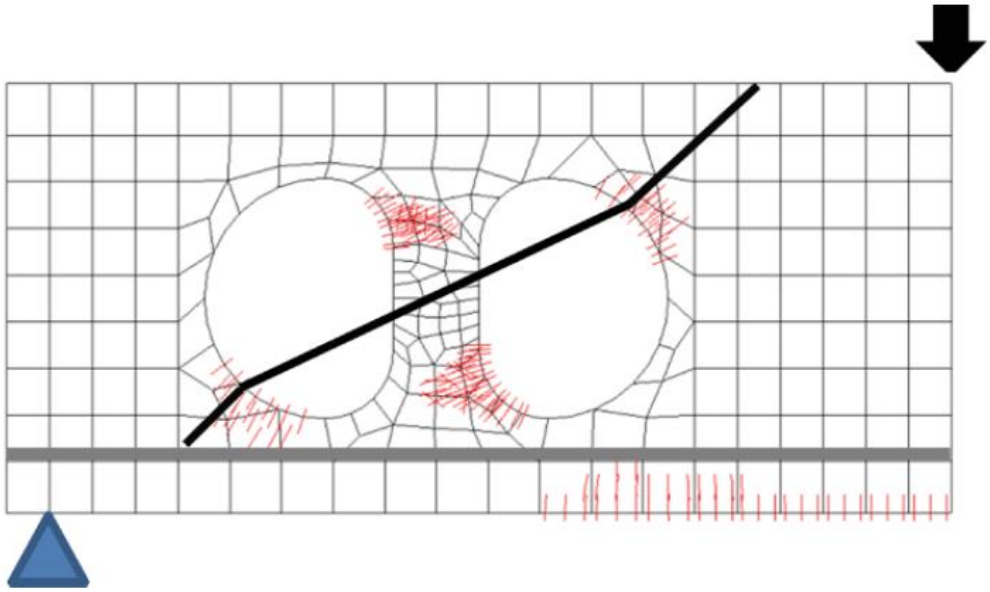

(b)

Figure 2.11 FE cracks result analysis (a) Distribution of equivalent stress. (b) Propagation of the shear (Chung et al., 2015).

2.5.1 Compressive strength of concrete

The compressive strength of concrete affects the behaviour of hollow concrete slabs (Anderson, 1987) (Committee et al., 2008). In a study by (Adel. A, 2016) where they tested the flexural behaviour of hollow concrete slabs manufactured with compressive strengths of 25, 38, and 45 MPa, they found that slabs with high compressive strength performed better than the slabs with

low compressive strength. Their results in Figure 2.12 suggest an almost double load capacity for a slab manufactured to 48 MPa concrete compared to a slab with 25 MPa concrete.

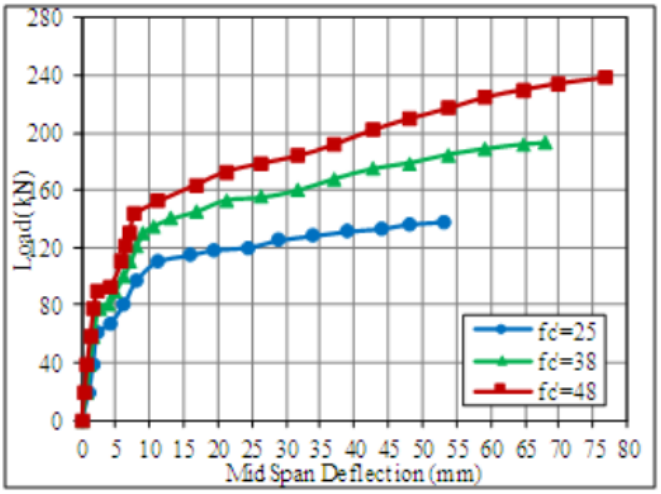

Figure 2.12 Concrete compressive strength effects on the hollow core slab (Adel. A, 2016).

2.5.2 Reinforcement ratio

(Adam et al., 2015) investigated the flexural behaviour of concrete beams reinforced with GFRP bars and found that the amount of reinforcement affected their ultimate load and serviceability. Narrower cracks and lower mid-span deflection were observed for beams with a higher rather than lower reinforcement ratio. (Kassem et al., 2011) also observed a smaller deflection and narrower cracks for slabs with a higher reinforcement ratio than slabs with less GFRP reinforcement.

2.5.3 Number of Voids

The presence of voids reduced the moment of inertia of slabs due to a reduction in the cross-section of concrete. The moment of inertia of a slab with voids located at mid-depth can be calculated by subtracting the moment of inertia of the voids from the solid slab, as shown in the equation below (Donohoe and Keogh, 2000).

$$I = I\ solid - I\ void = \frac{bd^3}{12} - \frac{n\pi dv^4}{64}$$

Where b is the width of the slab, d is the depth of the slab, n is the number of voids, and dv is the diameter of the voids. From another research, (Bhagat and Parikh, 2014) demonstrated that voids affect the stiffness of concrete slabs.

2.6 Methods to enhance the performance of hollow core slabs

(Meng, 2016) explored enhancing the capacity the voids of hollow concrete slabs by bonding Carbon Fibre Reinforced Polymer (CFRP) composite sheets, as shown in Figure 2.13 (a, b). CFRP sheets were saturated with epoxy resin so they would bond to the inner surface of the voids. While there was some enhancement in their capacity, shear failure and collapsing voids were still the dominant features of slab failure, as shown in Figure 2.14. Since reinforcing the voids was a weak solution, the resulting brittle failure for all the slabs showed that this technique did not improve the HCS behaviour. There was also debonding between the CFRP sheets and concrete before failure.

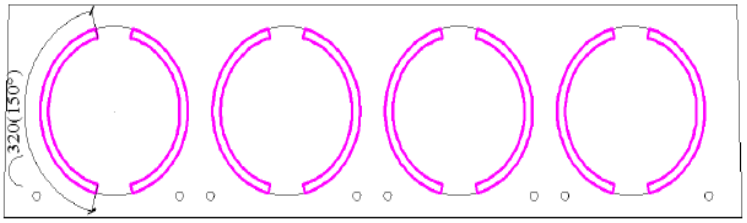

(a)

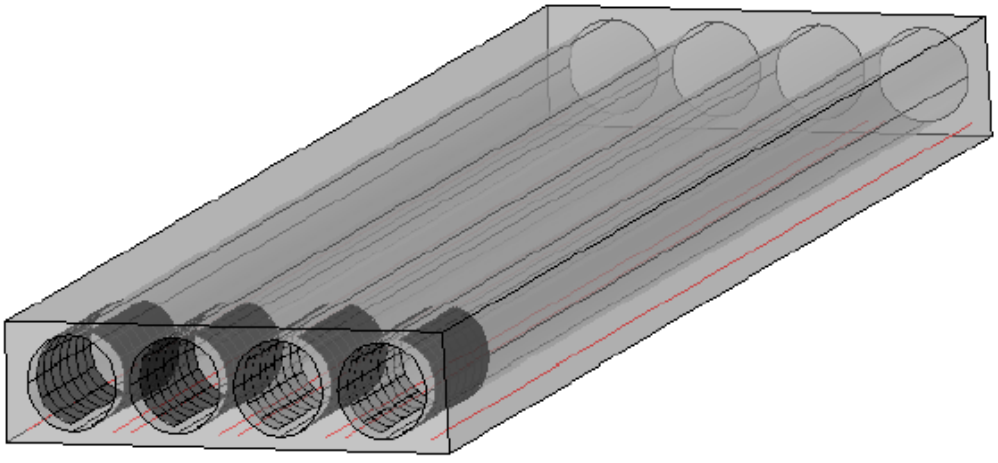

(b)

Figure 2.13 PHC slab strengthened by CFRP sheets (Meng et al., 2016).

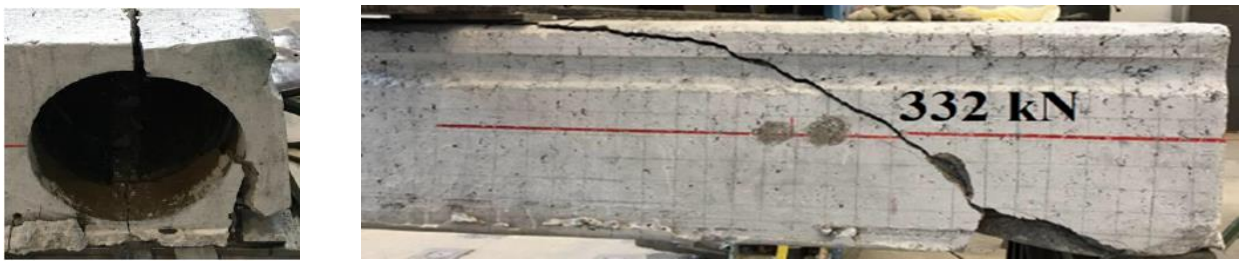

Figure 2.14 PHC slab failure modes (Meng et al., 2016).

Another suggestion for improving the shear capacity of HCS is to provide full CFRP composite sheets around the surface of the voids, as shown in Figure 2.15. This approach increased the shear capacity of hollow slabs by at least 20% compared to slabs without CFRP sheets. There was also no debonding failure but the researchers noted that attaching CFRP sheets, especially to smaller voids is complex.

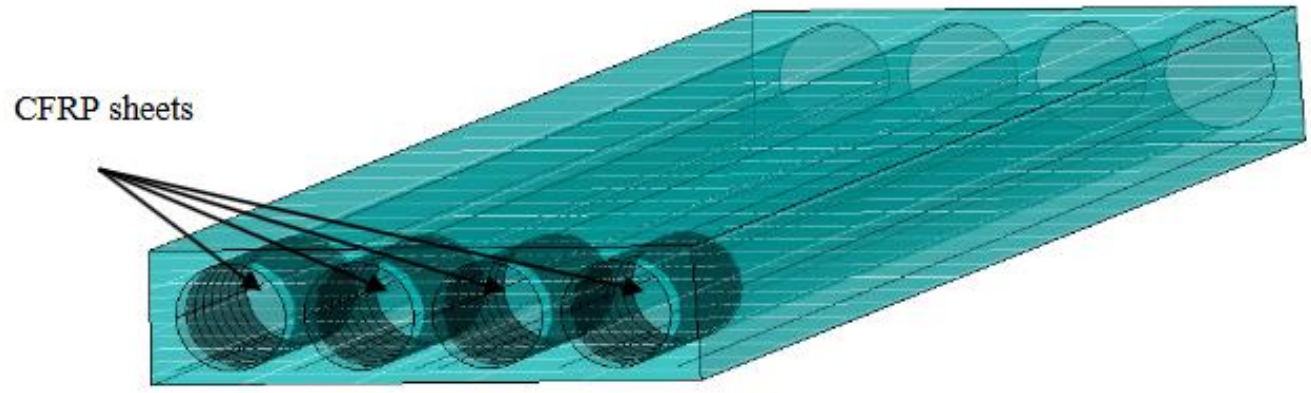

Figure 2.15 CFRP bonded sheet inside the HCS (Meng et al., 2016)

2.7 Shear connectors for reinforced concrete slabs

A number of studies introduced different types of shear connectors to increase the interaction between the reinforcement and the concrete. (Benayoune et al., 2008) used a truss shaped shear

connector (shown in Figure 2.16) for precast concrete sandwich panels with a layer of insulation. The results showed that this type of shear connector can improve the behaviour of precast sandwich panels such that the load deflection profile of sandwich panels and crack propagation, are similar to a solid slab. However, this system is complicated to fabricate and could not eliminate corrosion because the shear connector is made of steel.

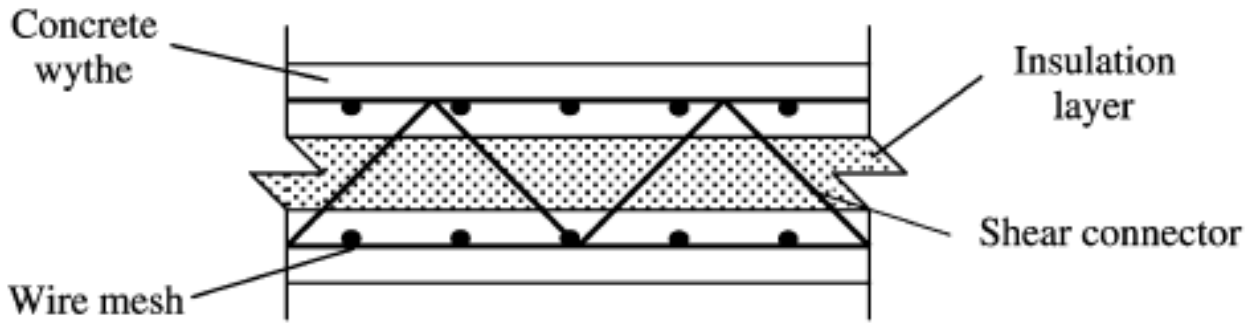

Figure 2.16 Precast concrete sandwich panels components (PCSP) (Benayoune et al., 2008).

In earlier studies, (Oguejiofor and Hosain, 1992) observed a considerable difference in behaviour between rib shear connecters (Figure 2.17a) and headed stud shear connecters (Figure 2.17b). They found that a rib shear connecter was better than a head stud shear connecter at providing a composite action between a steel girder and the overlying concrete deck.

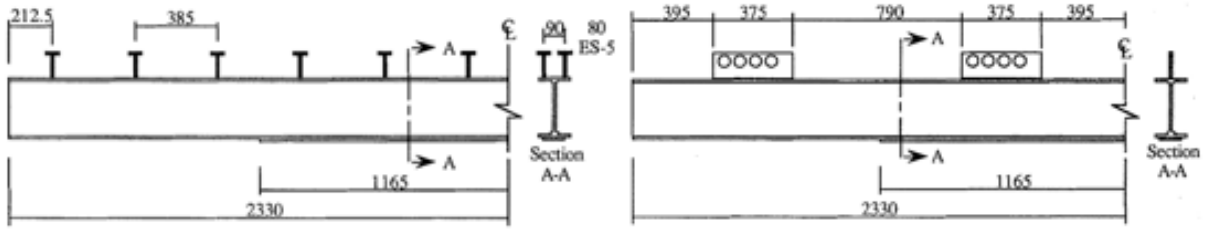

(a). Rib shear connecters (b). Headed stud shear connecters

Figure 2.17 Rib and headed stud shear connecters (Oguejiofor and Hosain, 1992).

(Hall and Mottram, 1998) worked on a hybrid concrete-FRP section incorporating FRP stay in place in an open structure form. The stay-in-place FRP sheet has shear ribs (Figure 2.18) to provide a composite action with a concrete slab (Figure 2.19). Their work suggested that this system would eliminate the need for mechanical shear studs or a bonded coarse aggregate coating on the surface of the framework.

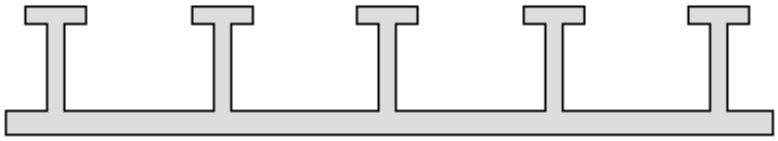

Figure 2.18 FRP shear connector section(Honickman, 2008a).

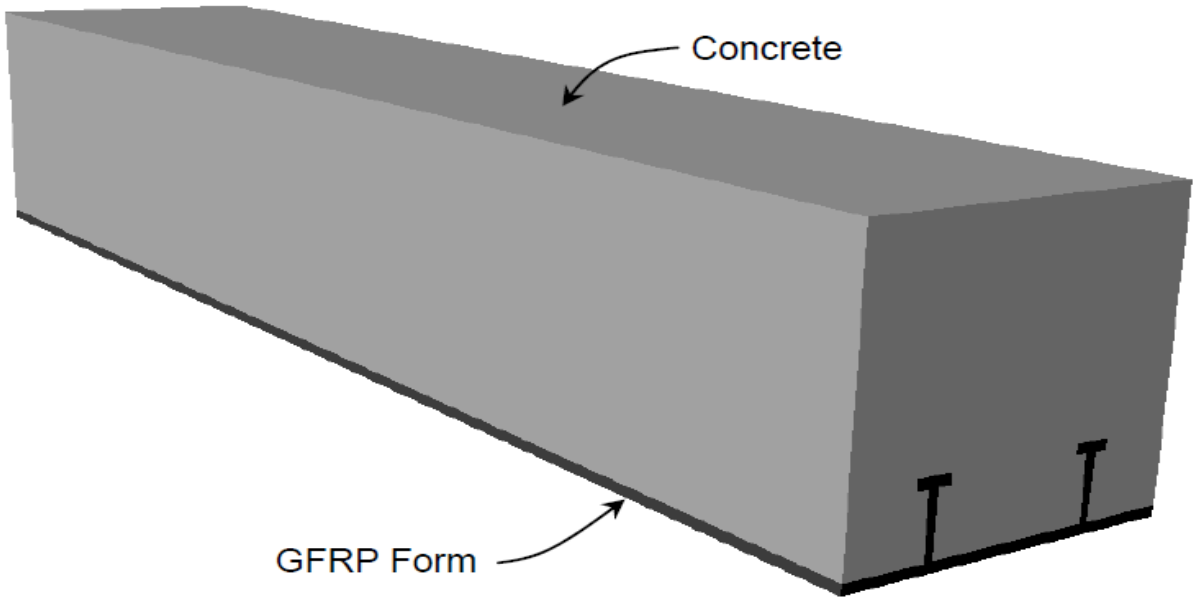

Figure 2.19 Concrete and GFRP ribbed sheet hybrid section(Hall and Mottram, 1998)

For strengthened concrete,(LIU et al., 2008) investigated the flexural capacity of slabs with FRP sheets. They used 7 specimens to test debonding on the FRP thickness and strength area. They observed that the slabs failed in in the mid span because the prestressed strands ruptured. They also reported that all the specimens failed at shear failure at the support and the FRP sheets failed in debonding.

However, the shear capacity of specimens improved from 48% to 109%, and when they yielding increased at mid span, vertical deflection improved due to the FRP sheets. (Xiangmin et al., 2014) investigated the flexural behaviour in PHC bonded by CFRP sheets. They found almost 67% improvement in the flexural capacity of the strengthened slab, whereas the average deflection at mid span for the strengthened specimens had doubled.

Another experimental study of hybrid composite material to reinforce flexural capacity was carried out by (Mosallam et al., 2012). They used high -performance concrete and CFRP composite sheets in a hybrid composite system located on the top surface of floor slabs or bridge decks. They found that the flexural capacity of the slabs improved by a maximum of 164% and 122% at the mid span for deflection. As a result, the overlay close to the support from the slab was horizontal, so the specimen failed its strength test. However, this solution still needs improvement because FRP sheets do not provide the design requirement for a structural member, so it is expected that HFRP will provide a shear connector at the same time as the FRP shell. Existing research has been applied where FRP sheets were used to increase the shear capacity of HCS concluded by (Lam and Teng, 2002) this experiment revealed that using full FRP wrap was better at increasing the shear capacity.

2.8 Hollow composite reinforcing systems for concrete slabs

Fibre reinforced polymer (FRP) composites have become an important material for constructing new infrastructures (Said et al., 2015). While a number of studies showed a reduction in material usage and overall weight, creating voids inside the slab led to a decrease in the shear and flexural capacity of the slab (Azad and Hakeem, 2016). The development of shear connectors to increase the strength of slabs, and bonding, was an important aspect needed to provide a successful design (Xiangmin et al., 2014) .

A composite reinforced system has been developed to create voids and shear connectors in reinforced concrete structures. This reinforcing system has four external flanges to facilitate mechanical bonding and interaction with concrete as shown in Figure 2.20. Moreover, the use of non-corrosive GFRP reinforcements in concrete structures is anticipated to increase the service life of the structure by eliminating steel corrosion, especially in structures located along the coastal areas in Australia (Deepa et al., 2016). The lighter weight of GFRP bars rather than traditional reinforcement (Dittenber and GangaRao, 2012, Robert and Benmokrane, 2009) is also an added benefit to manufacture highly durably and non-corrosive infrastructures.

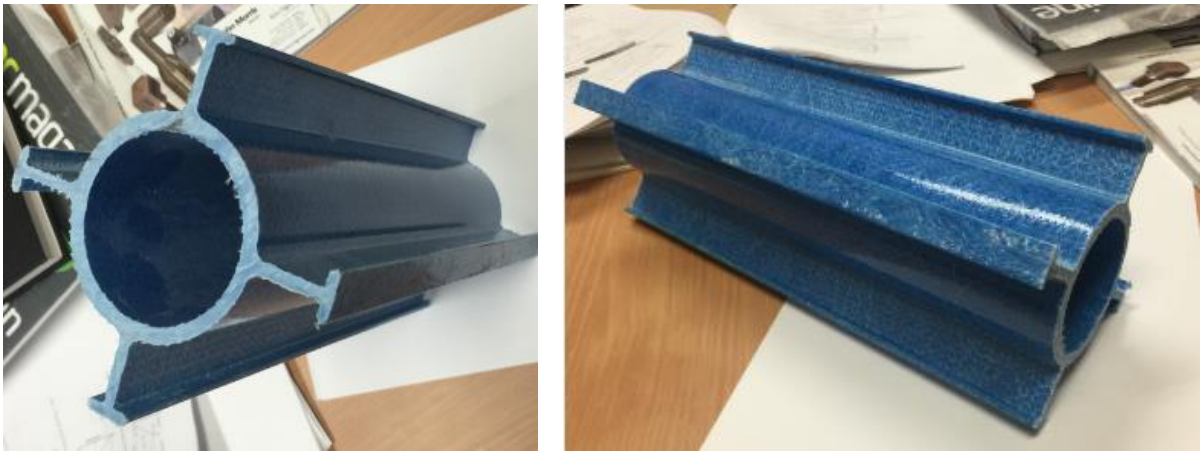

Figure 2.20 CRS.

2.9 Summary

The extensive review of the literature showed that hollow concrete slabs can minimise the amount of materials and reduce the overall weight of structures. Moreover, using GFRP reinforcements could eliminate the problem of steel corrosion. However, many studies indicate that voids create a weakness in a concrete slab, because when shear cracks develop around the voids they result in a reduced capacity. Some researchers explored bonding FRP sheets to the inner surface of a hollow core, and while there was some increase in strength, it is a difficult approach and the integrity of the bond is always a concern.

The development of a new hollow composite system could eliminate this problem in hollow core slabs because it can be used to create voids while the four flanges can enhance the interaction with concrete. However, the behaviour of concrete slabs with hollow composite system has yet to be investigated, so it will be the main focus of this study. The research gaps that have been identified and will be need addressed in this study are as follows:

- The flexural behaviour of one way concrete slabs with composite reinforced system (CRS) and GFRP bars.
- The performance of CRS and the effectiveness of this system in reinforcing hollow concrete slabs.
- Understanding the effect that important parameters have on the overall behaviour of slabs reinforced with GFRP bars and hollow composite systems.

Chapter 3

Experimental program

3.1 Introduction

This chapter illustrates and outlines the material properties of the test specimens and the experimental methodology used for this project; it also describes how the concrete slabs were prepared for flexural testing. The test setup procedure will be illustrated and explained. Since there is an inherent risk associated with any task where building materials or machinery is used, a risk assessment has been prepared to help mitigate any possible injuries.

3.2 Materials

3.2.1 Hollow composite system (CRS)

The hollow composite reinforcing system shown in Figure 3.1 was supplied by Composite Reinforcement Solutions in Perth (Australia). This material is manufactured using the pultrusion process and is made from glass fibres (mostly unidirectional) and reinforced vinylester resin. It also contains additives such as pigments, UV inhibitors, and fire retardant.

To reveal the pattern in which the glass fibres are woven in each part, a burnout test was carried out, as shown in Figure 3.2. The physical and mechanical properties of the hollow composite reinforcing systems were evaluated by following the appropriate ISO and ASTM test standards that are listed in Table 3.1.

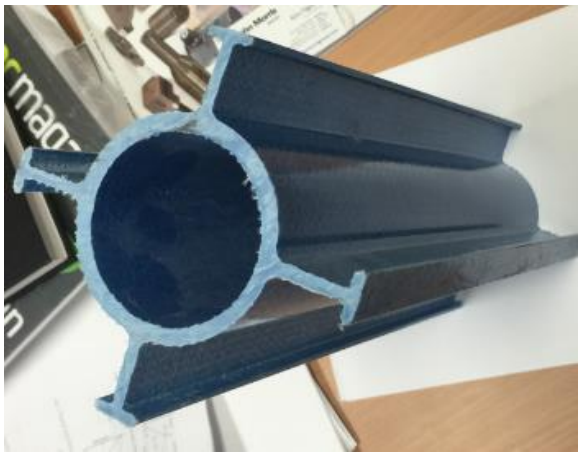

(a). CRS shape.

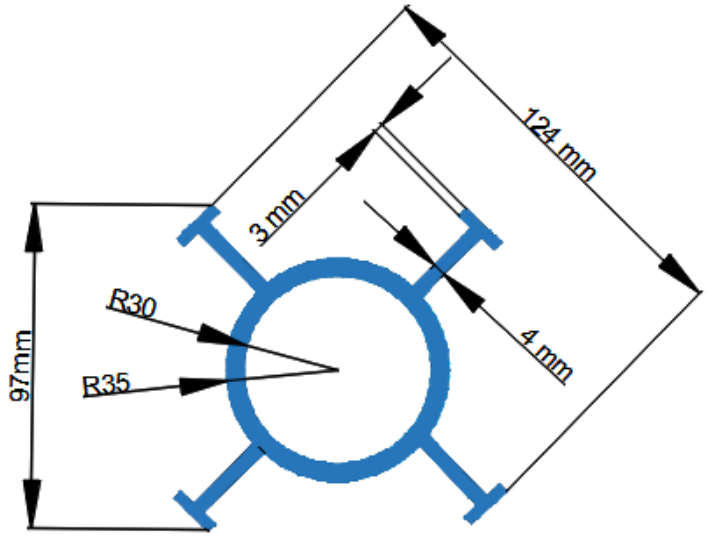

(b) CRS dimensions

Figure 3.1 Details of the composite reinforcing systems (CRS).

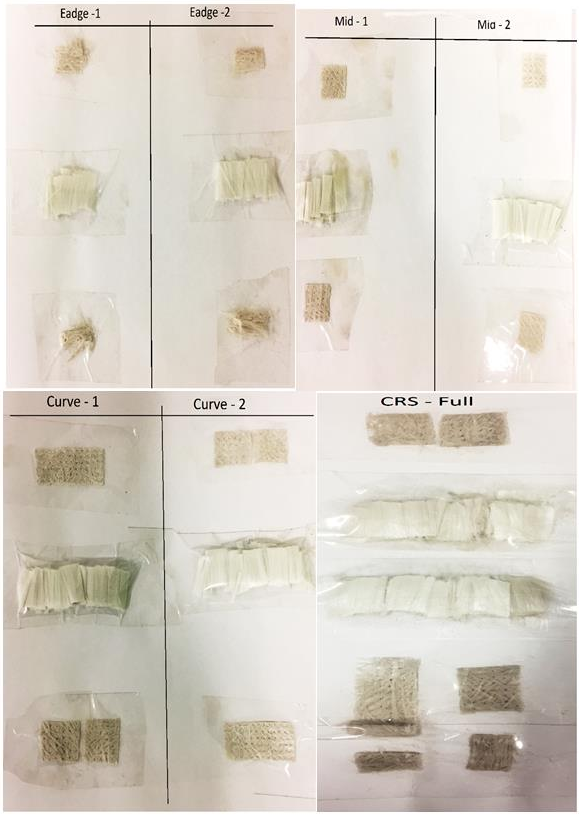

Figure 3.2 CRS fibre content (Manalo et al., 2017).

Table 3.1 Physical and mechanical properties of CRS.

Properties	Test standard	Values	Std.Dev.
Density, kg/m^3	ASTM D792 (Association, 2010)	1926.5	23.4
Fibre content by weight, %	ASTM D2584 (Standard, 2011a)	73.2	2.5
Glass transition temperature, ^{o}C	ASTM E1356 (ASTM, 2008b)	81.4	4.2
Axial compression, MPa	ASTM D695 (International, 2010)	120.4	7.11
Transverse compression, MPa	ISO 14125(1998) (ISO, 1998)	8.8	1.06
Transverse shear strength, MPa	ASTM D2344/D2344M-13 (Standard)	7.5	0.75
Interlaminar shear strength, MPa	ASTM D4475 (ASTM)	22.1	1.48
Flexural strength, MPa	ASTM D790 (ASTM, 2007)	201.1	28.7
Flexural modulus, GPa	ASTM D790 (ASTM, 2007)	42.1	1.3

3.2.2 GFRP bars

The slabs were reinforced with 12 mm diameter high-modulus (HM) GFRP bars (Grade III, CSA S807-10). The GFRP bars shown in Figure 3.3 were manufactured via the pultrusion process by impregnating E-type glass fibres in a thermosetting modified vinyl-ester resin. The external surfaces were coated with silica-sand particles to enhance the bond between the reinforcement and surrounding concrete. These bars were similar to those used by (Benmokrane et al., 2017), the mechanical properties are summarised in Table 3.2.

Figure 3.3 GFRP bars (12 mm diameter).

Table 3.2 Mechanical properties of GFRP bars (Benmokrane et al., 2017).

Properties	**Test standard**	**Values**	**Std-Dev**
Flexural strength	ASTM D4476/D4476M (ASTM, 2009)	1,588.1 MPa	93.5
Interlaminar shear strength	ASTM D4475-02 (ASTM, 2008a)	52.9 MPa	2.1
Tensile strength	ASTM D7205/D7205M-06 (ASTM, 2011)	1,281.5 MPa	35.3
Tensile modulus	ACI 440.6M (ACI, 2008) and CSA S807-10 (Association, 2010)	61.3 GPa	0.4
Tensile strain	ACI 440.6M (ACI, 2008) and CSA S807-10 (Association, 2010)	2.1	0.1

3.2.3 Steel bars

The steel reinforcement was standard grade 500N with a nominal diameter of 12 mm as shown in Figure 3.4. The characteristic strength and Young's modulus of this reinforcing steel was 500MPa and 200 GPa, with normal ductility as per the requirements of AS4671 (Standards Australia, 2001).

Figure 3.4 Steel bars (12 mm diameter).

3.2.4 Concrete

The concrete used for this project was a ready mix concrete with a nominal compressive strength of 32 MPa. The maximum aggregate size was 10mm and the maximum slump was 100mm determined in accordance with AS1379 Specification and supply of concrete (Standards Australia, 2007). A total of 8 cylinders were prepared and tested as per AS1012 methods for testing concrete (Standards Australia, 2014), the slabs were tested at the same time. The average compressive strength of the concrete was 31.8 MPa with a standard deviation of 3.54 MPa.

3.3 Slab details

Four full size slabs were prepared, 175mm thick by 750mm wide by 2400mm long; the dimensions of these slabs are based on industry practice for precast hollow core slabs, they consisted of a solid slab (S1), a hollow slab (S2), a slab with hollow composite reinforcing system (S3), and steel reinforced slab reinforced with hollow composite reinforcing system (S4). Table 3 provides details of the slab specimens. The S1, S2, and S3 slabs are reinforced at the top and bottom with 12 mm diameter GFRP bars in the centre, every 200 mm (both longitudinally and transversely), while the

slab S4 was reinforced with 12 mm diameter steel bars. The ratio for slabs reinforced by GFRP bars and steel is 0.44%; this led to an over-reinforced section for slabs S1 to S3 (ρ_b = 0.2%) and under-reinforced section for slab S4 (ρ_b = 2.1%), as outlined by the (Association, 2002b). The reinforcement is covered by 15 mm of concrete at the top and bottom and 25 mm of concrete at the edges of the slabs. All the details of the specimens are shown in Table 3.3.

Table 3.3 Concrete slab details.

Specimen name	Cross section layout	Description
S1	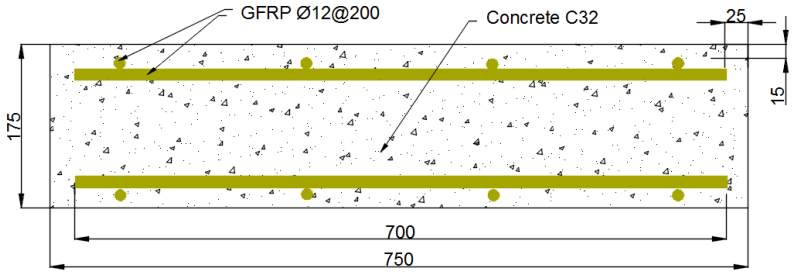	Solid concrete slab reinforced with GFRP bars
S2	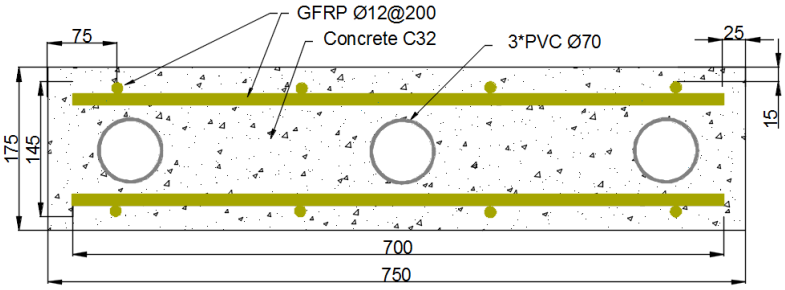	Hollow concrete slabs reinforced with GFRP bars
S3	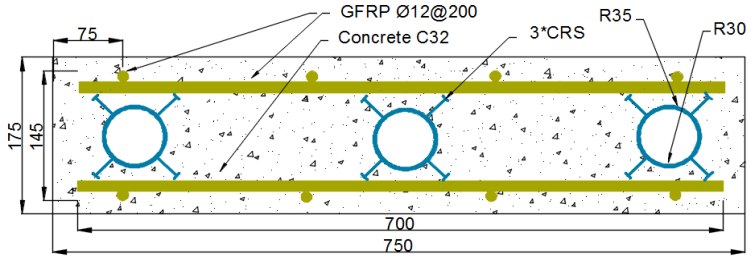	Slab reinforced with CRS and GFRP bars.
S4	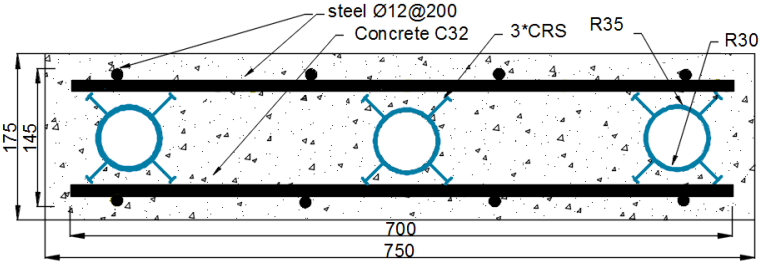	Slab reinforced with CRS and steel bars.

3.4 Specimen preparation

3.4.1 Assembly of bars

As mentioned previously the GFRP reinforcement bars in slabs (S1, S2, and S3) and the steel reinforcement in slab S4 have the same dimensions, but because there are no stirrups in these slabs the bars did have to be bent, but the bars did need cutting because each slab has longitudinal and transverse reinforcement at the top and bottom. The cutting machine was used to provide 8 bars (4 at the top and 4 at the bottom) 3950 mm long (to allow for a 25mm thick cover of concrete each side). For the transverse reinforcement, 24 bars were cut (12 at the top and 12 at the bottom), and then zip plastic wire was used to tie the top and bottom reinforcements layers together. All the reinforcing bars were assembled on a work table in the prescribed patterns to ensure the bars were spaced properly.

3.4.2 Installation of the reinforcement cage

Formwork made from 20 mm thick black plywood was screwed together in the dimensions of the slabs, as outlined previously. Bent 12 mm diameter steel bars were used as lifting hooks and under the bottom reinforcement, zip tie wire was placed at the four corners of the slabs to ensure the specimens would be lifted safely, as shown in Figure 3.5. Cut sections of CRS were used as spacers between the two layers of reinforcement for slabs S1 and S2, as shown in Figure 3.6, and PVC pipe, 70mm outside diameter by 1mm wall thickness were used to create voids inside the concrete in slab S2, as shown in Figure 3.6. The CRS for slabs S3 and S4, equally spaced 300 mm apart on the centres, and tied to the reinforcements to prevent them from moving while concrete was being poured. The reinforcement cage was then placed inside the formwork, and concrete spacers were used on the sides and the ends of the cage to ensuring that cover was maintained and the cage remained in the right place. All the slabs were then ready for casting, as shown in Figure 3.7.

Figure 3.5 Hook used for slab lifting.

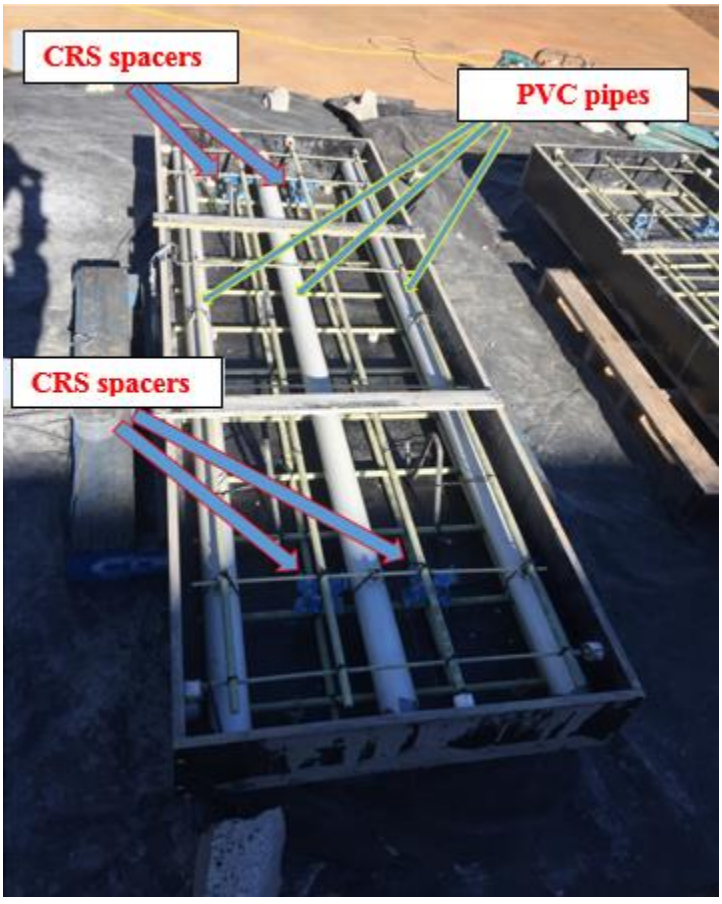

Figure 3.6 PVC pipes and CRS spacers before casting.

Figure 3.7 Specimens before casting.

3.4.3 Attachment of strain gauges

Uni-axial 3 mm strain gages were attached at the top and bottom reinforcements to measure the strains during the entire loading at mid-span, and at the top surface of the hollow composite reinforcing systems, as shown in Figure 3.8. Moreover, uni-axial 20 mm strain gauges, as shown in Figure 3.9, were attached to the top and bottom concrete surfaces of the slab. The strain gauges were installed after a section of the reinforcement (GFRP or steel) was ground smooth; the strain gauge wires were placed carefully to avoid any damage while pouring concrete; the wires were also bagged for protection and to make sure the strain gauges worked.

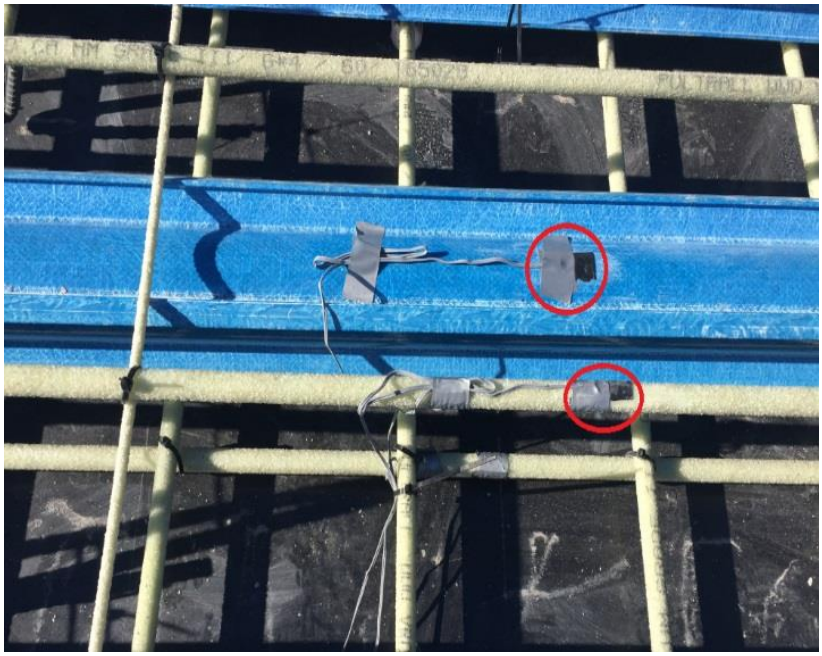

Figure 3.8 Strain gauges attached on the GFRP and CRS.

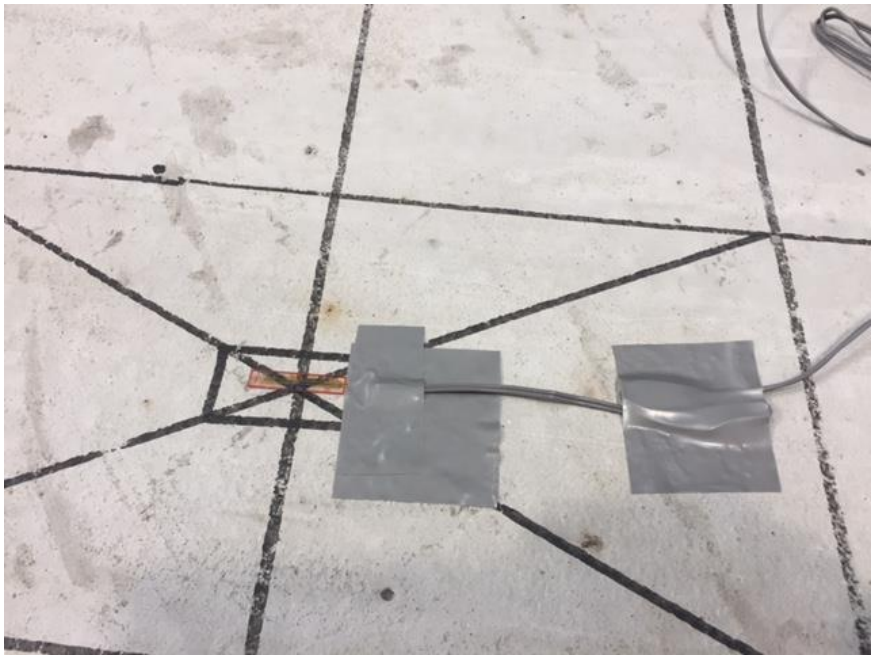

Figure 3.9 Strain gauges attached on the top concrete.

3.5 Concrete casting

The concrete was poured from the concrete mixer directly into the formwork while electrical vibrators were used to remove any air voids. Vibrating the concrete was a slow process, particularly around the strain gauges. After pouring the concrete and vibrating the moulds, the top surfaces were trowelled to create a smooth surface. Concrete cylinders were prepared and poured, and then removed and placed inside a curing tank the next day. A slump test was carried out on site during the pour and the result of 105mm was deemed allowable. During the curing stage, the concrete slabs were placed in water. Figure 3.10 shows the slabs with pouring complete, and the timber cross members used to save and support the formwork.

Figure 3.10 Specimens after casting.

3.6 Test set-up and instrumentation

The slabs were tested under the four-point static loading shown in Figure 3.11. The load was applied through a spreader steel I-beam using a using 2000 kN Enerpac hydraulic ram, and it was measured with a 444 kN load cell. Rubber matting was placed under the loading steel plate to ensure a uniform load distribution to the slab. A laser displacement transducer was used to measure the mid-span deflection. Prior to testing, gridlines were marked on the top surface and front side of the slab to trace any crack propagation during loading. The applied load, deflection, and strains were recorded using of the data acquisition system Vishay System 5000. All the specimens were tested up to failure.

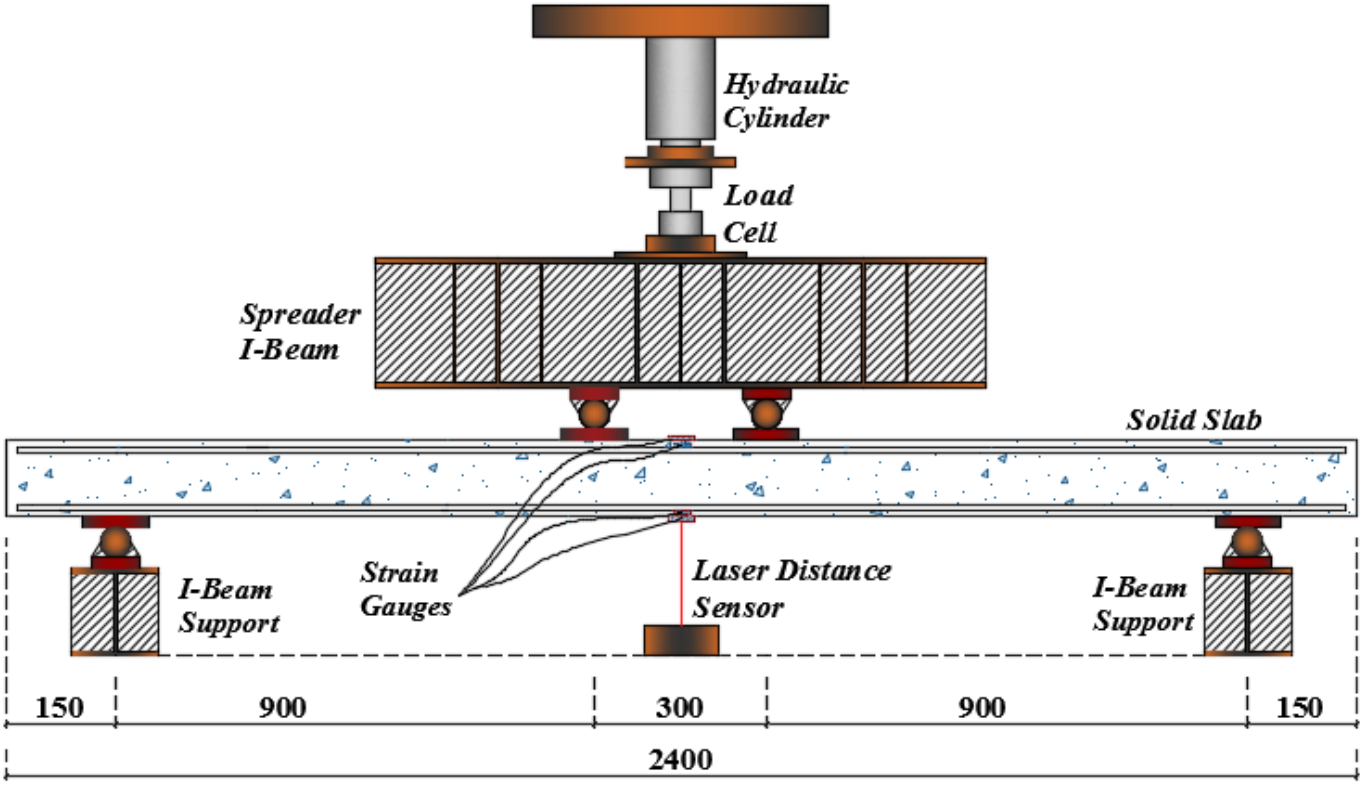

(a) Schematic diagram.

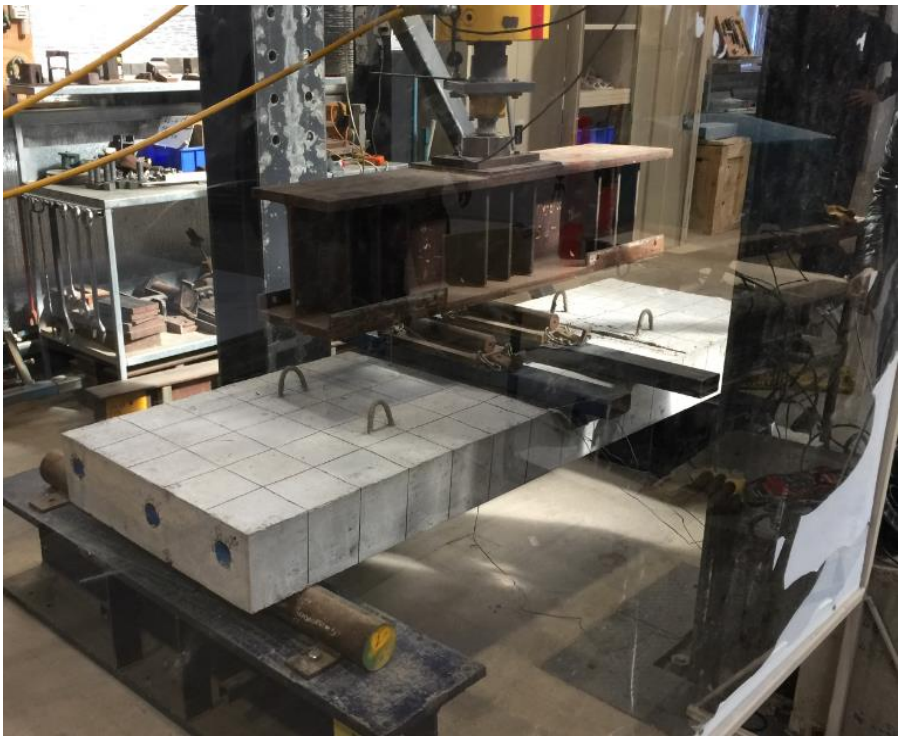

(b) Actual test set up.

Figure 3.11 Test set-up and instrumentation.

3.7 Summary

An experimental program was designed to investigate the flexural behaviour of reinforced concrete slabs. The details provided in this chapter include the material properties, slab details, materials required, specimen preparation, concrete casting, test set up and instrumentation. Four slabs (a solid slab reinforced by GFRP, a hollow slab reinforced by GFRP, a slab reinforced by GFRP and CRS, and a slab reinforced by steel and CRS) were prepared for testing under four-point static bending to better understand the performance of this new construction system. The results and observations from this testing will be presented in the next chapter.

Chapter 4

Results and Observations

4.1 Introduction

This chapter provides the results and observations from tests carried out on the hollow concrete slabs reinforced with GFRP bars and hollow composite reinforcing systems. It focuses on crack propagation and failure mode, load and deflection relationships, and the strains measured in concrete, as well as reinforcement and hollow composite reinforcing system. The tests are summarised in Table 4.1 and the details of the behaviour are presented in succeeding sections.

Table 4.1 Key observations of the tested samples.

Slab	First crack		Maximum		Failure mode
	Load (kN)	Cracking moment (kN-m)	Load (kN)	Bending moment (kN-m)	
S1	25	11.25	137	61.7	Shear failure with concrete crushing under the loading point and buckling of bars
S2	25	11.25	145	65	Shear failure with concrete crushing under the loading point and buckling of bars
S3	25	11.25	211	95	Concrete crushing at mid span with shear cracks
S4	25	11.25	208	94	Steel yielding followed by concrete crushing at mid span

4.2 Solid slab (S1)

4.2.1 Failure mode

The solid slab (S1) was the first slab tested under flexural loading; it initially showed elastic behaviour, it was uncracked, and it could carry a load over a very small deflection during prior loading. The first crack appeared close to the point load under approximately 25 kN, as shown in Figure 4.1, and as the load gradually increased, fine vertical cracks spread along the span. These vertical cracks formed from the tension area and propagated upwards, as shown in Figure 4.2, and as the load increased they became wider and deeper, especially around the points load.

Concrete crushing commenced in the compression zone, followed by a wider and deep crack on the right hand side of the slab as deflection increased. This crack reached the layer of compression concrete under the right load point, Shear cracks began under the loading point and propagated diagonally to the bottom of the slab, as shown in Figure 4.3, and then, without warning, the concrete was crushed. There was no rupture failure in the GFRP reinforcement, but the bars did buckle under compression; this resulted in the final failure of slab S1, as shown in Figure 4.4.

Failure was addressed by initiating cracks, increasing deflection, and concrete failure at different locations from the supports. The slabs reinforced with GFRP bars were actually over reinforced (Association, 2002a, Newhook and Svecova, 2007) whereas the slab reinforced with steel was under reinforced Australia (2009). With regards to the over reinforced sections of S1 when the reinforcement ratio was higher than the balance ratio ($\rho_f > \rho_{fb}$), failure was governed by concrete crushing (Grothe and Park, 2000, Association, 2002b).

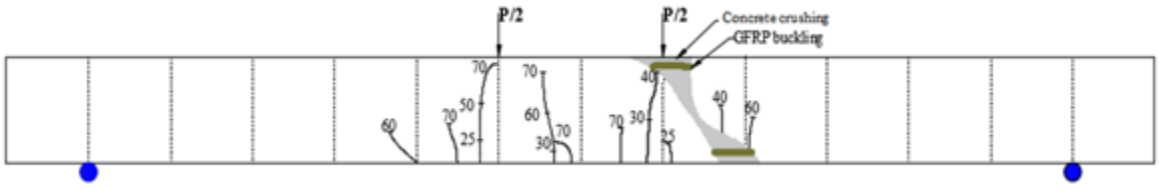

Figure 4.1 Crack propagation (S1).

Figure 4.2 Cracks propagated upwards (S1).

Figure 4.3 Crack propagated close to the point load (S1).

Figure 4.4 Final failure (S1).

4.2.2 Load- deflection behaviour

The load- mid span deflection of the solid slab is shown in Figure 4.5 where the load deflection curve of S1 has four segments. The first segment of the S1 curve was related to the uncracked and stiff section until the first crack appeared at a load around 25 kN and a mid-span deflection of 3 mm. When the concrete within the section exceeded its tensile strength, vertical cracks began at the bottom of the slab between the two loading points and they reduced the stiffness of the slab. As the load increased, more cracks developed along the length of the slab; this represented the beginning of the cracked condition which leads to segments two and three shown in Figure 4.5. The second segment presented almost linear behaviour (due to the GFRP linear behaviour) until the concrete reached its peak strength under an axial load of 137 kN with 50 mm deflection. The slab reinforced with GFRP then showed non-linear behaviour until the concrete crushed in the compression zone due to the over reinforced concrete section (segment 4). This non-linear response was due to wide cracks at the bottom or extensive concrete crushing, not because the GFRP yielded, as shown in segment three. At this stage the maximum load capacity shown in the curve was 137 kN with a maximum deflection of 56 mm. The stiffness of the second segment was 2.4 kN/mm. In the last segment, after the concrete failed, the GFRP bars began to buckle, as shown by the drop in load to 120 kN after the peak load, as shown by segment four. This slab totally failed due to GFRP buckling.

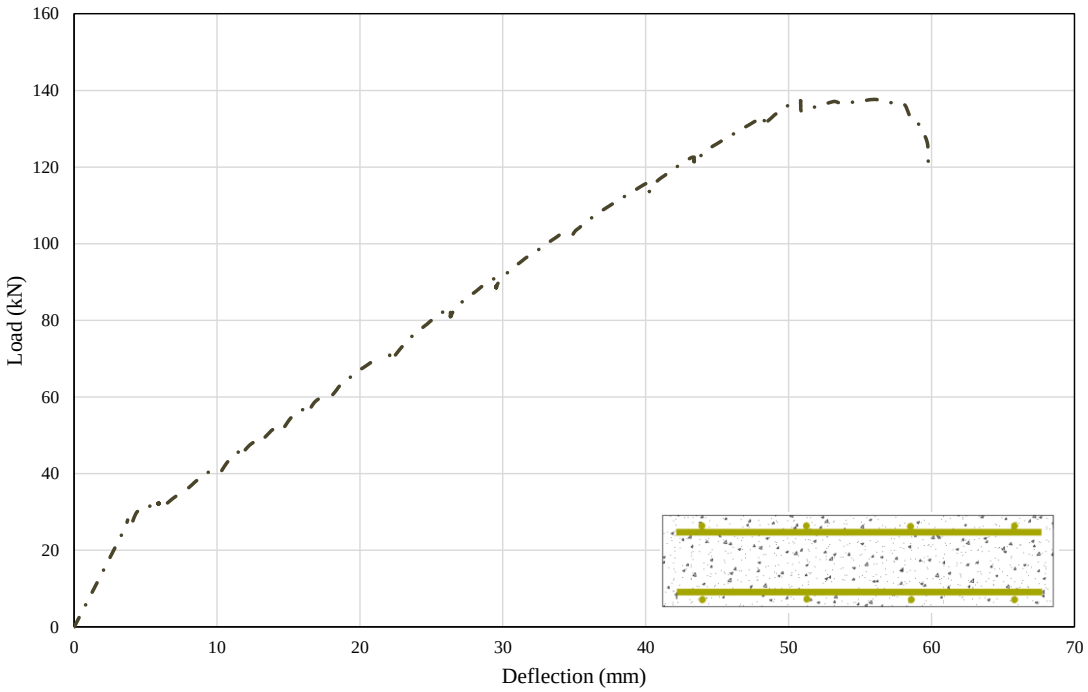

Figure 4.5 S1 load-deflection relationship.

4.2.3 Strain behaviour

4.2.3.1 Concrete strains

Figure 4.6 shows the relationship between load and strain at the top of the concrete of slab S1 as two segments; the first segment shows that the concrete slab carried the load without cracking until the first flexural cracking occurred at just before 25 kN (load level cracking) where the strain was recorded at 135 micro strains. This slab showed linear ascending behaviour after the first cracking, and then the concrete began to crack linearly until the peak load reached 137 kN and 2102 micro strains (segment 2). Unfortunately, the strain gauges at the bottom of the concrete were damaged during testing.

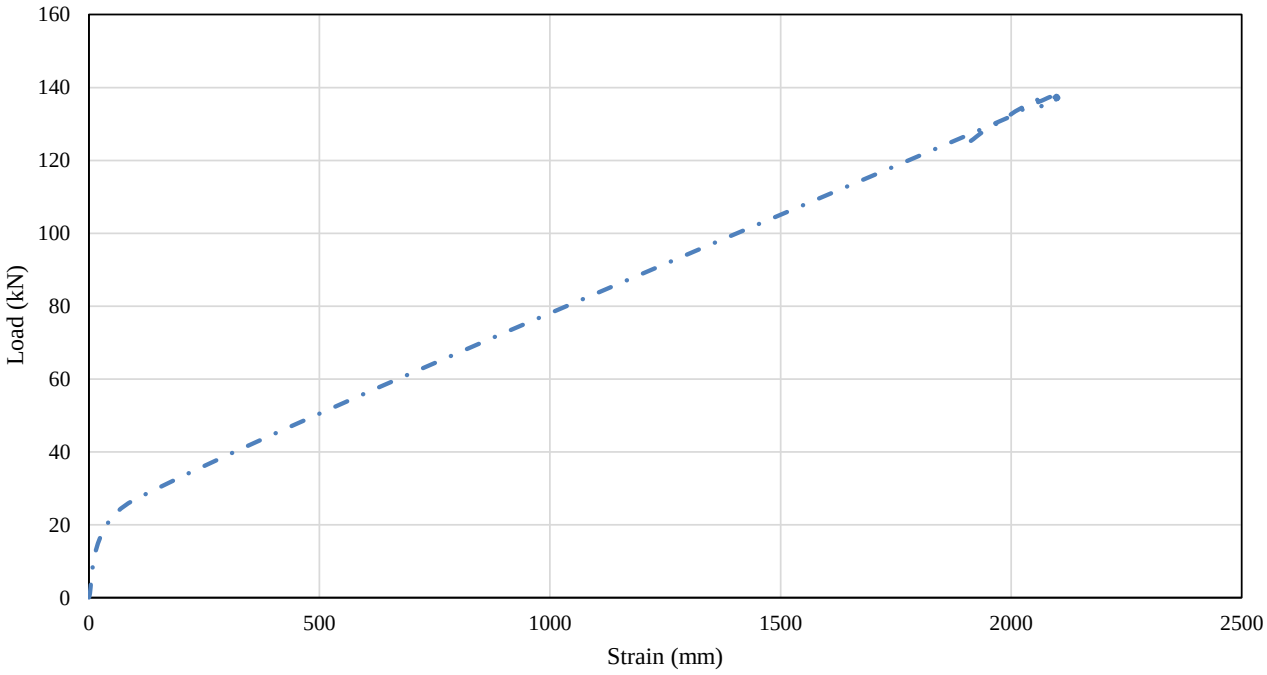

Figure 4.6 Load – strain behaviour for top concrete (S1).

4.2.3.2 GFRP strains

Figure 4.7 shows the relationship between the load and strain at the tensile reinforcement for slab S1. Before the concrete began to crack the GFRP bars had almost no strain, but after cracking commenced at around 25 kN, strains in the reinforcements rapidly increased. The load-strain behaviour in the tensile GFRP bars for slabs S1 and S2 was similar because at failure, when concrete crushing occurred, the strain in the over reinforced section and tensile GFRP bars reached 13,390 microstrains (less than the GFRP rupture strain) at a maximum load (137 kN).

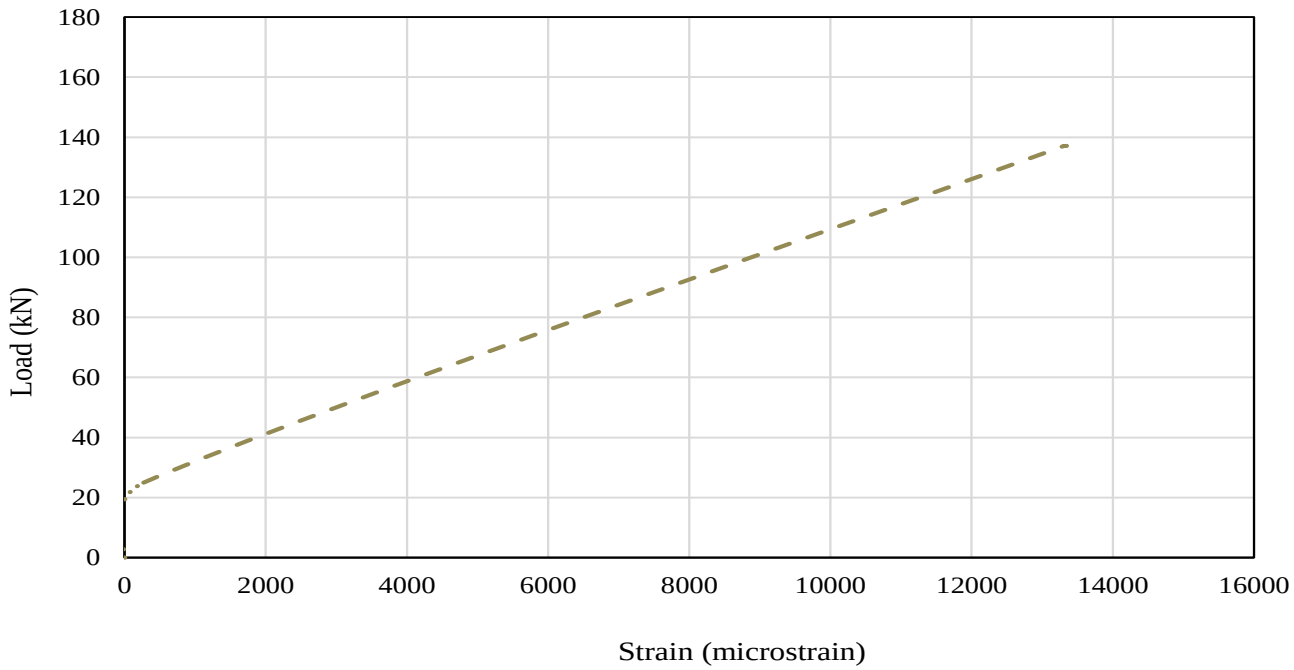

Figure 4.7 The load –strain for the bottom GFRP (S1).

4.3 Hollow slab (S2)

4.3.1 Crack propagation and failure mode

Figure 4.8 shows crack propagation in the S2 slab; the first crack began at 25 kN (load cracking level) and appeared close to the loading points. When the slab moved to a cracked condition under an increased load, fine cracks appeared at the bottom of the concrete between the two point loads, as marked, until the load reached 70 kN; as the load increased the cracks became wider and propagated towards the top e layer of concrete, as shown in Figure 4.9. With a further load increment, the vertical cracks near the point load became wider, as shown in Figure 4.10, and inclined cracks formed under the point loads due to shear stress and propagated towards the support points; concrete crushing then began in the compression zone. As a consequence, final failure was due to shear failure, as shown in Figure 4.11, where the concrete failed suddenly, and with a loud noise. Like slab S1, slab S2 was also over reinforced (Newhook and Svecova, 2007, Association, 2002b). With regards to the over reinforced section of S2, when the reinforcement ratio is higher than the balance ratio ($\rho_f > \rho_{fb}$), failure is due to concrete crashing (Grothe and Park, 2000, Association, 2002b). After failure, there was a massive amount of crushing at the left side of the

slab; the GFRP bars did not rupture, but buckling failure mode was associated with top GFRP reinforcements.

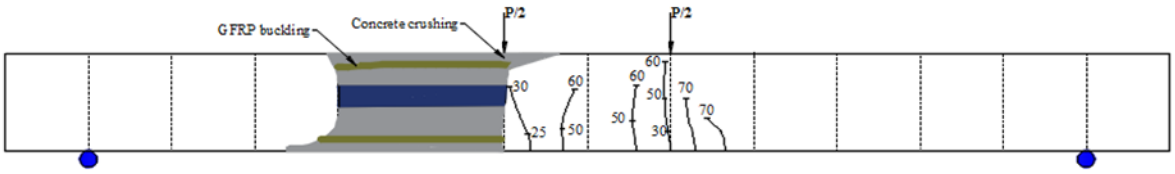

Figure 4.8 Crack propagation (S2).

Figure 4. 9 Cracks propagated upwards (S2).

Figure 4. 10 Cracks under the point load were wider (S2).

Figure 4. 11 Final failure (S2).

4.3.2 Load- deflection behaviour

Figure 4.12 shows the load- deflection behaviour of the hollow slab (S2). Overall, slab S2 showed almost the same behaviour as S1 because it began with a linear load-deflection until the first fine cracks appeared under a load of 25 kN and a deflection of 3 mm. After the first cracks appeared, the stiffness decreased to 2.6 kN/mm. but with further loadingdeflection increased linearly with a load up to 140 kN with a 50 mm deflection. At this point, S2 showed nonlinear behaviour because the concrete began to crush and the GFRP bars to buckle, as shown in Figures 4.8. There was an increase in deflection in response to a very small increase in the load; this continued up to a midspan deflection of around 60 mm and then the slab failed.

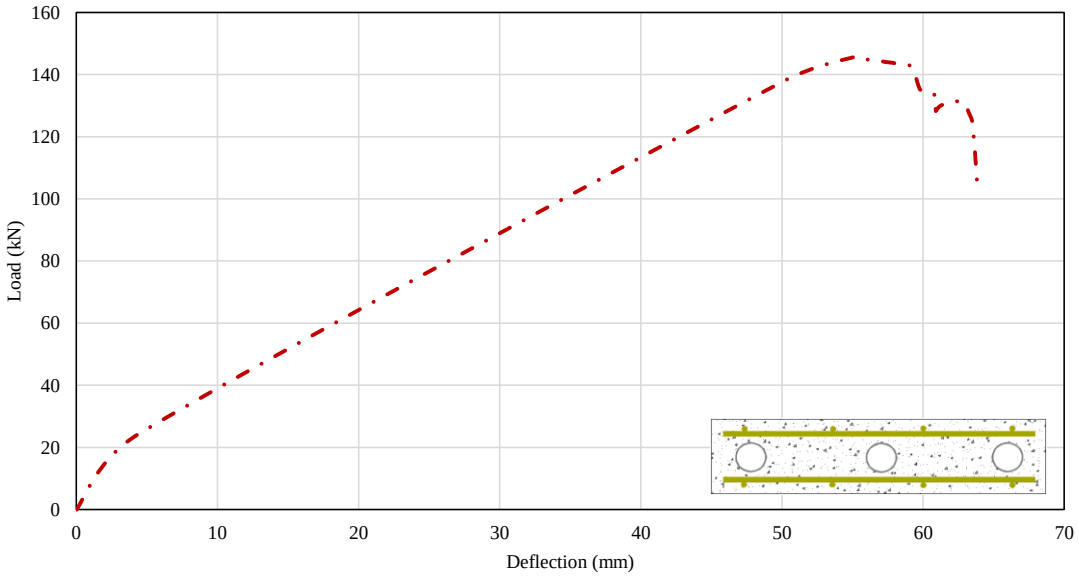

Figure 4. 12 S2 load-deflection relationship.

4.3.3 Strain behaviour

4.3.3.1 Concrete strains

Figure 4.13 shows the relationship between load and strain at the top surface of the concrete for slab S2. Strain in the concrete increased linearly with load up to 100 microstrains and then the first flexural tensile cracks appeared at the bottom of the slab at a load of 25 kN. As the load increased, the strain behaved linearly with load up to failure, but with a reduced stiffness. The maximum strain in the top concrete for slab S2 was 1995 microstrains.

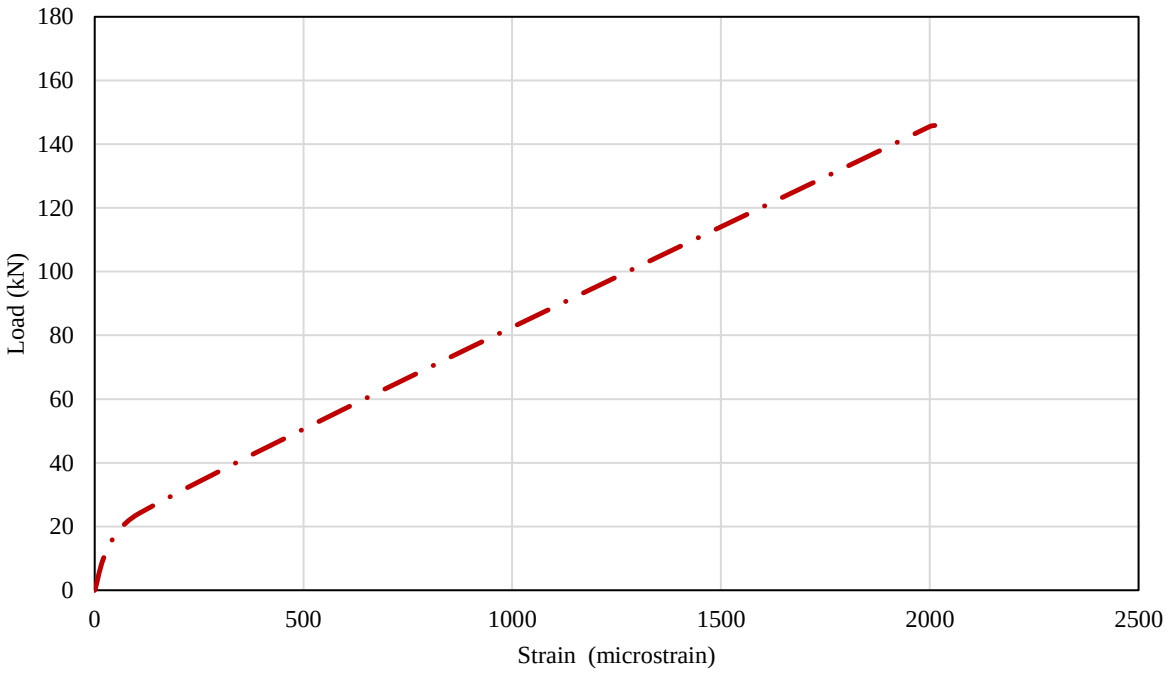

Figure 4. 13 Load-strain relationship for top concrete (S2).

4.3.3.2 GFRP strains

Figure 4.14 shows the relationship between the load and strain at the tensile GFRP reifnorcement for slab S2. Before cracking commenced, the GFRP bars had almost no strain values, but after the first cracks appeared at 25 kN, the strains in the GFRP bars rapidly increased. At failure, the strain in the GFRP bars reached almost 13,000 microstrains.

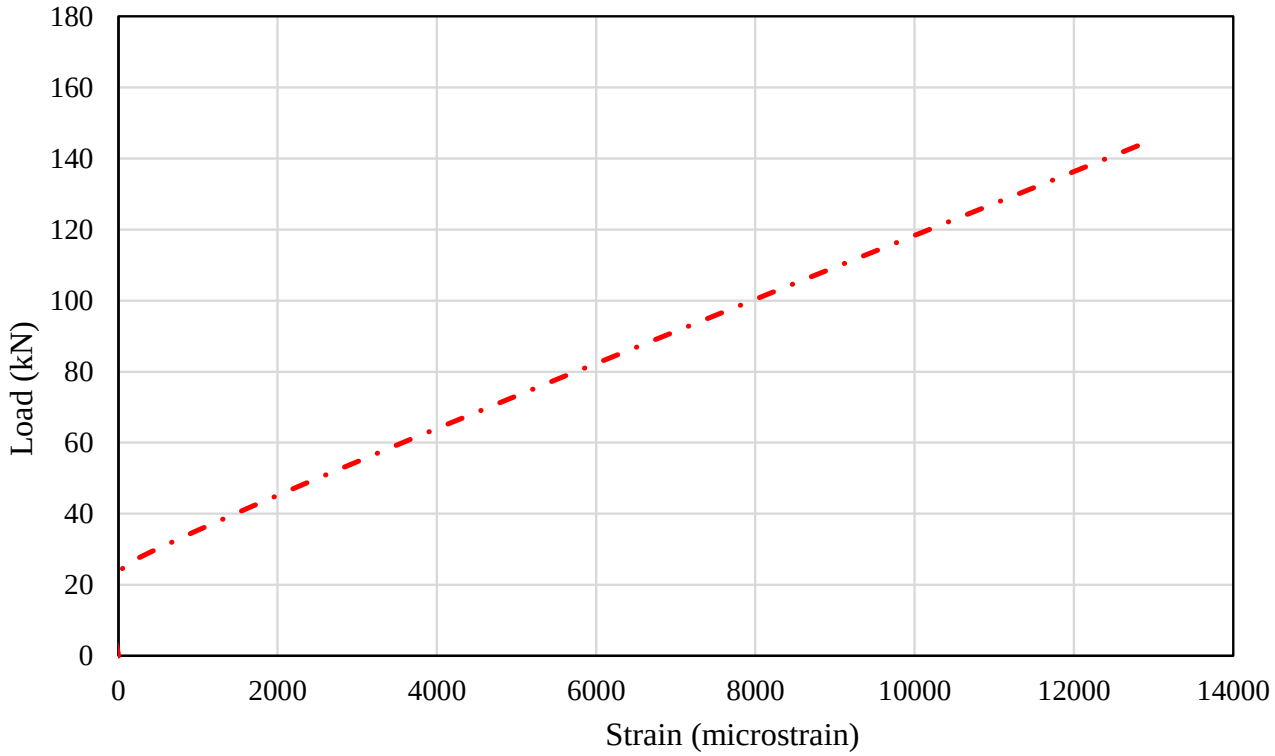

Figure 4.14 The load and strain behaviour for bottom GFRP (S2).

4.4. Slab reinforced with Hollow composite system and GFRP bars (S3)

4.4.1 Crack propagation and failure mode

Figure 4.15 shows the crack propagation in slab S3. The first cracks appeared at the bottom of the slab, between the loading points, at a load of 25 kN. As the load increased, fine flexural cracks began at the bottom of the concrete up to 80 kN, but as the load increased, these flexural vertical cracks became wider and propagated towards the top of the slab, as shown in Figure 4.16. At a load of 140 kN, concrete crushing began in the compression zone under the loading point, and then horizontal cracks developed, as shown in Figure 4.17. These cracks began under the loading point and propagated along the length of the CRS. Concrete crushing also began in the slab, as shown in Figure 4.18. Final failure occurred with a loud noise as the fibres in the bottom flanges of the CRS suddenly ruptured, as shown in Figure 4.19. At final failure, horizontal splitting cracks in the CRS appeared, as shown in Figure 4.20.

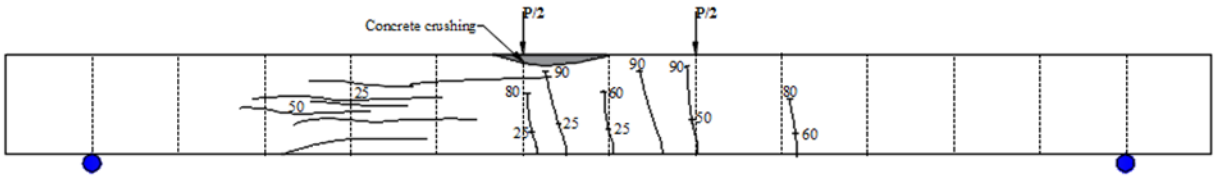

Figure 4. 15 Cracks propagation (S3).

Figure 4. 16 Initiation of horizontal cracks (S3).

Figure 4. 17 Cracks propagated upward (S3).

Figure 4. 18 Final failure (S3).

Figure 4. 19 CRS failure (S3).

Figure 4. 20 CRS debonding (S3).

4.4.2 Load- deflection behaviour

Figure 4.21 shows the load- deflection behaviour of slab S3 slab; it commenced with linear load-deflection until the first flexural cracking appeared at a load of 25 kN and deflection of 3 mm. In slab S3, the slope of the load-deflection curve decreased from 6.8 kN/mm to 4.8 kN/mm after the concrete first began to crack, but then deflection increased linearly as the load increased to around 200 kN with a deflection of 46 mm. Peak load was reached at 211 kN with a deflection of 57 mm, but then the load capacity decreased until the slab failed at a load of 150 kN and deflection of 75 mm.

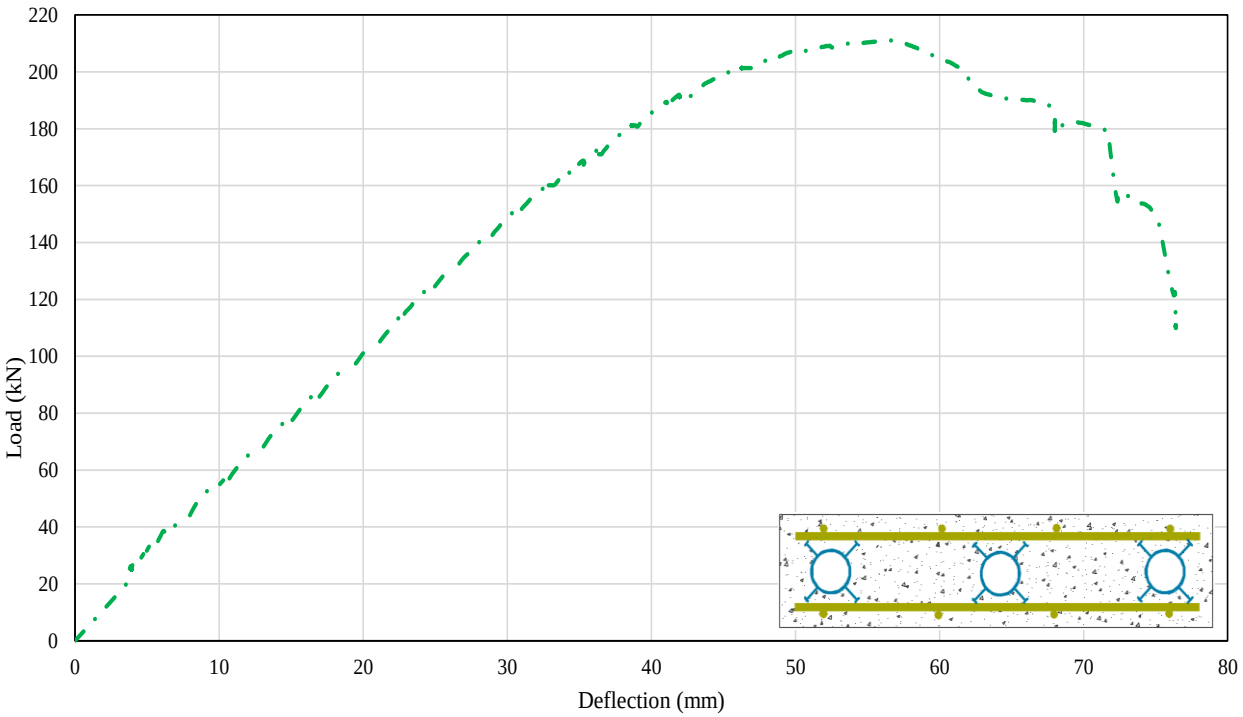

Figure 4.21 S3 load-deflection relationship.

4.4.3 Strain behaviour

4.4.3.1 Concrete strains

Figure 4.22 shows the relationship between the load and strain at the top and bottom of slab S3. At the top, strain in the first segment of the concrete behaved linearly up to 100 microstrains until the first flexural tensile cracks occurred at the bottom of the slab at a load of 25 kN; after this the strain again increased linearly with the load.

The maximum recorded strain in the top of slab S3 was 2855 microstrains, whereas . on the bottom, first crack appeared at 25 kN and only recorded 91 microstrains.

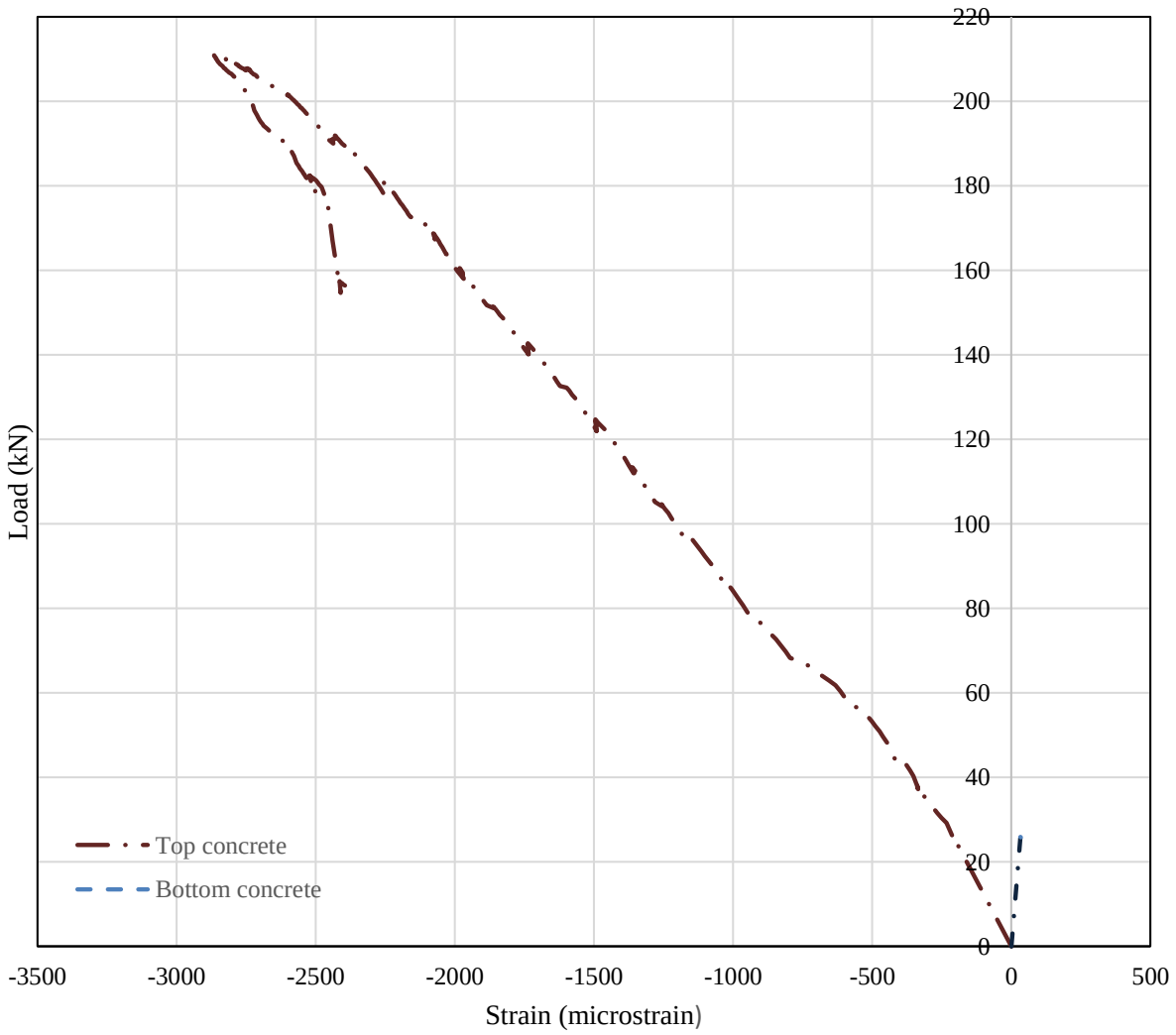

Figure 4.22 The load and strain behaviour for top and bottom concrete (S3).

4.4.3.2 GFRP strains

Figure 4.23 shows the relationship between the load and strain at the compression and tensile reinforcments for slab S3. The graph shows that the strain in the compressive GFRP bars in slab S3 increased linearly with load even after the concrete began to crack. A a load of 170 kN, the load-strain behaviour became nonlinear until the peak load, while the maximum strain recorded was around 2400 microstrain.

The same graph show that for tensile reinforcment, when the slab is very stiff and without cracks, the bottom GFRP bars had almost no strain values, but after the first first cracks appeared at 25 kN, the strains in the reinforcements rapidly increased. The load-strain in slab S3 was almost linear

after the concrete first began to crack, but the rate was slower than for slabs S1 and S2. The load-strain was nonlinear however until a peak load of 211 kN was reached. The strain at the bottom GFRP bars when slab S3 finally failed was around 14,000 microstrains, which was almost 70% higher than the failure strain of the GFRP bars in tension.

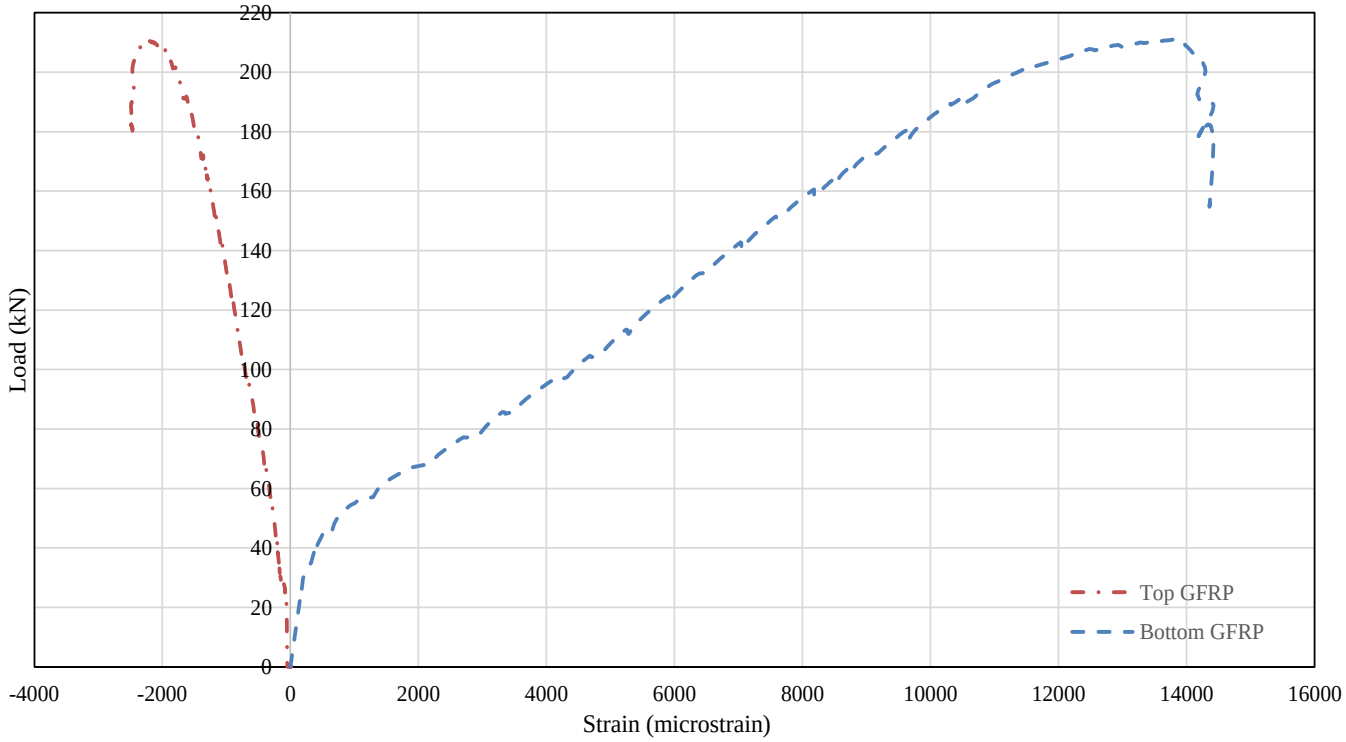

Figure 4.23 The load and strain behaviour for top and bottom GFRP (S3).

4.4.3.3 CRS strains

Figure 4.24 shows the relationship between the load and strain at the top surface of CRS for slab S3. At the initial application of load and until the first cracks appeared in the concrete, strain in the CRS was very low. The nonlinear and compressive strain was then measured at the top surface of CRS with the magnitude of strain, but then the strain shifted to tension at around 150 kN, until the slab finally failed. The graph shows that the maximum strain recorded in slab S3 was only 2500 microstrains, but then the load reduced gradually after CRS failure and failed completely at a load of around 145 kN with 2650 microstrains.

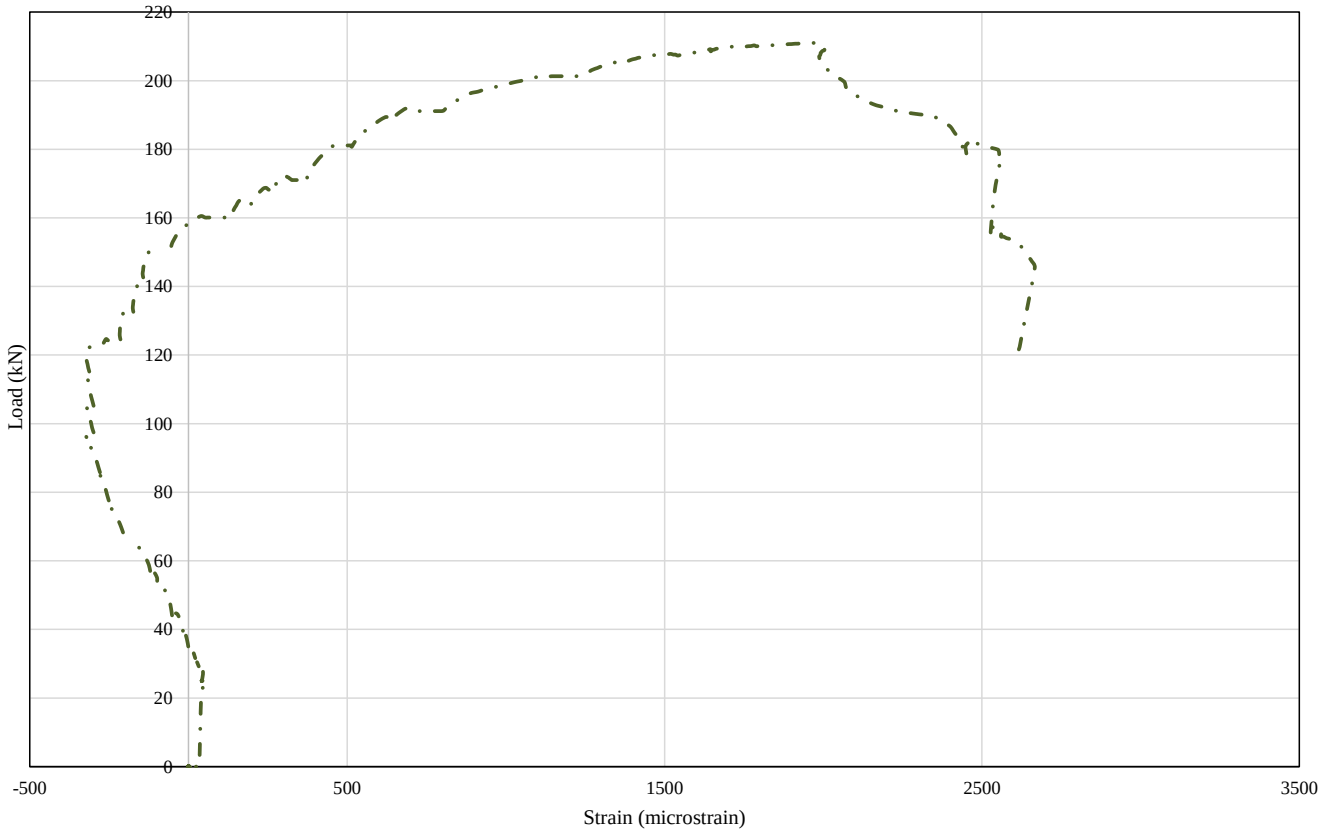

Figure 4.24 Load and strain relationship at the top of CRS (S3).

4.5 Slab reinforced with Hollow composite system and GFRP bars (S3)

4.5.1 Crack propagation and failure mode

Figure 4.25 shows the crack propagation in slab (S4); like the other three slabs, the first cracks began at the bottom of the slab between the loading points at an applied load of 25 kN. When the load increased, fine flexural cracks began at the bottom of the concrete up to a load of 70 kN, and with further load increments the flexural vertical cracks became wider and propagated towards the top of the slab, as shown in Figure 4.26. At an applied load of 150 kN, concrete crushing in compression occurred under the loading point, as shown in Figure 4.27, but after this load the crack in slab S4 became wider and deeper. The concrete in slab S4 was crushed as shown in Figure 4.28; there was a loud noise just before final failure as the fibres in the bottom flanges of the CRS ruptured, as shown in Figure 4.29. At final failure, there were horizontal splitting cracks along the

CRS, as shown in Figure 4.30; the steel bars did not break, but they did buckle under compression, as shown in Figure 4.29.

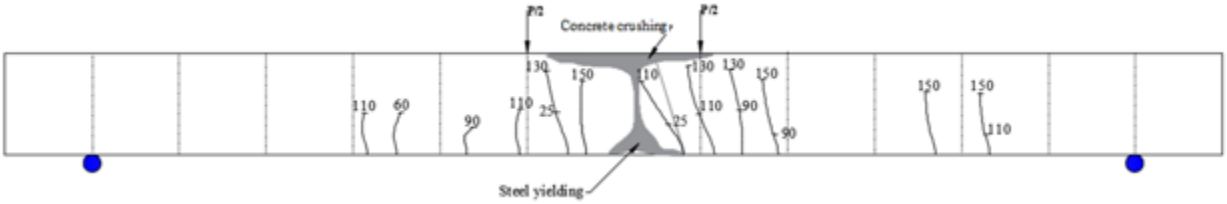

Figure 4. 25 Crack propagation (S4).

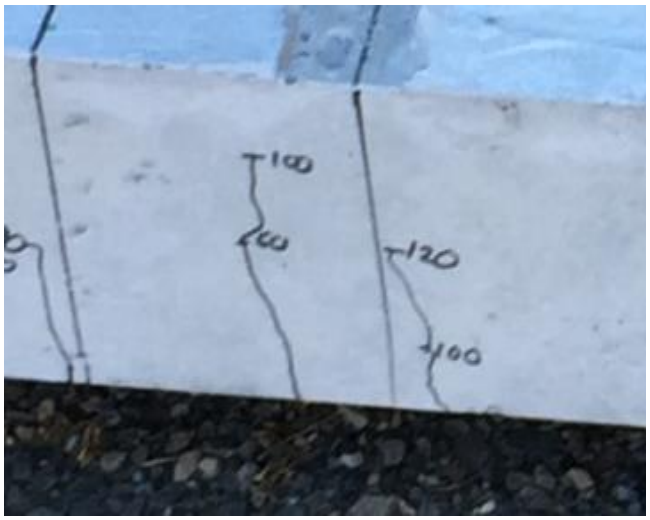

Figure 4. 26 Cracks propagated upward (S4)

Figure 4. 27 Cracks initiation in the top concrete (S4).

Figure 4. 28 Final failure (S4).

Figure 4. 29 Compressive steel buckling failure (S4).

Figure 4. 30 CRS failure (S4).

4.5.2 Load deflection behaviour

Figure 4.31 shows the load- deflection behaviour for slab S4. Slab S4 exhibited a linear load-deflection behaviour until the concrete began to crack at a load of 25 kN and deflection of 3 mm. When the concrete began to crack the stiffness decreased to 6.4 kN/mm, but deflection then increased linearly with load up to around 130 kN and a deflection of 16 mm. The slope of the load-deflection curve then decreased slightly after this load, and the behaviour of slab 4 became nonlinear. This continued until it reached a maximum load of 208 kN and a deflection of 45 mm; after this there was a slight decrease in the load capacity and the slab continued to deflect even without much increase in the load. Slab 4 then failed at a load of 150 kN and a midspan deflection of 80 mm due to concrete crushing and steel buckling.

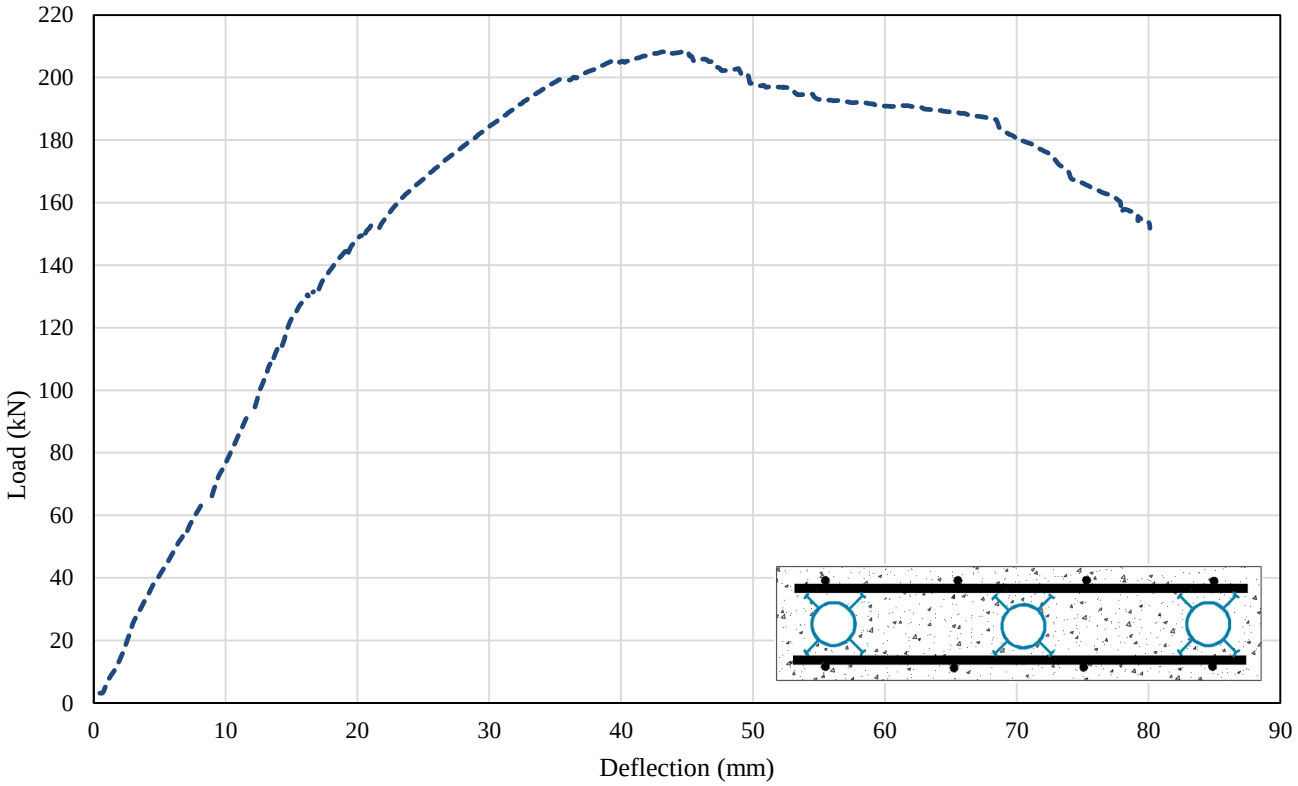

Figure 4. 31 S4 load-deflection relationship.

4.5.3 Strain behaviour

4.5.3.1 Concrete strains

Figure 4.32 shows the load- strain behaviour of the top concrete in S4. The strain increased linearly up to 100 microstrains and then the first flexural tensile cracks began at the bottom of the slabs at a load of 25 kN. After the concrete cracked, the strain at the top concrete for slab S4 also increased linearly with load, but at a slower rate than the other slabs, however, at a load of 130 kN and strain of 1100 microstrains, the strain readings became nonlinear. In fact, there was a significant increase in the load from 170 kN to 200 kN but the strain remained at 1500 microstrains. At 202 kN, the strain then increased to 1791 microstrains before the slab failed due to concrete crushing. The strain gauges at the bottom of the concrete recorded very small strain and completely stopped after tensile concrete commenced at a load of around 25 kN.

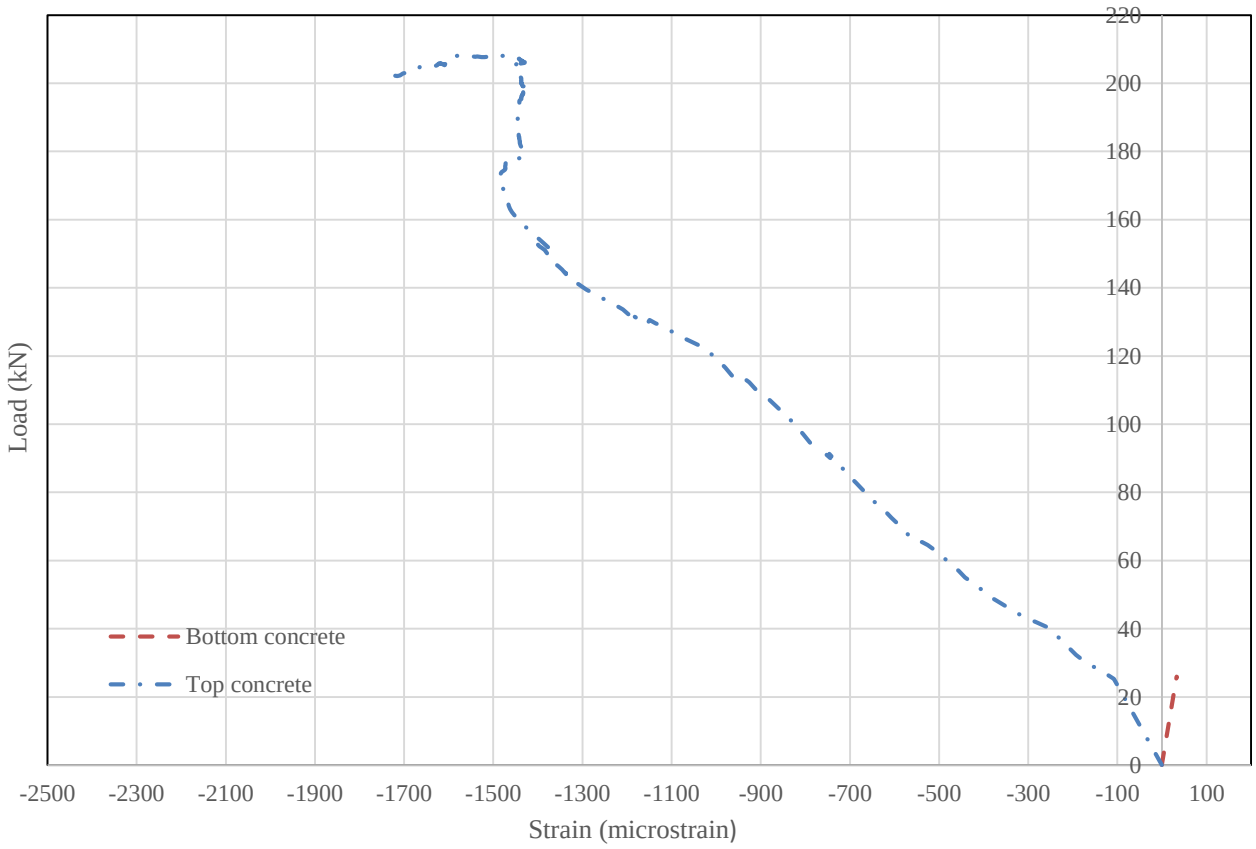

Figure 4. 32 The load and strain relationship for the top and bottom concrete (S4).

4.5.3.2 Steel strains

Figure 4.33 shows the relationship between the load and strain at the top and bottom reifnorcements for S4. Before the concrete began to crack, the steel reinforcements at the bottom of slab S4 had almost no strain values, but when the first cracks began at 25 kN, the strains in the reinforcements rapidly increased. The graph shows that as expected, the strain in the steel bars in slab S4 developed very slowly, but as the load increased from 130 kN to 208 kN the strain remained constant at around 2700 microstrains. This was followed by a significant increase in the strain even without any further increase in the applied load.

However, load-strain in the steel at the top of the slab S4 was nonlinear after the concrete began to crack, and continued up to failure. A strain of more than 3000 microstrains was recorded in the steel bars in compression at failure.

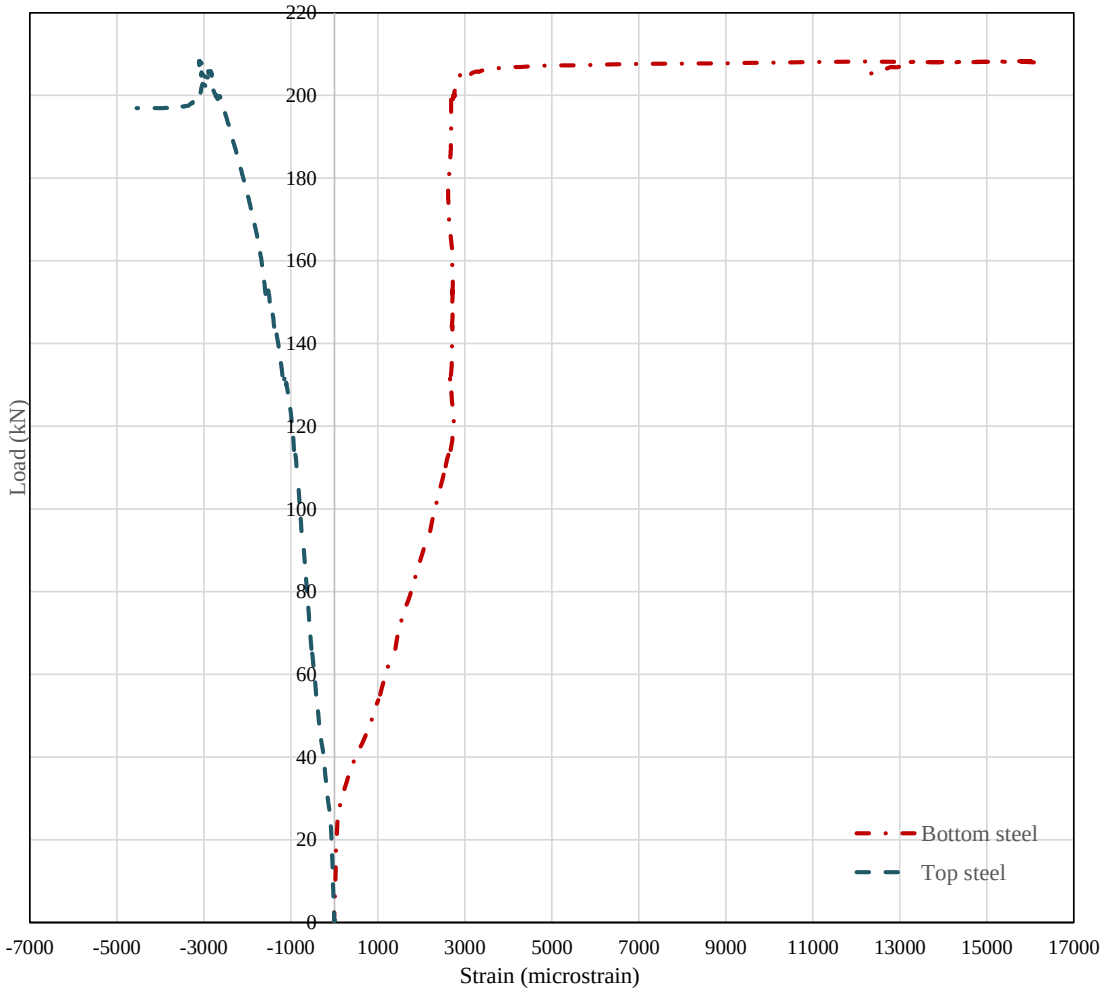

Figure 4.33 The load - strain behaviour for the top and bottom steel bars (S4).

4.5.3.3 CRS strains

Figure 4.34 shows the load - strain at the top surface of the CRS for slab S4. When the load was first applied and the first cracks appeared, strain in the CRS was very low. The graph shows that a nonlinear and compressive strain was then measured at the top surface of the CRS in slab S4, with a small strain value, but as the load increased to around 150kN the strain shifted to the tension zone and remained there until final failure. The CRS in slab S4 reached a maximum strain of up to 7100 microstrains before it failed completely.

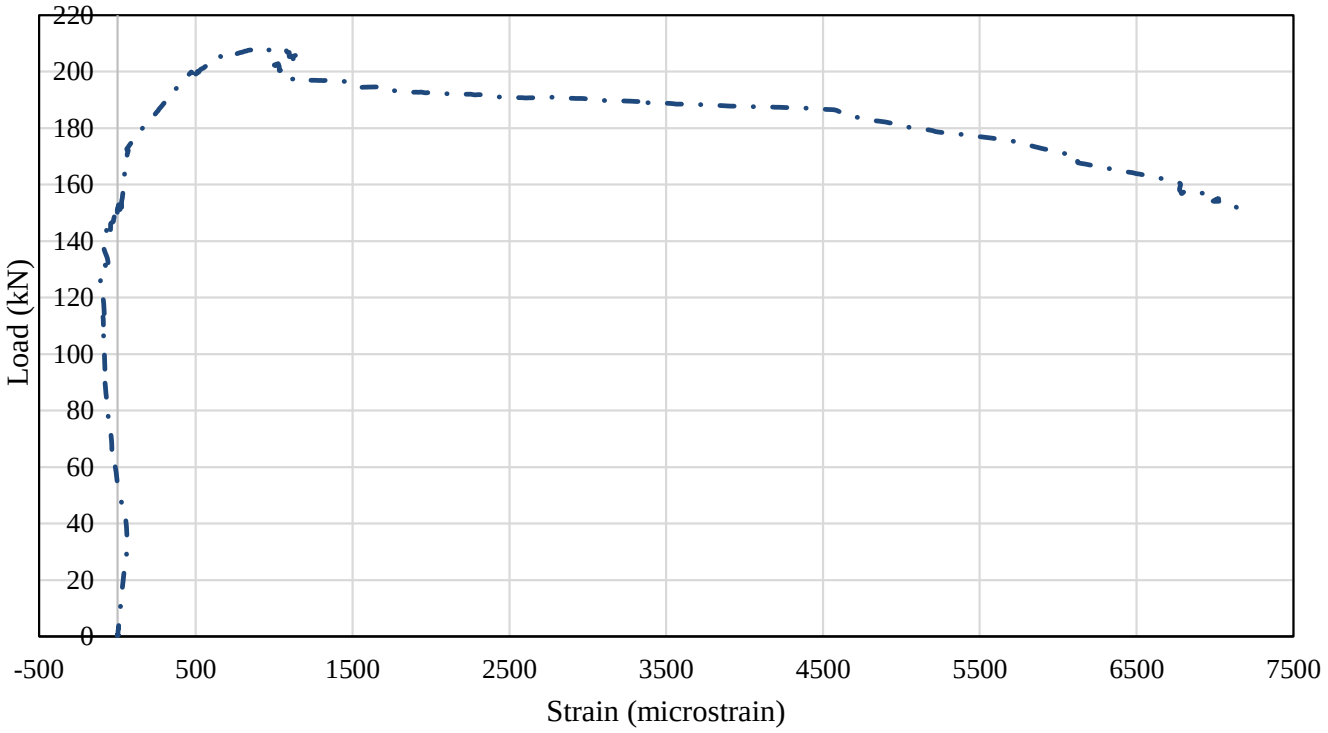

Figure 4.34 The load - strain behavioue for the top CRS (S4).

4.6 Summary

This chapter has presented the results and observations for the four point static bending tests of the four full-scale reinforced concrete slabs with hollow composite reinforcing systems. The effects that different parameters such as voids, the hollow composite reinforcing system, and the type of longitudinal reinforcements had on the structural performance of hollow concrete slabs are analysed and presented in the next chapter.

Chapter 5

Discussion and theoretical evaluation

5.1 Introduction

This chapter discusses the experimental results and observation for the four tested slabs. The effects of parameters such as voids, the effectiveness of a hollow composite reinforcing system, and how the type of longitudinal reinforcements affected the structural performance of hollow concrete slabs are analysed and presented. The behaviour of concrete slabs reinforced with GFRP bars and hollow composite reinforcement were analysed theoretically using the Fibre Model Analysis and then verified experimentally. This analysis was then extended to observe how the number of voids, the compressive strength of concrete, and the reinforcement ratio affected the overall behaviour of the slabs.

5.2 Discussing the experimental results

5.2.1 The influence of the hollow concrete core

The influence of a hollow concrete core in precast concrete slabs reinforced with GFRP bars was evaluated by comparing slabs S1 and S2. It was found that the structural behaviour of solid and hollow core slabs was similar because they both failed in diagonal shear, followed by concrete crushing and the bars buckling under compression. This type of failure was expected there was no shear reinforcement in these slabs. This was further confirmed by the maximum 2000 microstrains measured in slab S2. However, the hollow core slab (S2) showed more brittle failure behaviour than the solid slab (S1) because the reduced width of the slabs meant it could not resist the shear forces, so the voids collapsed.

Having a hollow core did not affect the overall stiffness or capacity of the concrete slab, possibly because the smaller voids matched the outside diameter of the CRS, thus resulting in only a 9% reduction in the gross area of slab S2 compared to slab S1. The similar behaviour of slabs S1 and S2 at peak load can be further explained by the location of neutral axis, it is higher than the top of the hollow core, so the contribution made by the uncracked concrete in compression was the same for both slabs. The strain measured in the top concrete in Figures 4.6 and 4.13, and strain at the bottom reinforcement in Figures 4.7 and 4.14 indicate that during the entire loading regime the depth of the neutral axis was 21 mm from the top of both slabs, so it is clearly above the hollow

core, as shown in Figure 5.1. This finding was similar to Wariyatno et al. (2017) who found that the void was lower than the neutral axis in the distribution of the stress and strain, as shown in Figure 5.2.

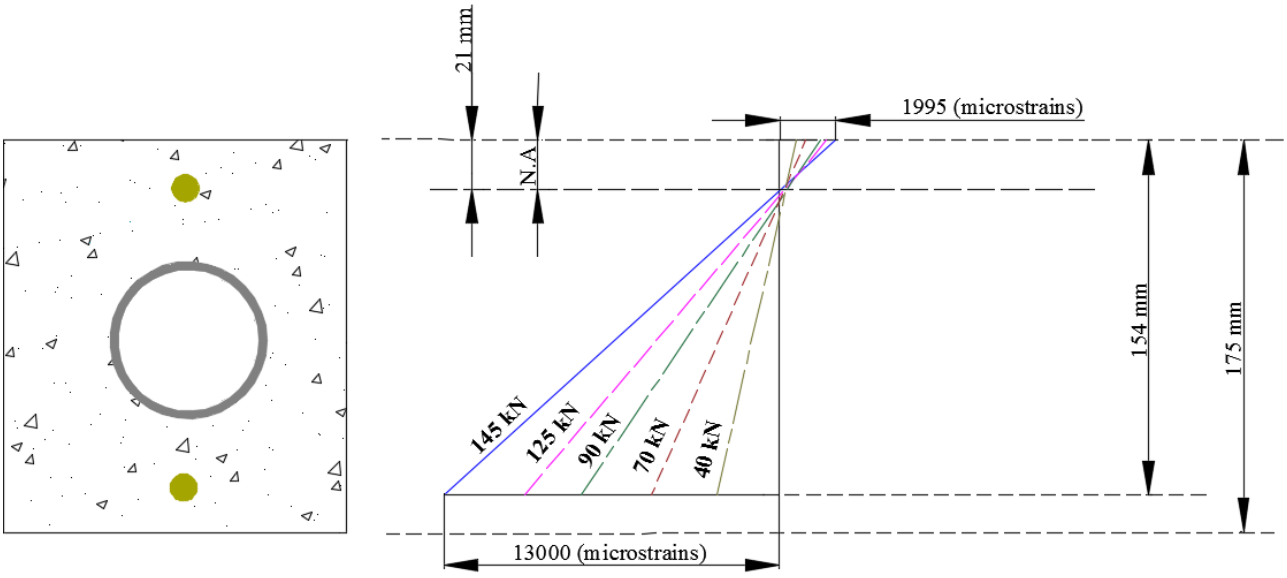

Figure 5.1 Strain distribution in slab S2.

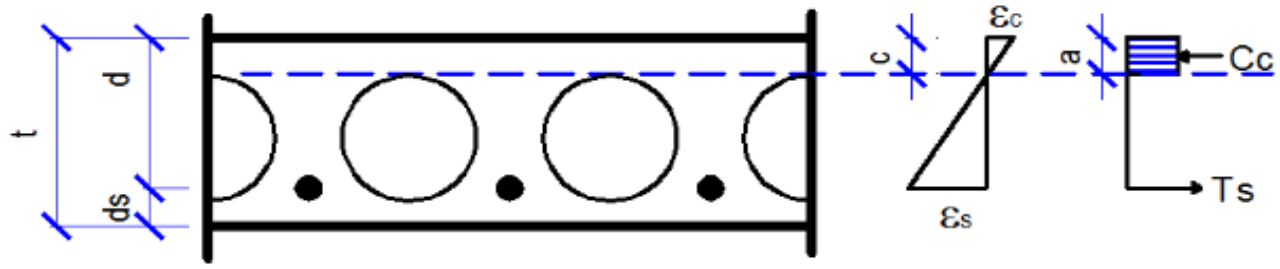

Figure 5.2 Stress and strain diagrams for hollow core slab (Wariyatno et al., 2017).

5.2.2 The effectiveness of CRS in reinforcing concrete slab

The CRS proved to be an effective reinforcement for hollow concrete slabs the behaviour of slabs S2 was compared to S3; in fact the provision of 3 pieces of CRS in slab S3 yielded more than 31% higher capacity than slab S2, which indicated that CRS was acting like an internal reinforcement

to slab S3. This finding was supported by the load and strain at the bottom GFRP bars where the addition of CRS reduced the strain in the bottom bars in slab S3, thus showing it provided additional tensile reinforcement. CRS also increased the bending stiffness of hollow concrete slabs by 85%, as well as changing the failure mode in slab S3 from shear failure to flexure, as shown in slab S2. This occurred because the hollow CRS stopped the vertical flexural cracks from reaching the top layer of concrete as well as massive concrete crushing at final failure. CRS controlled the direction of crack propagation and made the crack path longer because it had to pass through the CRS flanges; this enhanced the serviceability of slab S3. This finding is supported by Cuenca and Serna (2013) who showed that fibres can overcome shear failure because they increase the strength of the element to its full flexural capacity. This improved performance of the hollow core slab due to CRS was much better than attaching carbon fibre reinforced polymer (CFRP) sheets, as done by Meng (2016); there was only an 11% enhancement in load capacity which was not enough to stop the hollow core from collapsing completely while Meng attached the CFRP in order to avoid the shear failure experienced previously. Granted he enhanced the shear failure but not to any significant value. In this study however, it was possible to mitigate the shear failure by almost 45%, and there was debonding failure because the four flanges of CRS interacted effectively with the concrete. However, debonding failure observed by Meng (2016) on CFRP sheets occurred because the internal reinforcement inside the hollow was not stiff enough to stop the compressive and tensile forces from resisting bending loads; this was achieved in this study because thicker sheets of CRS were used in this study than the thin sheets of CFRP used in Meng's study; Elgabbas et al. (2010) used another CFRP technique for strengthening hollow core concrete slabs; this technique improved the load carrying capacity, but since it was not very efficient, shear failure and a sharp rupture failure of CFRP with debonding failure still occurred, unlike the slab reinforced with CRS in this study, shown in Figure 5.3. Here the concrete reinforced with CRS reinforced the voids perfectly, unlike the hollow core slabs where Ibrahim et al. (2016) using concrete as topping. This was clear evidence of failure where many cracks appeared around the voids, something that did not occur in the voids reinforced by CRS, as shown in Figure 5.4. Table 5.1 also summarises the comparisons between the effect of CRS and previous techniques used to improve failure, load capacity, and the stiffness of hollow core slabs; this table also shows that CRS is the perfect innovation that will provide a better performance.

(a) CFRP rupture failure in the bottom slab (Elgabbas et al., 2010).

(b) Hollow slab with CRS provided perfect failure behaviour as shown in the bottom slab.

Figure 5.3 Slabs with CFRP and CRS at the failure.

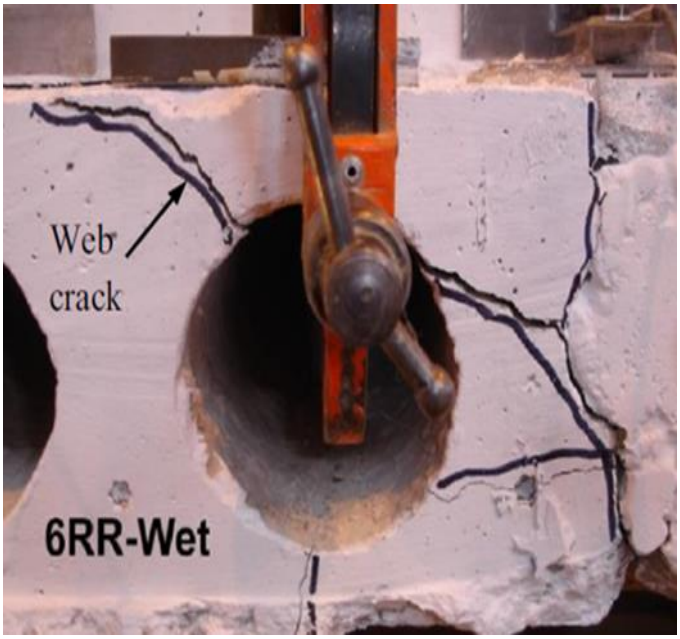

(a) Concrete cracks occurred around the voids at failure (Ibrahim et al., 2016).

(b) No concrete cracks occurred around the CRS.

Figure 5.4 Concrete around the voids at the failure.

Table 5.1 Compression between different materials and technique used in the hollow slabs.

Indicator	CRS	CFRP (Meng, 2016)	Concrete topping (Ibrahim et al., 2016)	CFRP different technics (Elgabbas et al., 2010)
Failure behaviour	**10**	**4**	**5**	**2**
Load capacity	**8**	**7**	**7**	**5**
Stiffness	**10**	**5**	**6**	**5**

*(1 to 10) level of improvement, 10 being the best

5.2.3 Effect of reinforcement type

The type of reinforcment had a signficant effect on the overall stiffness but had no effect on the load capacity of hollow concrete slabs. After the concrete first began to crack, slab S4 retained almost 94% of its initial and uncracked stiffness, while slab S3 only retained 75%. Slab S4 was stiffer because the modulus of elasticity of the steel was higher than the GFRP bars in slab S3, as seen by many researchers (Ombres et al., 2000, Ali et al., 2015, Abdalla, 2002, Benmokrane et al., 1995, Bischoff, 2005, Maranan et al., 2015). CRS enabled the hollow slab to retain most of its stiffness because it prevented wider cracks from developing. For example, El-Gamal et al. (2011) measured up to 72% higher stiffness for steel reinforced slabs over GFRP reinforced slabs with similar reinforcement ratios, whereas the steel reinforced slab (S4) was only 33% stiffer than the GFRP reinforced hollow slabs (S3) in this study, as shown in Figure 5.5. However, the flexural capacity of slabs S3 and S4 were almost the same because the failure of these slabs was governed by CRS, including the combined bending failure and interlaminar shear of CRS. Figure 4.23 shows that CRS reduced the strain experienced in the GFRP bars (slab S3) indicating how effectively it could utilise the tensile strength of the bars. Morever, the GFRP bars and CRS continued to carry the load to final failure. However, the stress was all transferred to the CRS when the tensile reinforcement in slab S4 yielded at a load of 140 kN. The bottom steel reinforcement experienced no strain (Figure 4.33). but the strain in CRS increased significantly after the steel bars yielded at

their maximum load (Figure 4.34). While slab S4 continued to carry the load until the CRS failed, the stiffness in the load-deflection curve reduced when the steel yielded (Figure 4.31). This result contradicted the comparison between the stiffness values at the beginning of this section, so the steel-reinforced slab S4 was stiffer than S3 from when cracking commenced until it reached the yielding point, but then the yielding case reversed because slab S3 continued to exhibit a linear stiffness due to the linear elastic behaviour of the GFRP bars, unlike the reduced stiffness of slabe S4 due to a reduction in the stiffness of steel reinforcement. This result suggests that the CRS and GFRP bars are more compatible than the steel bars because the stiffness of the composite materials was almost similar.

The presence of CRS prevented the concrete in slabs S3 & S4 from premature compressive failure but horizontal shear cracks still developed in the concrete at the level of the hollow reinforcing system. However, there were more horizontal cracks in slab S3 and they were deeper than those in slab S4. Chang and Seo (2012) made similar observations and then indicated that the wider cracks at the same level of load in GFRP-reinforced one way slabs compared to the steel-reinforced one way slabs were similar in size, whereas the reinforcement ratio reported occurred because the the GFRP bars were not as stiff as the steel bars. This also explaines the higher deflection in slab S3 than slab S4, where at peak load, concrete compressive crushing occurred in slab S3 while the bottom steel in slab S4 yielded.

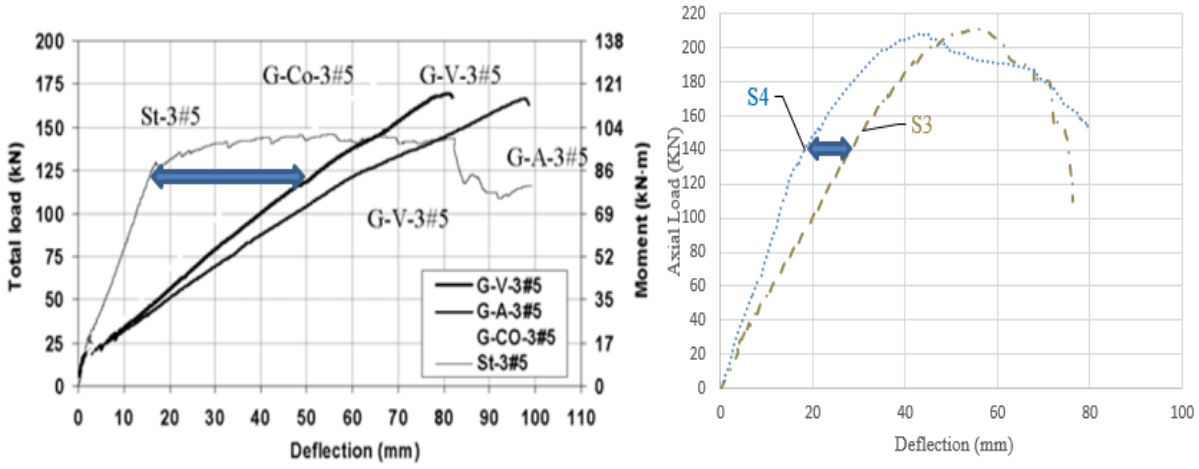

(a) Load –deflection behaviour without CRS (El-Gamal et al., 2011).

(b) Load-deflection behaviour with CRS.

Figure 5.5 Stiffness for slabs with steel and GFRP.

5.3 Theoretical evaluation

A theoretical analysis was carried out to evaluate two slabs reinforced with CRS (S3 and S4) only, and then the results provided theoretically by the Fibre Model Analysis were compared to the results from the experiment. This led to a better understanding of the behaviour of the slabs and the evaluation of CRS. In this section of the chapter three critical parameters are addressed with respect to the behaviour of the slabs.

5.3.1 Fibre Model Analysis

The behaviour of concrete slabs in flexure with a hollow composite reinforcing system was predicted using a simple Fibre Model Analysis (FMA). This layer-by-layer approach was used successfully by (Manalo and Aravinthan, 2012, Ashour, 2006) to reliably predict the flexural capacity of composite structures. In this approach the capacity of reinforced concrete slabs is predicted based on the cross section equilibrium, strain compatibility, and the constitutive material behaviour, as highlighted by Grothe and Park (2000). The internal force equilibrium principle was used to find the flexural capacity depending on the properties of the materials. It was assumed that a perfect bond exists between the reinforcement and the concrete, and the strains are directly proportional to the distance from the neutral axis of the section. The stress on each layer was calculated by multiplying the strain with the modulus of elasticity of the material, while the sectional equilibrium was maintained by balancing the net compressive and net tensile forces of the section. The flexural behaviour of the one-way slabs was then analysed using an excel spreadsheet. For a hollow composite reinforcing system, the four rectangular flanges replacing with an equivalent circular area with properties similar to the CRS; these basic assumptions are shown in Figure 5.6.

–

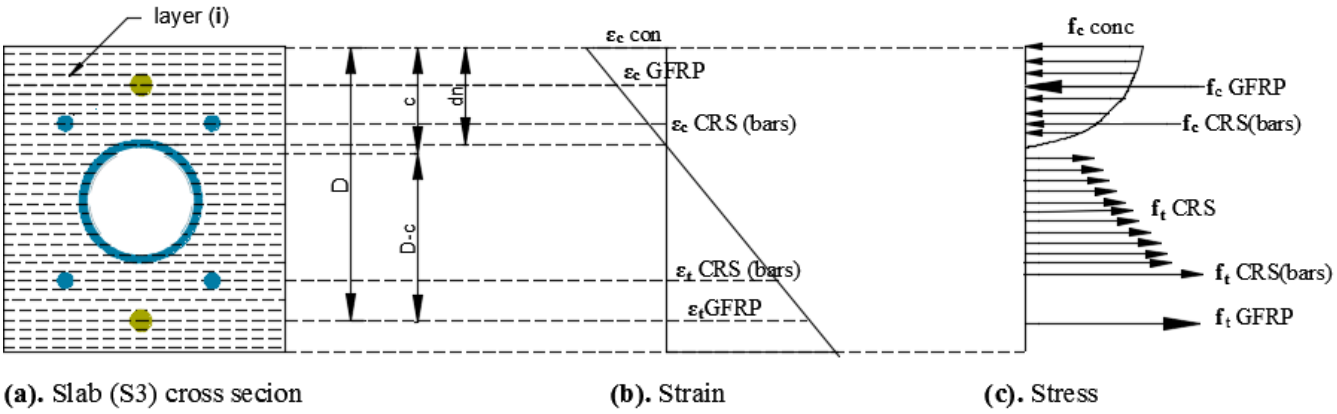

Figure 5.6 Basic assumptions in FMA.

In Figure 5.6, D is the effective depth, c is the depth of each layer from the compressive layer, d_n is the depth of the neutral axis, ε_c con corresponds to the top concrete strain, ε_c GFRP corresponds to the top GFRP strain, ε_t GFRP corresponds to the bottom GFRP strain, f_c conc is the compressive concrete stress, f_c GFRP is the compressive GFRP stress, f_c CRS is the compressive CRS stress, f_t CRS is the tension CRS stress, and f_t GFRP is the tension GFRP stress. In the FMA, Popovics (1973) model was used for the stress-strain behaviour of concrete. The concrete was considered as being with tensile strength and without tensile strength. whereas the GFRP bars and CRS were analysed as linear elastic material in both tension and compression while the steel was simplified with bilinear behaviour Wolanski (2004), i.e. linear elastic before yielding and a constant stress after yield. Two cases were also considered for the CRS, the first considered the flanges and the other was omitted the flanges. This step was to prove the advantage of using the load carrying capacity of the flange. The constitutive models for the concrete, GFRP, steel, and CRS are shown in Figure 5.7.

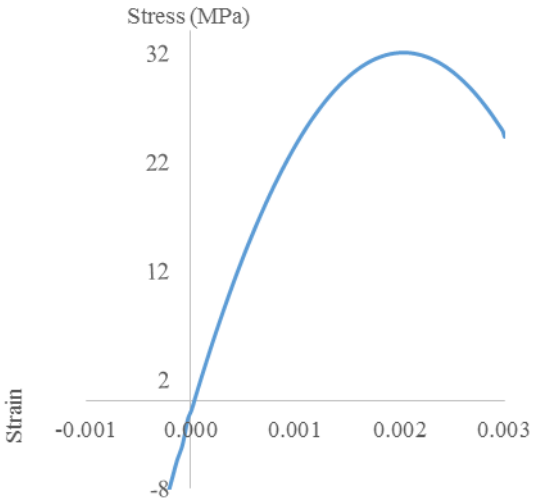

(a) Concrete

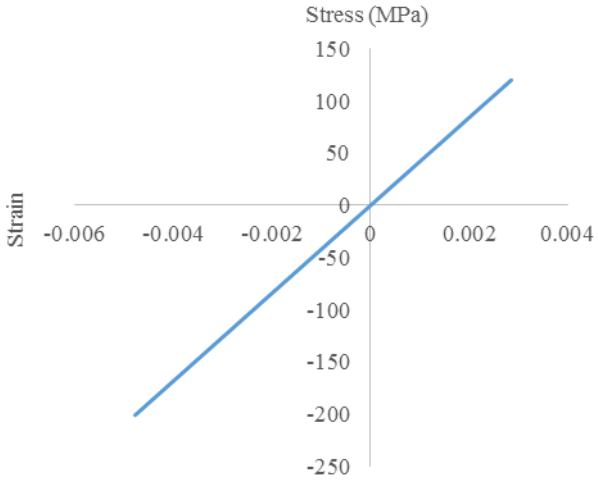

(b) CRS

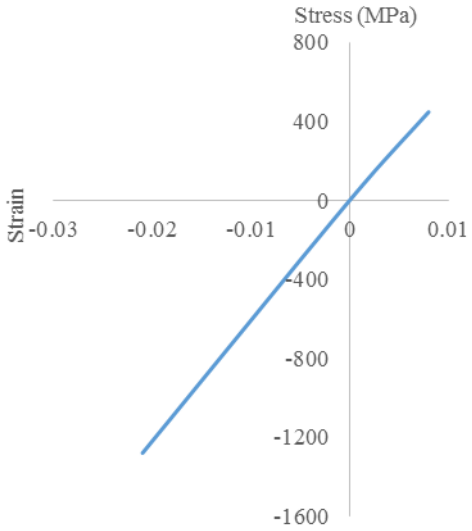

(c) GFRP bars

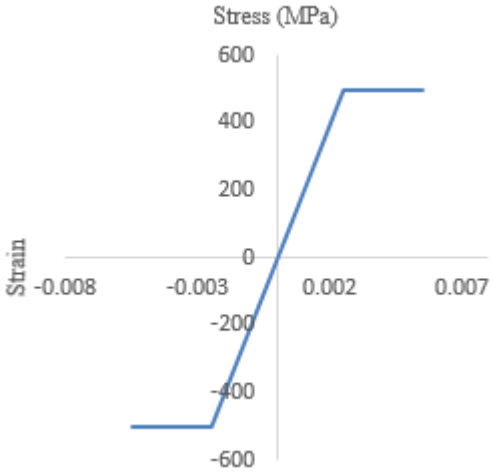

(d) Steel bars

Figure 5.7 Model of constitutive materials.

Assuming that the compressive strain at the top of the reinforced concrete slab was the first step in FMA, the bottom strain was determined by repeating the top strain until the summation of forces became zero. While the slab had still not crack, all the layers or element i contributed to the moment capacity of the section. The depth of the corresponding neutral axis d_n for these adjustments are for the strains in the top and bottom which set the force equilibrium principle which is calculated in the relation 1. Moreover, the strain $\varepsilon_{(i)}$ at element i is related for the top strain (assumed to be 0.003 for the top concrete). The stress was then calculated from the strain for each layer multiplied by its corresponding elastic modulus. The strain equation shown below was used in the FMA.

$$\varepsilon_{i=} \frac{\varepsilon_{c*(dn-di)}}{dn}$$

Where ε_0 is the top concrete strain while ε_c is the concrete strain at depth d_i. To calculate the load and moment for the slabs, the following equations were used.

$$\sum p = \sum_{i=1}^{n} f_i conc \ A_i conc + \sum_{i=1}^{n=3} f_i CRS \ A_i CRS + \sum_{i=1}^{n=4} f_i \, GFRP \, A_i \, GFRP = 0$$

$$\sum M = \sum_{i=1}^{n} f_{i\,Conc} \ A_i conc \, di + \sum_{i=1}^{n=3} f_i \, CRS \, A_i CRS \, di + \sum_{i=1}^{n=4} f_i \, GFRP \, A_i GFRP \ \ di$$

Where:

P = Sum of forces, kN.

$f_{i\ Conc}$= strength of concrete at layer i, MPa.

A_i conc = Concrete area at layer i, mm^2.

f_i GFRP= Stress GFRP bars, MPa.

A_i GFRP = Area of main reinforcement at layer i, mm^2.

f_i = CRS strength at layer i, MPa.

A_{hi} = CRS area at layer i, mm^2.

M = Moment, kN mm.

di= depth of layer from upper compressive layer, mm

5.3.2. Comparing the predicted failure load and with the experiments

A summary of the different cases analysed using FMA are shown in Table 5.2. The experimental results indicate that slabs S3 and S4 failed when the topmost concrete reached its maximum strain; this was considered to be the failure criteria used to calculate the maximum capacity of the concrete slabs with CRS.

Table 5.3 summarises the loads predicted for the cases considered and the results from the experiments. The predicted results indicate that including the tensile contribution of concrete predicted a 7 % higher load than by leaving it out, while including the flanges resulted in an almost 8% higher predicted load than only the hollow portion of the CRS was included. Overall, the predicted results using FMA, while including the tensile strength of the concrete and the CRS flanges were similar to the experiments carried out on slabs S3 and S4. In fact the load predicted in Case 3 was only 13.8 % more conservative than the actual load measured from the experiment. This small difference between the predicted load and the actual load could be due to the inherent variability of the compressive strength of concrete or to some portions of the flange not being included in the analysis, but which helped to carry the load applied to the slabs during the experiment.

Table 5.2 The different cases considered in the FMA.

Cases	Details of the FMA
Case 1	Omit the tensile strength of concrete and include the CRS flanges.
Case 2	Omit the tensile strength of concrete and the CRS flanges.
Case 3	Include the tensile strength of concrete and the CRS flanges.
Case 4	Include the tensile strength of concrete and omit the CRS flanges.

Table 5.3 Predicted and actual failure load.

Slab	Failure load (kN)				
	Case 1	**Case 2**	**Case 3**	**Case 4**	**Experiment**
S3	167	156	182	171	211
S4	166	146	173	157	208

5.4 Parametric evaluation of the hollow concrete slabs

The literature review in Chapter 2 showed that hollow concrete slabs are affected by the compressive strength of concrete, the reinforcement ratio, and the number of voids. The FMA developed in the previous section was therefore used to determine how these critical parameters affected the load capacity of hollow composite slabs reinforced with GFRP bars and hollow composite reinforcing systems.

5.4.1 Compressive strength of concrete

The effect of the compressive strength of concrete f'_c was predicted theoretically by analysing the maximum bending moment of slab S3. This slab had similar reinforcement details and three hollow composite reinforcing systems, but the concrete had different compressive strengths, i.e., 25 MPa, 40 MPa and 80 MPa. The FMA showed that the capacity of hollow concrete slabs increased with the compressive strength of concrete, so from 25 MPa where the predicted maximum bending moment was 71.8 kN-m it increased by 22 % for 40 MPa and 45 % for 80 MPa. Table 5.4 shows that the bending moment increased when the compressive strength of concrete increased and the strains increased rapidly until the slab reached its maximum capacity. Because the slab was over reinforced and the GFRP reinforcement bars did not rupture at failure, the increasing strength of concrete improved its overall strength. Moreover, the bending moment increased by 30 % when the compressive strength increased from 40 MPa to 80 MPa, however this result was higher than Goldston (2016) who found that when the compressive strength increased from 40 MPa to 80 MPa the bending moment increased by 13.8 % (note that the reinforcement ratio was 0.5%). This increase in the bending moment shows how effectively CRS was as reinforcement and then the slab continued to carry heavier loads. The CRS recorded more strains when the concrete compressive strength increased as shown in the Table 5.4. This evidenced the efficiency of CRS when increased the concrete compressive strength $f'c$, Then that resulted decreasing in the neutral axis depth. Consequently, slab capacity increased due to increased concrete compressive strength with more moment coming from CRS.

Table 5.4 Effect of compressive strength of concrete.

f'_c	Strain in GFRP bars (microstrains)		Strain in CRS (microstrains)		Strain in CRS's flange (microstrains)		Bending moment (kN-m)
	Top	Bottom	Top	Bottom	Top	Bottom	
25	2000	6000	120	4800	480	5300	71.8
40	2000	7000	200	5700	220	6200	92
80	1000	8000	500	6600	65	7100	131

f'_c : Concrete compressive strength.

5.4.2 Reinforcement ratio

Table 5.5 shows the reinforcement ratios for slabs S3 and S4 with their maximum load capacity from the FMA, but note that this included the top and bottom reinforcement. The failure load predicted by the FMA for different reinforcement ratios for slab S3 was evaluated. In the FMA the reinforcement ratio was reduced by 25 % from 0.0044 to 0.0033 and increased by 25 % from 0.0044 to 0.0055. The results for slabs S3 show that the load capacity decreased when the reinforcement ratio was reduced by just 11.5 % whereas as the reinforcement ratio increased, the load capacity increased by just 2.7 % for slabs S3. These results from FMA indicate that even then the reinforcement ratio increased the load carrying capacity of the slab did not increased to the point where the concrete experienced crushing failure. As expected, slab (S3) was an over reinforced section so failure was controlled by concrete crushing. This finding was similar to Kassem et al. (2011), who found that increasing the reinforcement ratio by 50 % and 100% increased the flexural load capacity of a beam by just 4% and 16%. Moreover, Kara and Ashour

(2012) showed that beams reinforced with FRP bars experienced a modest increase in their load carrying capacity. This was also seen by Esfahani et al. (2007) who showed that the flexural capacity of beam increased with CFRP sheets, even when the steel ratio was small. The experimental program from Ceroni (2010) for beams strengthened by FRP laminate and near surface mounted (NSM) reported that the load capacity of reinforced beams increased between 26 to 50%. The effect of the longitudinal steel ratio on the behaviour of reinforced beam strengthened with FRP composites was investigated by Almusallam et al. (2014), who found that bonded FRP enhanced the flexural capacity of the beam. This proved that CRS not only reduced the amount of concrete used it can also reduce the reinforcement ratio and provide perfect result, all this while contributing to a low slab weight with a high load carrying capacity. However, when the reinforcement ratio increased the CRS strain reading decreased as shows in Table 5.5. This indicated the less of the CRS contribution when the reinforcement ratio increased due to the increased the neutral axis depth and in slab mechanism behaviour.

Table 5.5 Effect of the reinforcement ratio.

ρ_{fn}	**Strain in GFRP bars (microstrains)**		**Strain in CRS (microstrains)**		**Strain in CRS flange (microstrains)**		**Bending moment (kN-m)**
	Top	**Bottom**	**Top**	**Bottom**	**Top**	**Bottom**	
0.0033	2000	8000	700	5600	200	6200	75.4
0.0044	2000	8000	600	5400	200	6000	80.7
0.0055	2000	7000	600	5300	100	5900	86

ρ_{fn}: reinforcement ratio

5.4.3 Number of voids

Table 5.6 shows the load capacity of slab S3 using grade 32 concrete and the same reinforcement ratio, but with different numbers of voids reinforced with CRS. As expected, slab S3 shows that when four voids were reinforced with CRS the load capacity increased by approximately 10%, but when only two voids were reinforced with CRS the load capacity was only 7.5 %. The presence of voids reduced the moment of inertia of the slabs due to the reduced cross-section of concrete (Donohoe and Keogh (2000), but with slabs reinforced with CRS, any change in the cross section of concrete was not noticed due small section of CRS, but CRS provided highest load capacity when four voids were reinforced with CRS. Although Bhagat and Parikh (2014) showed that voids do affect the stiffness of concrete slabs, the FMA showed that as the number CRS increased, this means the number of voids increased, the slab became stiffer and carried more load. However, from three to four CRS, as shown in the Table 5.6, the 3.1 % increase in the bending moment was small with decreased the strain results for CRS, so three CRS would be the most efficient number in this particular size slab.

Table 5.6 Effectiveness of the number of voids.

Number of CRS	**Strain in GFRP bars (microstrains)**		**Strain in CRS (microstrains)**		**Strain in CRS flange (microstrains)**		**Bending moment (kN-m)**
	Top	**Bottom**	**Top**	**Bottom**	**Top**	**Bottom**	
2	2000	7000	446	5053	54	5804	80.4
3	2000	7000	500	5300	100	6000	83
4	2000	7000	400	4900	12	5600	85.7

5.5 Summary

This chapter has shown how parameters such as the presence of voids, the effectiveness of a hollow composite reinforcing system, and the type of longitudinal reinforcements affected the structural performance of hollow concrete slabs. An analysis of the results showed that these parameters had a significant effect on failure behaviour and the capacity of hollow concrete slabs. A theoretical evaluation of the behaviour of concrete slabs reinforced with GFRP bars and hollow composite reinforcement was carried out using the Fibre Model Analysis and showed results that were comparable with the experimental results. A parametric investigation using FMA was then carried out to analyse how the compressive strength of concrete, the reinforcement ratio, and the number of composite reinforcing systems affected the maximum bending moment of the slabs. The findings from this work and recommendations for future study will be presented in the Conclusions in the next Chapter.

Chapter 6

Conclusion

6.1 Summary

Reinforced concrete slabs are very important structural members in building and construction, and while hollow core slabs can reduce their weight many researchers have found that hollow core slabs have a lower capacity than solid slabs due to premature failure when the voids collapse. As a result, a number of methods have been used to address this issue such as bonding CFRP sheets inside the voids and providing a topping to hollow core slabs. While these methods have improved the overall behaviour of hollow core slabs, bonding CFRP sheets inside the voids is very difficult, particularly with small voids. While providing a concrete topping adds to the overall weight of hollow core slabs and thus eliminates their lightweight property, this did reveal a research gap when using a hollow composite reinforcing system in a hollow slab design.

An experimental program was carried out in this study to increase our understanding of how concrete slabs reinforced with glass fibre reinforced polymer bars (GFRP) and hollow composite reinforcing system (CRS) behave under load. To that end the behaviour of large-scale hollow concrete slabs (solid slabs, hollow slabs, hollow slabs reinforced with GFRP bars and CRS, and hollow slabs reinforced with steel bars and steel were evaluated under four-point static bending tests. The results were then collated and analysed to evaluate the effects of the hollow core, the effectiveness of CRS, and the types of reinforcements. The capacity of hollow concrete slabs reinforced with GFRP bars and CRS were also evaluated using a simplified Fibre Model Analysis; this FMA was then used to determine how critical design parameters such as the compressive strength of concrete, the reinforcement ratio, and number of voids affects the load bearing capacity of hollow core concrete slabs.

6.2 Conclusions from the experimental results

An experimental investigation into the behaviour of concrete slabs reinforced with GFRP bars and hollow CRS has been successfully carried out in this study, and the significant findings are highlighted in the following conclusions:

6.2.1 Influence of hollow core concrete

A hollow core concrete slab reinforced with GFRP bars behaves the same as a solid slab because their failure is governed by shear cracks that originate under the loading point and then propagate diagonally to the bottom of the slab; this is followed by concrete crushing and compression

buckling of the GFRP bars which leads to final failure of slabs. Both slabs also exhibited similar load-deflection and load-strain behaviour during the entire loading because the gross area of concrete in the hollow slab was only 9% less than the solid slab while the area of concrete in compression for the hollow slab was located above the hollow core. However, the hollow core concrete slab displayed more brittle failure behaviour than the solid slab because the hollow core collapsed.

6.2.2 The effectiveness of CRS in reinforced concrete slabs

The composite reinforcing system effectively enhanced the structural performance of hollow core concrete slabs; in fact 3 pieces of composite reinforcing increased the stiffness of the GFRP reinforced concrete hollow slab by 85% and increased the load carrying capacity by 32%, and the CRS also reduced the strain in the bottom GFRP bars, thus proving it was also acting as internal reinforcement. Moreover, the addition of CRS changed the failure mode in hollow core concrete slab from shear to flexural failure because the hollow composite system prevented vertical flexural cracks from propagating up to the top concrete layer; this did however, result in ductile failure. Furthermore, there was no debonding failure either because the four flanges of the CRS interacted with the concrete.

6.2.3 Effecting of the type of reinforcement (GFRP bars and steel)

The types of reinforcement had a significant effect on the overall stiffness but none at all on the load capacity of the hollow concrete slabs. The provision of CRS enabled the GFRP reinforced hollow concrete slab to retain most of its stiffness even after the first flexural cracks began because it stopped them from becoming wider. The hollow composite reinforcing system was also found to be more compatible to GFRP bars than steel bars due to their similar modulus of elasticity, because while the slab reinforced with steel was stiffer than the slab reinforced with GFRP, when the concrete first began to crack, the latter exhibited almost constant stiffness until it reached the maximum load. Moreover, the GFRP bars and the CRS simultaneously resisted the load up to failure whereas the total load was transferred to the CRS once the steel yielded in steel reinforced slab. Despite this, the flexural capacity of slabs reinforced with GFRP bars and steel bars were almost same, probably because the slabs reinforced by CRS failed due to a combination of bending failure and inter-laminar shear.

6.3 Conclusions from the theoretical evaluation

The failure load of hollow core concrete slabs was predicted using the simplified Fibre Model Analysis and Excel spreadsheets, while taking into account the contribution made by different materials in the hollow core concrete slabs, including the concrete, the top and bottom reinforcements, and the hollow composite reinforcing systems. The significant findings from the FMA are listed below:

- The capacity of concrete slabs reinforced with GFRP bars and a hollow composite reinforcing system can be reliably predicted by considering the tensile strength of the concrete and the flanges of the hollow composite reinforcing system. The predicted results indicated that including the tensile contribution made by concrete will result in a 7 % higher load than by excluding it, whereas including the flanges resulted in an almost 8% higher predicted load than if only the hollow portion of the CRS was included. Overall, the predicted failure load was only 13% less than the experimentally measured failure load.
- The increase in the compressive strength of concrete in hollow concrete slabs reinforced with GFRP bars and CRS increased the depth of the concrete compression block, and this resulted in in increasing the bending moment capacity. Increasing the compressive strength from 25 MPa to 40 MPa increased the tensile strain in the CRS and GFRP bars by at least 16% and the bending moment capacity by 22%. This result suggests that the high tensile strength properties of GFRP bars and CRS can be utilised effectively when a high compressive strength concrete is used.
- The increase in the number of CRS from 2 to 4 only increased the flexural capacity of the hollow concrete slab by 6%. This minimal increase was due to the limited thickness of the concrete compression block to provide the compressive force to counteract the increase in the tensile force provided by the hollow composite reinforcing system.
- The increase in the reinforcement ratio from 0.33% to 0.55% (a 67% increase) resulted in only a 14% increase in the bending moment capacity. This was due to the behaviour of the GFRP reinforced hollow core concrete slab and when the CRS was governed by concrete crushing in compression.

6.4 Recommendations for Future Research

The following recommendations will further increase our understanding of the overall behaviour of hollow concrete slabs reinforced with GFRP bars and CRS.

- The behaviour of hollow concrete slabs was similar to solid slabs because the voids were small; it is therefore recommended that further research is needed to comparing the behaviour of hollow core slabs with larger voids with solid slabs in order to further evaluate how voids affect the capacity and failure of GFRP reinforced hollow concrete slabs.
- The comparison showed that CRS reinforced slabs behaved better than hollow core concrete slabs, so an investigation into hollow core slabs with different amounts of CRS is needed to determine the optimal number that will provide the highest level of improvement in the overall behaviour of hollow core concrete slabs.
- At the level of the reinforcement ratios investigated in this study, GFRP bars were more compatible than steel bars for concrete slabs with hollow composite reinforcing system. Therefore, an experimental investigation into the behaviour of hollow core concrete slabs with different reinforcement ratios should be carried out to further verify the findings from this conclusion.
- The Fibre Model Analysis reliably predicted the flexural capacity of hollow core concrete slabs reinforced with GFRP bars and hollow composite reinforcing systems, but this simplified method could not account for the shear failure of material components. Thus, a more refined theoretical model and/or finite element simulation is needed to describe the overall behaviour of hollow core concrete slabs that exhibit different types of shear failure.

References

ABDALLA, H. 2002. Evaluation of deflection in concrete members reinforced with fibre reinforced polymer (FRP) bars. *Composite Structures,* 56**,** 63-71.

ACI 2008. Metric specification for carbon and glass fiber–reinforced polymer bar materials for concrete reinforcement.

ADAM, M. A., SAID, M., MAHMOUD, A. A. & SHANOUR, A. S. 2015. Analytical and experimental flexural behavior of concrete beams reinforced with glass fiber reinforced polymers bars. *Construction and Building Materials,* 84**,** 354-366.

ADEL. A, S. A. 2016. NUMERICHAL ANALYSIS OF REINFORCED CONCRETE HOLLOW - CORE SLABS. *ARPN Journal of Engineering and Applied Sciences,* 11**,** -.

ALI, A. H., AFIFI, M. Z., ABDULSALAM, B., HAGGAG, H., EL HASHIMY, A., EL-SAYED, T. & MOHAMED, H. M. 2015. Performance Evaluation of One-Way Concrete Slabs Reinforced with New Developed GFRP Bars. *Materials Sciences and Applications,* 6**,** 420.

ALMUSALLAM, A. A. 2001. Effect of degree of corrosion on the properties of reinforcing steel bars. *Construction and Building Materials,* 15**,** 361-368.

ALMUSALLAM, T., ELSANADEDY, H. & AL-SALLOUM, Y. 2014. Effect of Longitudinal Steel Ratio on Behavior of RC Beams Strengthened with FRP Composites: Experimental and FE Study. *Journal of Composites for Construction,* 19**,** 04014028.

ALSAYED, S. H. & ALHOZAIMY, A. M. 1999. Ductility of concrete beams reinforced with FRP bars and steel fibers. *Journal of composite materials,* 33**,** 1792-1806.

ANDERSON, R. 1987. Web Shear Strength of Prestressed Concrete Members. *Technical Bulletin 85B1. Tacoma, WA: Concrete Technology Associates*.

APOSTOLOPOULOS, C. & PAPADAKIS, V. 2008a. Consequences of steel corrosion on the ductility properties of reinforcement bar. *Construction and Building Materials,* 22**,** 2316-2324.

APOSTOLOPOULOS, C. A. & PAPADAKIS, V. 2008b. Consequences of steel corrosion on the ductility properties of reinforcement bar. *Construction and Building Materials,* 22**,** 2316-2324.

APOSTOLOPOULOS, C. A., PAPADOPOULOS, M. & PANTELAKIS, S. G. 2006. Tensile behavior of corroded reinforcing steel bars BSt 500s. *Construction and building Materials,* 20**,** 782-789.

ARAVINTHAN, T. & MANALO, A. Field applications and case studies of FRP in civil infrastructure: the Australian experience. Proceedings of the 6th International Conference on FRP Composites in Civil Engineering (CICE 2012), 2012. International Institute for FRP in Construction (IIFC), 1-8.

ASHOUR, A. 2006. Flexural and shear capacities of concrete beams reinforced with GFRP bars. *Construction and Building Materials,* 20**,** 1005-1015.

ASSOCIATION, C. S. 2002a. CSA S806 02 Design and construction of building components with fibre reinforced polymers. Toronto, Canada: Canadian Standards Association International.

ASSOCIATION, C. S. 2002b. CSA S806 02 Design and construction of building components with fibre reinforced polymers. *Canadian Standards Association International, Toronto, Canada*.

ASSOCIATION, C. S. 2010. CAN/CSA S807-10 "Specification for fibre-reinforced polymers. *Canadian Standards Association, Rexdale, Ontario, Canada*.

ASTM 2008a. Standard test method for apparent horizontal shear strength of pultruded reinforced plastic rods by the short beam method.

ASTM 2009. Standard test method for flexural properties of fiber reinforced pultruded plastic rods.

ASTM 2011. Standard test method for tensile properties of fiber reinforced polymer matrix composite bars. *ASTM D7205-11*.

ASTM, D. 4475 (2002). *Standard Test Method for Apparent Shear Strength of Pultruded Reinforced Plastic Rods by the Short-beam Method*.

ASTM, I. 2007. Standard test methods for flexural properties of unreinforced and reinforced plastics and electrical insulating materials. *ASTM D790-07*.

ASTM, S. 2008b. Standard test method for assignment of the glass transition temperatures by differential scanning calorimetry.

AUSTRALIA, S. 2009. Concrete structures. *Standards Australia, AS***,** 3600-2009.

AZAD, A. K. & HAKEEM, I. Y. 2016. Flexural behavior of hybrid hollow-core slab built with ultra high performance concrete faces. *Materials and Structures,* 49**,** 3801-3813.

BENAYOUNE, A., SAMAD, A. A., TRIKHA, D., ALI, A. A. & ELLINNA, S. 2008. Flexural behaviour of pre-cast concrete sandwich composite panel–experimental and theoretical investigations. *Construction and Building Materials,* 22**,** 580-592.

BENMOKRANE, B., CHAALLAL, O. & MASMOUDI, R. 1995. Glass fibre reinforced plastic (GFRP) rebars for concrete structures. *Construction and Building Materials,* 9**,** 353-364.

BENMOKRANE, B., MANALO, A., BOUHET, J.-C., MOHAMED, K. & ROBERT, M. 2017. Effects of Diameter on the Durability of Glass Fiber–Reinforced Polymer Bars Conditioned in Alkaline Solution. *Journal of Composites for Construction,* 21**,** 04017040.

BHAGAT, S. & PARIKH, K. 2014. Comparative Study of Voided Flat Plate Slab and Solid Flat Plate Slab. *International Journal of Innovative Research and Development*.

BISCHOFF, P. H. 2005. Reevaluation of deflection prediction for concrete beams reinforced with steel and fiber reinforced polymer bars. *Journal of Structural Engineering,* 131**,** 752-767.

BOUGUERRA, K., AHMED, E., EL-GAMAL, S. & BENMOKRANE, B. 2011. Testing of full-scale concrete bridge deck slabs reinforced with fiber-reinforced polymer (FRP) bars. *Construction and building materials,* 25**,** 3956-3965.

BRUNESI, E., BOLOGNINI, D. & NASCIMBENE, R. 2015. Evaluation of the shear capacity of precast-prestressed hollow core slabs: numerical and experimental comparisons. *Materials and Structures,* 48**,** 1503-1521.

CAIRNS, J. & MILLARD, S. Reinforcement corrosion and its effect on residual strength of concrete structures. Proc., 8th Int. Conf. on Structural Faults and Repair, 1999. Engineering Technics Press London.

CERONI, F. 2010. Experimental performances of RC beams strengthened with FRP materials. *Construction and Building Materials,* 24**,** 1547-1559.

CHANG, K. & SEO, D. 2012. Behavior of One-Way Concrete Slabs Reinforced with GFRP Bars. *Journal of Asian Architecture and Building Engineering,* 11**,** 351-358.

CHERNIN, L., VAL, D. V. & VOLOKH, K. Y. 2010. Analytical modelling of concrete cover cracking caused by corrosion of reinforcement. *Materials and Structures,* 43**,** 543-556.

CHUNG, J.-H., CHOI, H.-K., LEE, S.-C. & CHOI, C.-S. 2015. One-way shear strength of circular voided reinforced concrete floor slabs. *Proceedings of the Institution of Civil Engineers-Structures and Buildings,* 168**,** 336-350.

COMMITTEE, A., INSTITUTE, A. C. & STANDARDIZATION, I. O. F. Building code requirements for structural concrete (ACI 318-08) and commentary. 2008. American Concrete Institute.

CORONELLI, D. & GAMBAROVA, P. 2004. Structural assessment of corroded reinforced concrete beams: modeling guidelines. *Journal of structural engineering,* 130**,** 1214-1224.

CRS PERTH, A. Composite Reinforcement Solutions | CRS Perth, Australia". Composite Reinforcement Solutions | CRS Perth. N.p., 2016. . 5th International Symposium on Underwater Technology, 18 Oct. 2016 2016. Web.

CUENCA, E. & SERNA, P. 2013. Failure modes and shear design of prestressed hollow core slabs made of fiber-reinforced concrete. *Composites Part B: Engineering,* 45**,** 952-964.

DAVALOS, J. F., KODKANI, S. S., RAY, I. & LIN, C. 2008. Fracture evaluation of GFRP—concrete interfaces for freeze—thaw and wet-dry cycling. *Journal of composite materials,* 42**,** 1439-1466.

DE CASTILHO, V. C., DO CARMO NICOLETTI, M. & EL DEBS, M. K. 2005. An investigation of the use of three selection-based genetic algorithm families when minimizing the production cost of hollow core slabs. *Computer methods in applied mechanics and engineering,* 194**,** 4651-4667.

DEEPA, A., PADMANABHAN, K. & RAGHUNADH, G. 2016. Effect of Hygrothermal Loading on Laminate Composites. *Indian Journal of Science and Technology,* 9.

DITTENBER, D. B. & GANGARAO, H. V. 2012. Critical review of recent publications on use of natural composites in infrastructure. *Composites Part A: Applied Science and Manufacturing,* 43**,** 1419-1429.

DOMONE, P. & ILLSTON, J. 2010. *Construction materials: their nature and behaviour,* CRC Press.

DONOHOE, S. & KEOGH, D. Orthotropic analysis of voided slab bridges. International conference on engineering computational technology, 2000. 71-79.

DU, Y., CLARK, L. & CHAN, A. 2005. Effect of corrosion on ductility of reinforcing bars. *Magazine of Concrete Research,* 57**,** 407-419.

EL-GAMAL, S., ABDULRAHMAN, B. & BENMOKRANE, B. 2011. Deflection Behaviour of Concrete Beams Reinforced with Different Types of GFRP Bars. *Advances in FRP Composites in Civil Engineering.* Springer.

ELGABBAS, F., EL-GHANDOUR, A., ABDELRAHMAN, A. & EL-DIEB, A. 2010. Different CFRP strengthening techniques for prestressed hollow core concrete slabs: Experimental study and analytical investigation. *Composite Structures,* 92**,** 401-411.

ELLIOTT, K. S. 2016. *Precast concrete structures*, Crc Press.

ESFAHANI, M. R., KIANOUSH, M. & TAJARI, A. 2007. Flexural behaviour of reinforced concrete beams strengthened by CFRP sheets. *Engineering structures,* 29**,** 2428-2444.

FERNANDEZ, I., BAIRÁN, J. M. & MARÍ, A. R. 2015. Corrosion effects on the mechanical properties of reinforcing steel bars. Fatigue and σ–ε behavior. *Construction and Building Materials,* 101**,** 772-783.

GOLDSTON, M. W. 2016. Behaviour of concrete beams reinforced with GFRP bars under static & impact loading.

GROTHE, B. & PARK, T. J. 2000. Structure and function of the bat superior olivary complex. *Microscopy Research and Technique,* 51**,** 382-402.

GU, X., YU, B. & WU, M. 2016. Experimental study of the bond performance and mechanical response of GFRP reinforced concrete. *Construction and Building Materials,* 114**,** 407-415.

HAG-ELSAFI, O., ALAMPALLI, S. & KUNIN, J. 2001. Application of FRP laminates for strengthening of a reinforced-concrete T-beam bridge structure. *Composite structures*, 52**,** 453-466.

HALL, J. & MOTTRAM, J. 1998. Combined FRP reinforcement and permanent formwork for concrete members. *Journal of Composites for Construction,* 2**,** 78-86.

HONICKMAN, H. N. 2008a. *Pultruded GFRP sections as stay-in-place structural open formwork for concrete slabs and girders.*

HONICKMAN, H. N. 2008b. Pultruded GFRP sections as stay-in-place structural open formwork for concrete slabs and girders.

IBRAHIM, I., ELLIOTT, K., ABDULLAH, R., KUEH, A. & SARBINI, N. 2016. Experimental study on the shear behaviour of precast concrete hollow core slabs with concrete topping. *Engineering Structures,* 125**,** 80-90.

INTERNATIONAL, A. 2010. *Standard Test Method for Compressive Properties of Rigid Plastics*, ASTM International.

ISO, I. 1998. 14125: 1998 (E). *Fibre reinforced plastic composites–determination of flexural properties*.

KARA, I. F. & ASHOUR, A. F. 2012. Flexural performance of FRP reinforced concrete beams. *Composite Structures,* 94**,** 1616-1625.

KASSEM, C., FARGHALY, A. S. & BENMOKRANE, B. 2011. Evaluation of flexural behavior and serviceability performance of concrete beams reinforced with FRP bars. *Journal of composites for construction,* 15**,** 682-695.

KING, R., HOWARD, P., MALE, S. & HOFFMANN, P. Systemic Approaches to Improving Engineering Education in Australia.

LIU, S., YAN, C., WANG, G., LI, J. & WANG, Y. 2008. Experimental analysis on flexural capacity and ductility of pre-stressed RC hollow core slab strengthened by CFRP. *Journal of Building Structures,* 29**,** 125-128.

LUNDGREN, K. 2005. Bond between ribbed bars and concrete. Part 1: Modified model. *Magazine of Concrete Research,* 57**,** 371-382.

LUTZ, L. A. & GERGELY, P. Mechanics of bond and slip of deformed bars in concrete. Journal Proceedings, 1967. 711-721.

MAGNUSSON, J. 2000. *Bond and anchorage of ribbed bars in high-strength concrete*, Chalmers University of Technology.

MANALO, A., AL-FAKHER, U. & AL-RUBAYA, M. 2017. FRP Hollow Bar Characterisation. University of Southern Qeensland

MANALO, A. & ARAVINTHAN, T. 2012. Behaviour of glued fibre composite sandwich structure in flexure: experiment and fibre model analysis. *Materials & Design*, 39**,** 458-468.

MANALO, A., BENMOKRANE, B., PARK, K.-T. & LUTZE, D. 2014. Recent developments on FRP bars as internal reinforcement in concrete structures. *Concrete in Australia,* 40**,** 46-56.

MARANAN, G., MANALO, A., BENMOKRANE, B., KARUNASENA, W. & MENDIS, P. 2015. Evaluation of the flexural strength and serviceability of geopolymer concrete

beams reinforced with glass-fibre-reinforced polymer (GFRP) bars. *Engineering Structures,* 101**,** 529-541.

MARANAN, G., MANALO, A., BENMOKRANE, B., KARUNASENA, W. & MENDIS, P. 2016. Behavior of concentrically loaded geopolymer-concrete circular columns reinforced longitudinally and transversely with GFRP bars. *Engineering Structures,* 117**,** 422-436.

MARANAN, G., MANALO, A., KARUNASENA, K. & BENMOKRANE, B. 2014. Bond stress-slip behavior: case of GFRP bars in geopolymer concrete. *Journal of Materials in Civil Engineering,* 27**,** 04014116.

MARANAN, G. B. 2016. *Structural behaviour of geopolymer concrete beams and columns reinforced with glass fibre reinforced polymer bars.* University of Southern Queensland.

MASMOUDI, A., OUEZDOU, M. B. & BOUAZIZ, J. 2012. New parameter design of GFRP RC beams. *Construction and Building Materials,* 29**,** 627-632.

MATOS, B., CORREIA, J. R., CASTRO, L. M. & FRANÇA, P. 2012. Structural response of hyperstatic concrete beams reinforced with GFRP bars: Effect of increasing concrete confinement. *Composite Structures,* 94**,** 1200-1210.

MEHTA, P. K. 2002. *Concrete in the marine environment,* Crc Press.

MENG, X. 2016. *Shear Strengthening of Prestressed Hollow Core Slabs Using Externally Bonded Carbon Fiber Reinforced Polymer Sheets.* University of Windsor (Canada).

MENG, X., CHENG, S. & EL RAGABY, A. 2016. STR-946: EXPERIMENTAL STUDY ON A NOVEL SHEAR STRENGTHENING TECHNIQUE FOR PRECAST PRESTRESSED HOLLOW-CORE SLABS.

MONES, R. M. & BREÑA, S. F. 2013. Hollow-core slabs with cast-in-place concrete toppings: A study of interfacial shear strength. *PCI journal,* 58**,** 124-141.

MOSALLAM, A., TAHA, M. M. R., KIM, J. J. & NASR, A. 2012. Strength and ductility of RC slabs strengthened with hybrid high-performance composite retrofit system. *Engineering Structures,* 36**,** 70-80.

NEWHOOK, J. & SVECOVA, D. 2007. Reinforcing concrete structures with fibre reinforced polymers. *ISIS Canada: Design Manual*.

NPCAA 2002. *Precast Concrete Handbook,* Australia National Precast Concrete Association Australia & Concrete Institue of Australia

OGUEJIOFOR, E. & HOSAIN, M. 1992. Behaviour of perfobond rib shear connectors in composite beams: full-size tests. *Canadian Journal of Civil Engineering,* 19**,** 224-235.

OKELO, R. & YUAN, R. L. 2005. Bond strength of fiber reinforced polymer rebars in normal strength concrete. *Journal of composites for construction,* 9**,** 203-213.

OMBRES, L., ALKHRDAJI, T. & NANNI, A. Flexural analysis of one-way concrete slabs reinforced with GFRP rebars. International meeting on composite materials, PLAST, 2000. 243-250.

PAJARI, M. 2009. Web shear failure in prestressed hollow core slabs. *Journal of Structural Engineering,* 42**,** 83-104.

PARK, R. & GAMBLE, W. L. 2000. *Reinforced concrete slabs*, John Wiley & Sons.

POPOVICS, S. 1973. A numerical approach to the complete stress-strain curve of concrete. *Cement and concrete research,* 3**,** 583-599.

ROBERT, M. & BENMOKRANE, B. 2009. Behavior of GFRP reinforcing bars subjected to extreme temperatures. *Journal of Composites for Construction,* 14**,** 353-360.

ROBERT, M. & BENMOKRANE, B. 2010. Effect of aging on bond of GFRP bars embedded in concrete. *Cement and Concrete Composites,* 32**,** 461-467.

ROBERT, M., COUSIN, P. & BENMOKRANE, B. 2009. Durability of GFRP reinforcing bars embedded in moist concrete. *Journal of Composites for Construction,* 13**,** 66-73.

SACKS, R., EASTMAN, C. M. & LEE, G. 2004. Parametric 3D modeling in building construction with examples from precast concrete. *Automation in construction,* 13**,** 291-312.

SAID, S. H., RAZAK, H. A. & OTHMAN, I. 2015. Flexural behavior of engineered cementitious composite (ECC) slabs with polyvinyl alcohol fibers. *Construction and Building Materials,* 75**,** 176-188.

SMITH, P. 2016. Design and specification of marine concrete structures. *Marine Concrete Structures: Design, Durability and Performance***,** 65.

STANDARD, A. D2344/D2344M," Standard Test Method for Short-Beam Strength of Polymer Matrix Composite Materials and Their Laminates," ASTM International, West Conshohocken, PA, 2013, DOI: 10.1520/D2344_D2344M.

STANDARD, A. 2011a. Standard test method for ignition loss of cured reinforced resin. *West Conshohocken (PA): ASTM,* 100.

STANDARD, A. A. Building Code Requirements for Structural Concrete (ACI 318-11). American Concrete Institute, 2011b.

STANDARDS AUSTRALIA 2001. Steel reinforcing materials. *4671-2001.* Australia: Standards Australia.

STANDARDS AUSTRALIA 2007. Specification and supply of concrete. *AS1379-2007* Australia SIA Global.

STANDARDS AUSTRALIA 2014. Methods of testing concrete Method 1: Sampling of concrete. *AS 1012.1-2014* Australia: Standards Australia.

TAHERSHAMSI, M. 2016. *Structural effects of reinforcement corrosion in concrete structures,* Chalmers University of Technology Gothenburg, Sweden.

TAWFIK, Q. H., KARUNASENA, W. K. & CARDONA, F. Strengthening of corroded steel angles using CFRP. Proceedings of the Composites Australia and the CRC for Advanced Composite Structures Conference 2012, 2012. Composites Australia, 1-12.

TAYLOR, R., MAHER, D. & HAYES, B. 1966. Effect of the arrangement of reinforcement on the behaviour of reinforced concrete slabs. *Magazine of concrete research,* 18**,** 85-94.

TEPFERS, R. & CONCRETE, T. G. B. M. I. F. F. S. 2000. *Bond of reinforcement in concrete: state-of-art report*, Internat. Fed. for Structural Concrete.

WARIYATNO, N. G., HARYANTO, Y. & SUDIBYO, G. H. 2017. Flexural behavior of precast hollow core slab using PVC pipe and styrofoam with different reinforcement. *Procedia Engineering*, 171**,** 909-916.

WOLANSKI, A. J. 2004. *Flexural behavior of reinforced and prestressed concrete beams using finite element analysis.*

XIANGMIN, L., FUWEN, Z. & QINGFENG, X. 2014. Experimental study and computational analysis on PC hollow core slabs strengthened with different FRP strips. *China Civil Engineering Journal,* 47.

YANG, L. 1994. Design of prestressed hollow core slabs with reference to web shear failure. *Journal of Structural Engineering,* 120**,** 2675-2696.

YARDIM, Y., WALEED, A., JAAFAR, M. S. & LASEIMA, S. 2013. AAC-concrete light weight precast composite floor slab. *Construction and Building materials,* 40**,** 405-410.

YEE, A. A. & ENG, P. H. D. 2001. Structural and economic benefits of precast/prestressed concrete construction. *PCI journal,* 46**,** 34-43.

Appendix A

The flexural behaviour of concrete slabs reinforced with GFRP bars and hollow composite reinforcing systems

Mohammed Al-Rubaye[1], Allan Manalo[2*], Omar Alajarmeh[3], Weena Lokuge[4], Brahim Benmokrane[5], and Azam Edoo[6]

Abstract

Glass Fibre Reinforced Polymer (GFRP) bars are now an alternative reinforcement for concrete slabs because they eliminate corrosion caused by steel bars. Moreover, hollow concrete slab systems are also being used to reduce the amount of concrete used, and to minimise their self-weight, but the internal voids makes them prone to shear failure and collapse. A hollow composite reinforcing system (CRS) with four flanges to improve the bond with concrete has recently been developed to stabilise the void in concrete members. This study investigated the flexural behaviour of concrete slabs reinforced with GFRP bars and CRS. Four full-scale concrete slabs (solid slab reinforced with GFRP bars; hollow slab reinforced with GFRP bars; slab reinforced with GFRP bars and CRS; and slab reinforced with steel bars and CRS) were prepared and tested under four-point static bending to understand how this new construction system would perform. We found that CRS enhanced the structural performance of hollow concrete slabs because it was more compatible with GFRP bars than steel bars due to their similar modulus of elasticity. A simplified Fibre Model Analysis (CRS) reliably predicted the capacity of hollow concrete slabs by considering the tensile strength of concrete and the flanges of the hollow composite reinforcing system.

Keywords: Flexural behaviour; Hollow concrete slabs; Composite reinforcing system; GFRP bars; Fibre Model Analysis.

[1]Master student, Centre for Future Materials (CFM) , School of Civil Engineering and Surveying, University of Southern Queensland , QLD 4350, Australia. Email: Mohammed.Al-Rubaye@usq.edu.au,

[2](Corresponding Author) Associate Professor, Centre for Future Materials (CFM), School of Civil Engineering and Surveying, University of Southern Queensland, QLD 4350, Australia. Email: allan.manalo@usq.edu.au

[3]PhD Student, Centre for Future Materials (CFM), School of Civil Engineering and Surveying, University of Southern Queensland, QLD 4350, Australia. Email: Omar.Alajarmeh@usq.edu.au

[4]Senior Lecturer in Civil Engineering, Centre for Future Materials (CFM), School of Civil Engineering and Surveying, University of Southern Queensland, QLD 4350, Australia. Email: weena.lokuge@usq.edu.au

[5]Professor of Civil Engineering, University of Sherbrooke, Department of Civil Engineering, Sherbrooke, Quebec, Canada. Email: Brahim.Benmokrane@USherbrooke.ca

[6]Manager, Composite Reinforcing Solutions Pty Ltd, 48 Lucraft Gardens, Winthrop, WA 6150, Australia. Email: azam@crsperth.com

1. INTRODUCTION

Reinforced concrete slabs are very important structural members in building and construction because they carry loads and transfer them to the beams (Yardim et al., 2013, Taylor et al., 1966). However, the steel bars traditionally used as reinforcement inevitably corrode, which then affects the integrity of concrete slabs by reducing their strength and limiting their serviceability, which ultimately leads to failure. The corrosion of steel bars is practically critical in structures built close to marine or industrial environments (Smith, 2016). For example, the million dollar 20-storey Iluka high-rise apartment complex in Surfers Paradise, Australia which was built in 1972 was demolished in 2013 due to corrosion of the steel reinforcement in the concrete slabs and other structural elements (Dalton, 2014). In fact the Australian Corrosion Association (ACA) has reported that more than AU$10 billion is lost every year due to the corrosion of steel reinforcement (Goldston, 2016). Obviously, the need to explore the use of alternative reinforcing materials that will minimise or eliminate corrosion in concrete structures is great.

The non-corrosive properties of Glass Fibre Reinforced Polymer (GFRP) bars are an effective alternative reinforcement for concrete structures. GFRP bars will massively reduce the cost of maintenance and repairs of concrete structures (Abdalla, 2002). Moreover, GFRP bars have a higher longitudinal tensile strength than steel, and they are lighter and non-magnetic (Manalo et al., 2014). Many studies have reported that GFRP bars have been used successfully as internal reinforcement for concrete structures, including the beams (Maranan et al., 2015), columns (Maranan et al., 2016), and slabs (Bouguerra et al., 2011). However, the lighter weight of GFRP bars is not always realised in concrete slabs because more concrete is needed with the reinforcement that is normally provided just within the minimum requirements (Hag-Elsafi et al., 2001). Since slabs are the main structural members that consume the largest amount of concrete

in a building, they are large contributors to the dead load (Sacks et al., 2004), so these structural components must be designed to reduce the overall weight. The result is that many researchers (de Castilho et al., 2005, Pajari, 2009) have created voids inside the slab to reduce the amount of concrete and its overall weight.

A hollow core slab (HCS) is a common structural form used for precast concrete slabs and wall panels in industrial, commercial and residential applications, and in bridge decks (Mones and Breña, 2013). However, several researchers found that voids can cause early shear failure and significantly reduce the capacity of the slab (Azad and Hakeem, 2016, Brunesi et al., 2015). Meng (2016) suggested that CFRP sheets saturated with epoxy resin and bonded inside the voids would increase the shear capacity of HCS, but this is a difficult system to implement, especially for small diameter voids, so a strong bond between the CFRP sheets and concrete cannot be ensured. There is a need to find new technology to improve structural efficiency and provide light weight features for hollow core slabs. A new type of FRP system that will create a hollow inside a slab and stabilise the voids, while fully interacting with the concrete needs to be developed.

A new type of hollow composite reinforcing system (CRS) has recently been designed and developed to create voids in reinforced concrete slabs. This CRS system has four flanges that act as shear connectors, much like the rib shear connector in the stay-in-place FRP decks introduced by many researchers (Benayoune et al., 2008, Oguejiofor and Hosain, 1992, Honickman, 2008a, Hall and Mottram, 1998), to provide a composite action with the concrete. This paper investigated the flexural behaviour of a one-way concrete slab reinforced with GFRP bars and CRS. Four concrete slabs (a solid slab reinforced with GFRP, a hollow slab reinforced with GFRP, a GFRP reinforced slab with CRS, and a steel-reinforced slab with CRS) were cast and tested under static four-point bending to evaluate the effectiveness of hollow CRS. The capacity of the hollow concrete slab was also predicted theoretically by simplified Fibre Model Analysis (FMA) and compared with the experimental results. The results obtained from this study will advance our understanding on the behaviour of hollow concrete slabs reinforced with GFRP bars and hollow composite systems, and will provide new light weight slabs for civil engineering and construction.

2. EXPERIMENTAL PROGRAM

2.1. Materials

2.1.1. Hollow composite reinforcing system (CRS)

The hollow composite reinforcing system (CRS) shown in Figure 1 was supplied by Composite Reinforcement Solutions in Perth, Australia. This material was manufactured through the pultrusion process and is made from glass fibres (mostly unidirectional) reinforced with vinylester resin. It also contains additives such as pigments, UV inhibitors, and fire retardant. The physical and mechanical properties of this CRS were evaluated by following the appropriate ISO and ASTM test standards that are listed in Table 1.

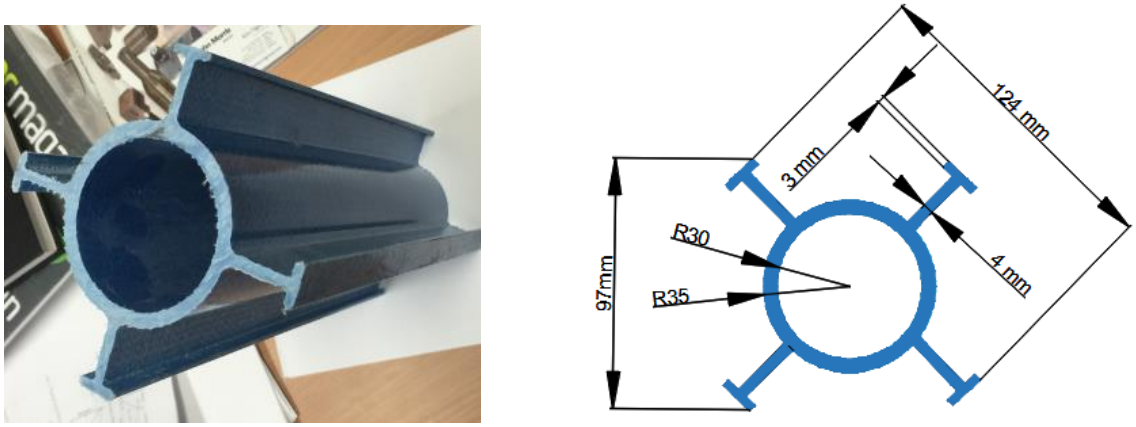

(a) CRS shape **(b)** CRS dimensions

Figure 1: Details of the composite reinforcing systems (CRS Perth)

Table 1. Physical and mechanical properties of CRS.

Properties	**Test standard**	**Values**	**Standard Deviation**
Density, kg/m^3	ASTM D792 (Association, 2010)	1926.5	23.4
Fibre content by weight, %	ASTM D2584 (Standard, 2011a)	73.2	2.5
Glass transition temperature, ^{o}C	ASTM E1356 (ASTM, 2008b)	81.4	4.2
Axial compression, MPa	ASTM D695 (International, 2010)	120.4	7.1

Transverse compression, MPa	ISO14125(1998) (ISO, 1998)	8.8	1.1
Transverse shear strength, MPa	ASTM D2344 (2013)	7.5	0.7
Inter-laminar shear strength, MPa	ASTM D4475 (ASTM)	22.1	1.5
Flexural strength, MPa	ASTM D790 (ASTM, 2007)	201.1	28.7
Flexural modulus, GPa	ASTM D790 (ASTM, 2007)	42.1	1.3

2.1.2. GFRP bars

The concrete slabs were reinforced with 12 mm diameter high-modulus (Grade III) GFRP bars (CSA S807-10). These bars were manufactured through the pultrusion process by impregnating E-type glass fibres in a thermosetting modified vinyl-ester resin. The external surfaces of the GFRP bars were coated with particles of silica-sand to enhance the bond between the reinforcement and surrounding concrete. The mechanical properties of these bars are summarised in Table 2, as reported by Benmokrane et al. (2017).

Table 2. Mechanical properties of GFRP bars (Benmokrane et al., 2017).

Properties	**Test standard**	**Values**	**Standard Deviation**
Flexural strength, MPa	ASTM D4476/D4476M (ASTM, 2009)	1,588.1	93.5
Interlaminar shear strength, MPa	ASTM D4475-02 (ASTM, 2008a)	52.9	2.1
Tensile strength, MPa	ASTM D7205/D7205M-06 (ASTM, 2011)	1,281.5	35.3
Tensile modulus, GPa	ACI 440.6M (ACI, 2008) and CSA S807-10 (Association, 2010)	61.3	0.4
Tensile strain	ACI 440.6M (ACI, 2008) and CSA S807-10 (Association, 2010)	2.1	0.1

2.1.3. Steel bars

The steel reinforcing bars were standard grade 500N with a nominal diameter of 12 mm. The characteristic strength and Young's modulus of the reinforcing steel were 500MPa and 200 GPa, respectively.

2.1.4. Concrete

The concrete was a ready mix with a nominal compressive strength of 32 MPa. The aggregate was a maximum of 10mm and maximum slump was 100mm determined in accordance with the AS1379 Specification and supply of concrete (Standards Australia, 2007). A total of 8 cylinders were prepared and tested as per the AS1012 methods of testing concrete (Standards Australia, 2014) at the same time of testing the slabs. The average compressive strength of concrete was 31.8 MPa with a standard deviation of 3.54 MPa and a modulus of elasticity of 29.9 GPa.

2.2. Slab details

Four full-scale slabs, 2400 mm long by 750mm wide by 175mm thick were prepared; these dimensions are based on industry practice for precast hollow core slabs. Of these four slabs, one was a solid slab reinforced with GFRP (S1), one was a hollow slab reinforced with GFRP (S2), one was a GFRP reinforced slab with CRS (S3), and one slab was reinforced with and CRS (S4). Table 3 gives details of the slab specimens. Slabs S1, S2, and S3 were reinforced at the top and bottom with 12 mm diameter GFRP bars spaced 200 mm apart on the centre (both longitudinally and transversely), while slab S4 was reinforced with 12 mm diameter steel bars spaced 200 mm apart on the centre. The reinforcement ratio for slabs reinforced by GFRP bars and steel was 0.44%; this resulted in an over-reinforced section for slabs S1 to S3 (balanced reinforcement ratio, $\rho_b = 0.2\%$) and under-reinforced for slab S4 ($\rho_b = 2.1\%$) as per the CSA S806 (2012). Slab S2 had 3 voids measuring 70 mm in diameter. On the other hand, slabs S3 and S4 had 3 CRS spaced at 300 mm on the centre. A 15mm thick cover of concrete was provided at the top and bottom reinforcements, and a 25 mm thick cover of concrete was provided at the edges of the slabs. Details of these specimens are listed in Table 3.

Table 3. Concrete slab details.

Specimen name	Cross section layout	Description
S1	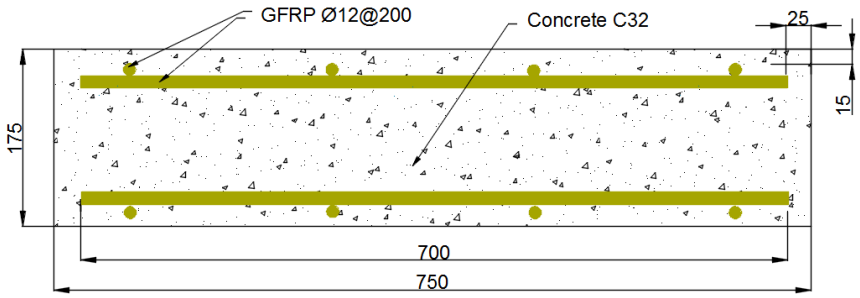	Solid concrete slab reinforced with GFRP bars
S2	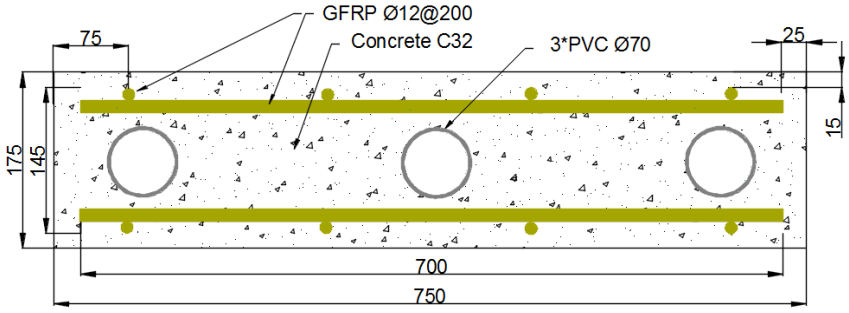	Hollow concrete slabs reinforced with GFRP bars
S3	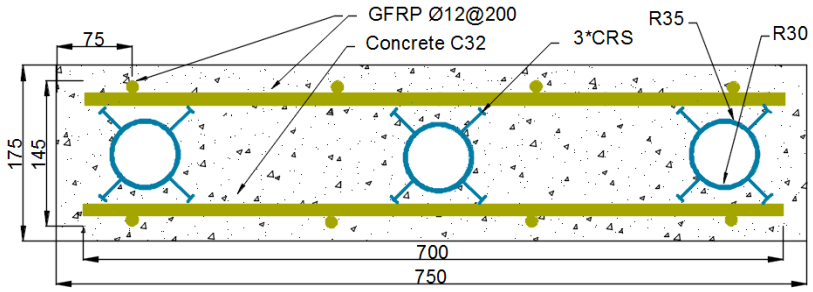	Slab reinforced with CRS and GFRP bars.
S4	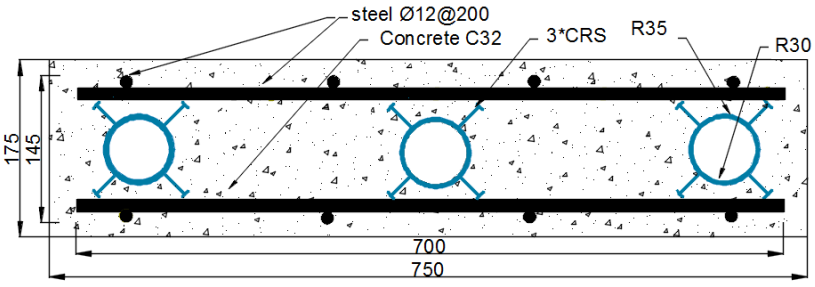	Slab reinforced with CRS and steel bars.

2.3. Specimen preparation

All the reinforcements were assembled on a work table with patterns drawn to ensure the bars were spaced properly, and cut sections of CRS were used as spacers between the top and bottom reinforcement for slabs S1 and S2. Moreover, 70mm outside diameter by 1mm thick wall PVC pipes used to create voids inside the concrete in slab S2, as shown in Figure 2 (a). With slabs S3 and S4, the CRS was spaced equally at 300 mm centres and tied to the top and bottom longitudinal reinforcements to prevent movement while pouring concrete. Bent 12 mm diameter steel bars were placed at each corner of the slabs as lifting hooks.

3mm uni-axial strain gages were attached at the top and bottom reinforcements at mid-span and the top surface of the CRS to measure strain during loading, as shown in Figure 2(b); 20 mm uni-axial strain gauges were also attached in the top and bottom concrete surfaces of the slab.

(a) Slab S2 with PVC pipes before casting

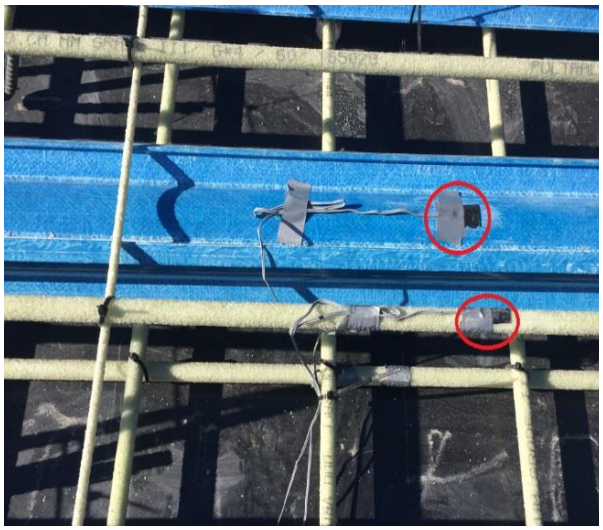

(b) Strain gauges attached to the bars and CRS

Figure 2. Assembly of reinforcement and attachment of strain gauges

2.4. Test set-up and instrumentation

The slabs were tested under four-point static bending, as shown in Figure 3. The load was applied through a spreader steel I-beam using a 2000 kN Enerpac hydraulic ram, and was measured using a 444 kN load cell. Rubber matting was placed under the loading steel plate to ensure a uniform load distribution to the slab. A laser displacement transducer was used to measure mid-span deflection. Prior to testing, gridlines were marked on the front side of the slab to trace the propagation of cracks during loading. The applied load, deflection, and strains were recorded using Vishay System 5000. All the specimens were tested up to failure.

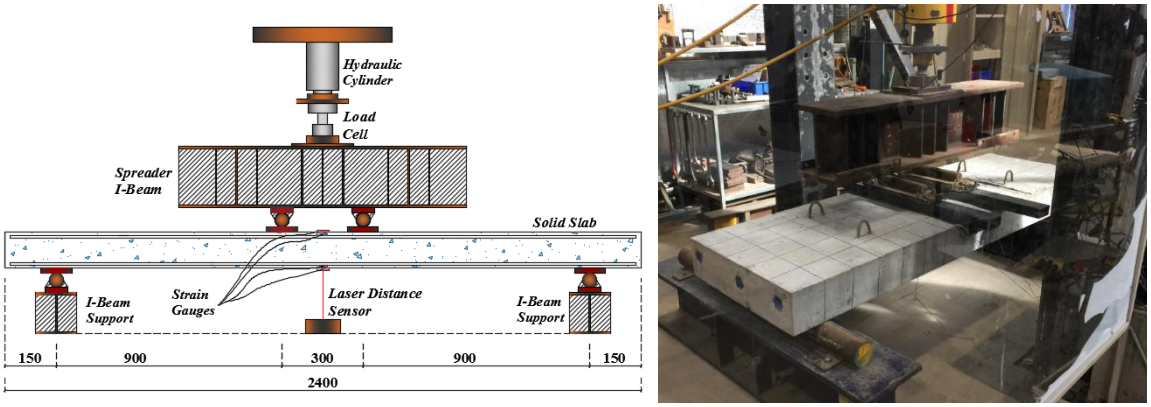

(a) Schematic diagram **(b)** Actual test set up

Figure 3. Test set-up and instrumentation.

3. TEST RESULTS AND OBSERVATION

3.1. Crack propagation and failure behaviour

Table 4 reports the moment at first cracking, the maximum bending moment, and the failure mode of the slabs at the maximum load.

Table 4. Experimental failure modes of reinforced concrete slabs.

Slab	First crack		Maximum		Failure mode
	Load (kN)	Cracking moment (kN-m)	Load (kN)	Bending moment (kN-m)	
S1	25	11.25	137	61.7	Shear failure with concrete crushing under the loading point and buckling of the bars

S2	25	11.25	145	65	Shear failure with concrete crushing under the loading point and buckling of the bars
S3	25	11.25	211	95	Concrete crushing at mid span with shear cracks
S4	25	11.25	208	94	Steel yielding followed by concrete crushing at mid span

Figure 4 shows the propagation of cracks in the slabs. In every slab, the first crack occurred at the bottom portion and between the loading points at an applied load of 25 kN. As the load increased, the cracks that propagated in slabs S1 and S2 were similar, as shown in Figures 4(a) and 4(b). Fine vertical cracks began at the bottom of the slab near the loading points, up to a load of 70 kN, and then the vertical cracks widened and propagated towards the top of the slab. At a load of 140 kN, the concrete began to be crushed on the compression side under the loading point. As the load continued to be applied, shear cracks began under the loading point and propagated diagonally to the bottom of the slab. This was followed by the concrete being crushed and the GFRP bars experiencing compression buckling that caused slabs S1 and S2 to fail completely. Interestingly, the concrete crushed in slab S2 was worse than slab S1, as shown in Figures 5(a) and 5(b); this indicated that the voids in slab S2 had collapsed. The fibre in the bottom GFRP reinforcements in both slabs did not rupture either.

Similar crack propagation occurred in slabs S3 and S4 up to an applied load of 140 kN, as shown in Figures 4(c) and 4(d), but then the crack in slab S4 became wider than slab S3. However, horizontal cracks had also developed in slab S3; they began under the loading point and propagated along the level of the CRS (Figure 5c). At final failure, concrete was crushed under the loading point and at the midspan of slabs S3 and S4 (Figures 5c and 5d). Before both slabs ruptured, there was a loud noise in the slabs as the fibres in the bottom flanges of the CRS ruptured. There were also horizontal splitting cracks along the length of the CRS in both slabs, but the top and bottom reinforcements did not rupture.

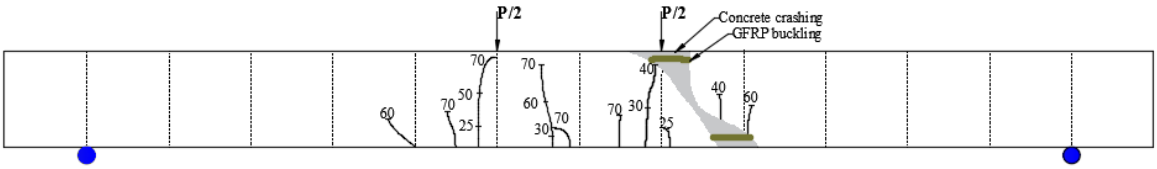

(a) Slab S1.

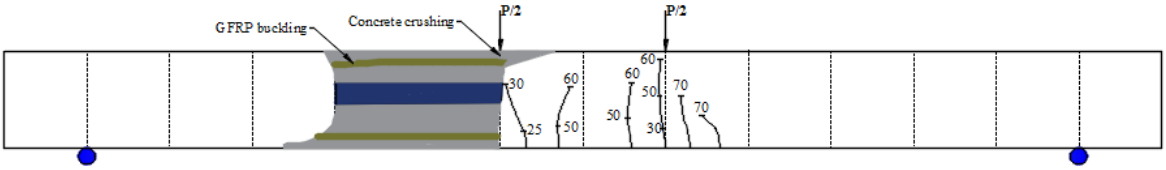

(b) Slab S2.

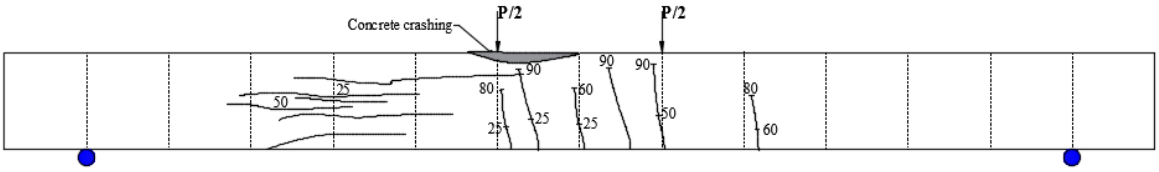

(c) Slab S3.

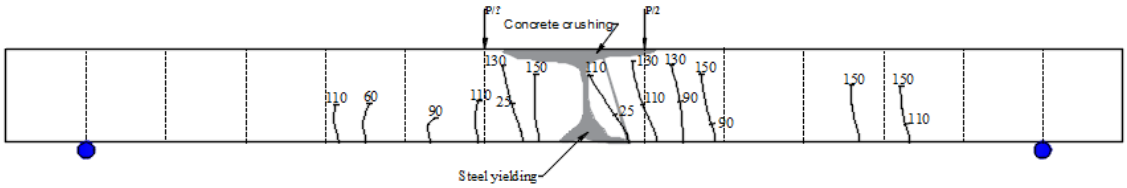

(d) Slab S4.

Figure 4. Slabs crack propagation.

(a) Slab S1

(b) Slab S2

(c) Slab S3

(d) Slab S4

Figure 5. Final failure of concrete slabs

3.2 Load -deflection

Figure 6 shows the load and mid span deflection of the four tested slabs. Every slab exhibited linear load-deflection until the concrete experienced its first flexural cracking at 25 kN and a deflection of 3 mm. When the concrete cracked, slabs S1 & S2 experienced a reduced but similar stiffness (2.6 kN/mm), after which the deflection increased linearly with load up to around 140 kN and a deflection of 50 mm. Under this load both slabs experienced a nonlinear behaviour as the concrete began to collapse (crush) and develop shear cracking under the loading point, as shown in Figures 4a and 4b. Both slabs then failed abruptly with a midspan deflection of around 60 mm due to shear failure, as shown in Figures 5a and 5b.

The slope of the load-deflection curve in slab S3 decreased from 6.8 kN/mm to 4.8 kN/mm after the concrete first began to crack. This is significant compared to slabs S1 and S2 where the stiffness increased by 85%. Deflection then increased linearly up to around 200 kN load and a deflection of 46 mm; peak load was then reached non-linearly at 211 kN with a deflection of 57 mm. The load cpacity then began to decrease until the slab failed at 150 kN with a deflection of 80 mm. However, with slab S4, there was only a slight decrease in stiffness (6.4 kN/mm) after flexural tensile cracking but with a 33% increasing in stiffness compared to S3. Deflection then increased linearly with load up to around 130 kN with a deflection of 16 mm. The slope of the load-deflection curve decreased again after this load, and the behaviour of S4 became nonlinear until it reached a maximum load of 208 kN with a deflection of 45 mm. There was a slight decrease in the load capacity under this load and the slab continued to deflect even without any increase in

the load. Slab 4 then failed at 150 kN with a midspan deflection of 76 mm due as the concrete collapsed (crushed) and the steel buckled, as shown in Figure 5d.

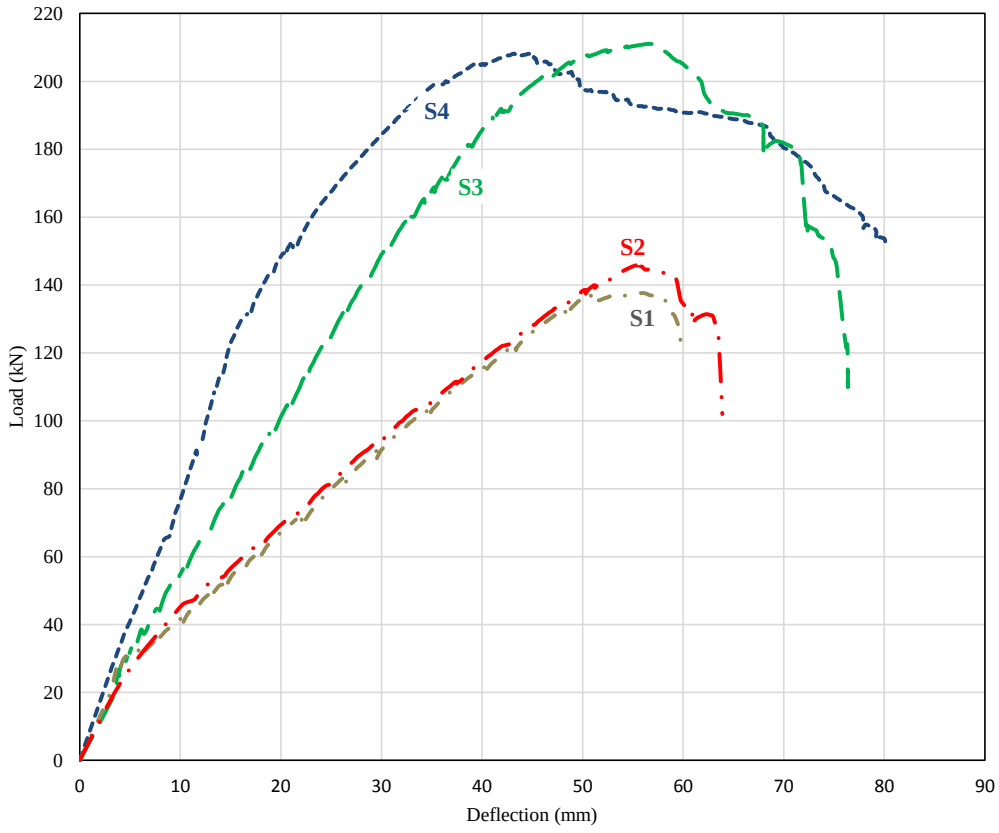

Figure 6. The load-deflection relationship of concrete slabs.

3.3 Load and strain behaviour

Figure 7 shows the relationship between load and strain at top surface of the concrete slabs. The strain increased linearly up to 100 microstrains until the first flexural tensile cracks occurred at the bottom of the slabs at a load of 25 kN. The strain then increased linearly but at a faster rate than before cracking; this linear load-strain behaviour continued until slabs S1, S2, and S3 failed. The maximum strain(s) recorded in the concrete at the top of these slabs was 2100 microstrains, 1995 microstrains, and 2855 microstrains, respectively. The level of strain in the top of the concrete for slabs S1 and S2 further confirmed that they failed prematurely in shear, whereas slab S3 failed by bending. After the concrete began to crack, strain at the top of the concrete for slab S4 also

increased linearly with load but at a slower rate than the other slabs. However, at a load of 130 kN and strain of 1100 microstrains, the strains became nonlinear; in fact there was a significant increase in the load from 170 kN to 200 kN but the strain remained at 1500 microstrains. At 202 kN, the strain then increased to 1791 microstrains before the slab failed due to concrete crushing.

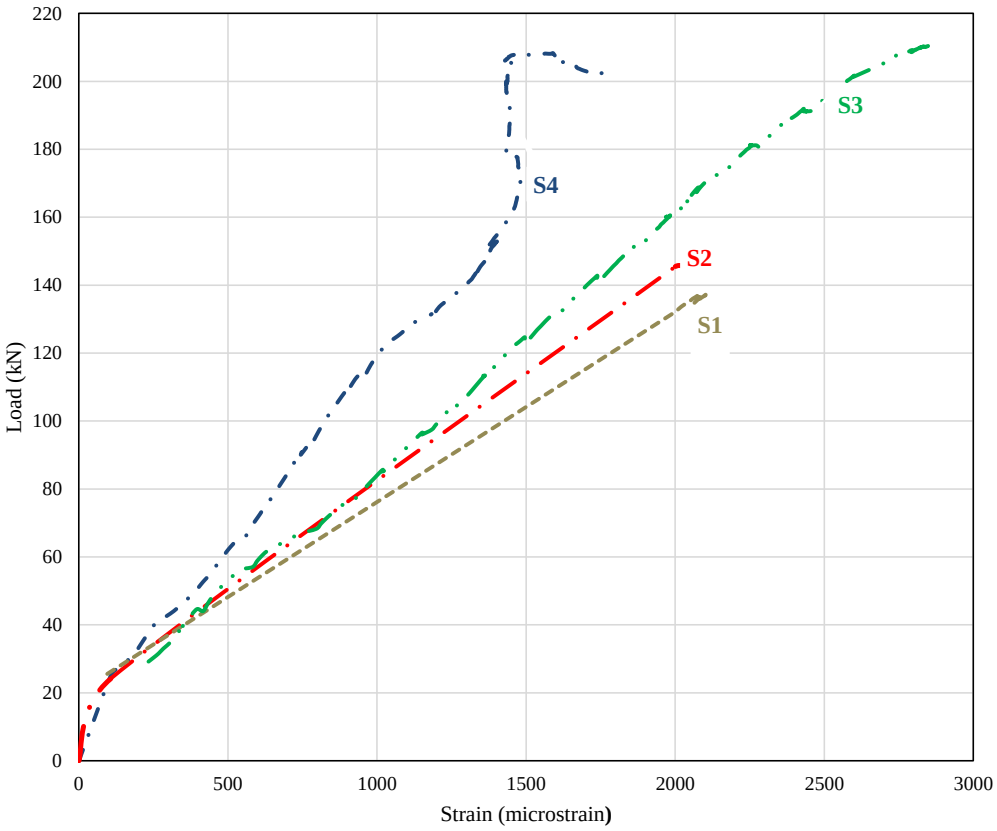

Figure 7. The load and strain relationship at the top concrete.

Figure 8 shows the relationship between the load and strain at the tensile reinforcement for every slab. Before the concrete began to crack, the GFRP bars for slabs S1 to S3 and the steel reinforcements in slab S4 recorded almost no strain, but after the first cracks appeared at 25 kN, the strain in the reinforcement increased rapidly. The load-strain behaviour in the tensile GFRP bars for slabs S1 and S2 was similar, and at failure, the strain in the GFRP bars for these slabs was almost 13,000 microstrains.The load-strain behaviour in slab S3 was almost linear after the concrete first began to crack, but compared to slabs S1 & S2, the rate was slower, however, the

load-strain behaviour when the peak load reached 211 kN was non lineare. The strain measured at the bottom GFRP bars when slab S3 finally failed was around 14,000 microstrains, which was almost 70% of the failure strain of the GFRP bars in tension. As expected, strain in the steel bars in slab S4 developed at a slower rate than the GFRP bars in slabs S1 to S3, but from 130 kN to 208 kN, the strain remained constant at around 2700 microstrains, which is the level of yield strain for 500 MPa steel bars. This was followed by a large increase in strain even without any further increase in the applied load.

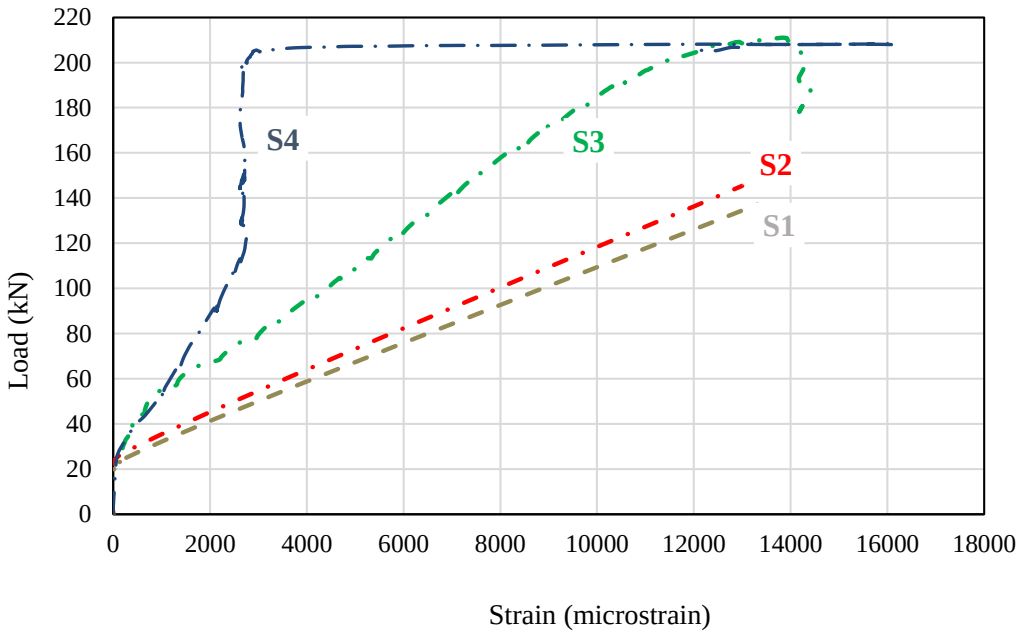

Figure 8. The load and strain relationship at the bottom GFRP and steel bars.

Figure 9 shows the relationship between load and strain at the compression reinforcement for slabs S3 and S4. The graph shows that the strain in the compressive GFRP bars in slab S3 increased linearly with load even after the concrete began to crack, but at a load of 170 kN, the load-strain behaviour became nonlinear until it reached peak load. The maximum strain recorded was around 2400 microstrains. However, the load-strain behaviour in the top steel bars in slab S4 was non linear after the concrete began to crack, and up to failure. More than 3000 microstrains were recorded in the steel bars in compression at failure.

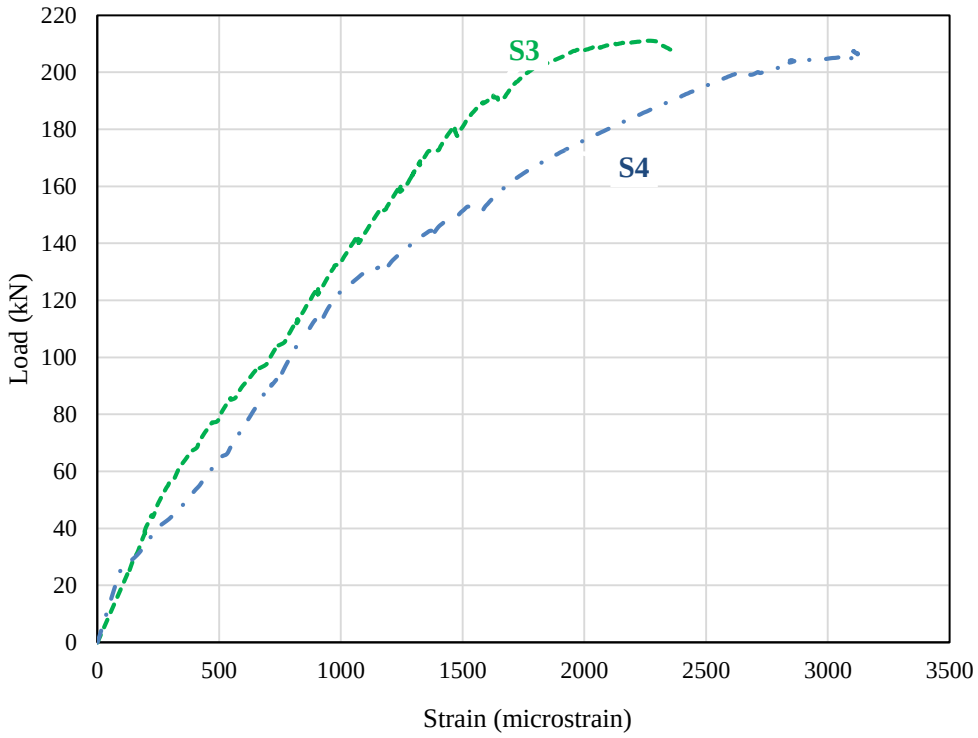

Figure 9. The load and strain relation at top GFRP and steel bars.

Figure 10 shows the relationship between the load and strain r at the top surface of the CRS for slabs S3 and S4. When the load was first applied, until the concrete first began to crack, the strain in the CRS was very low. A nonlinear and compressive strain was then measured at the top surface of the CRS in both slabs and showed that the strain in slab S3 was higher than slab S4 at the same load levels. Then the strain shifted to tension at around 150 kN and until both slabs failed. Interestingly, the CRS in slab S4 reached almost 7100 microstrains before it failed whereas the maximum strain recorded in slab S3 was only 2500 microstrains.

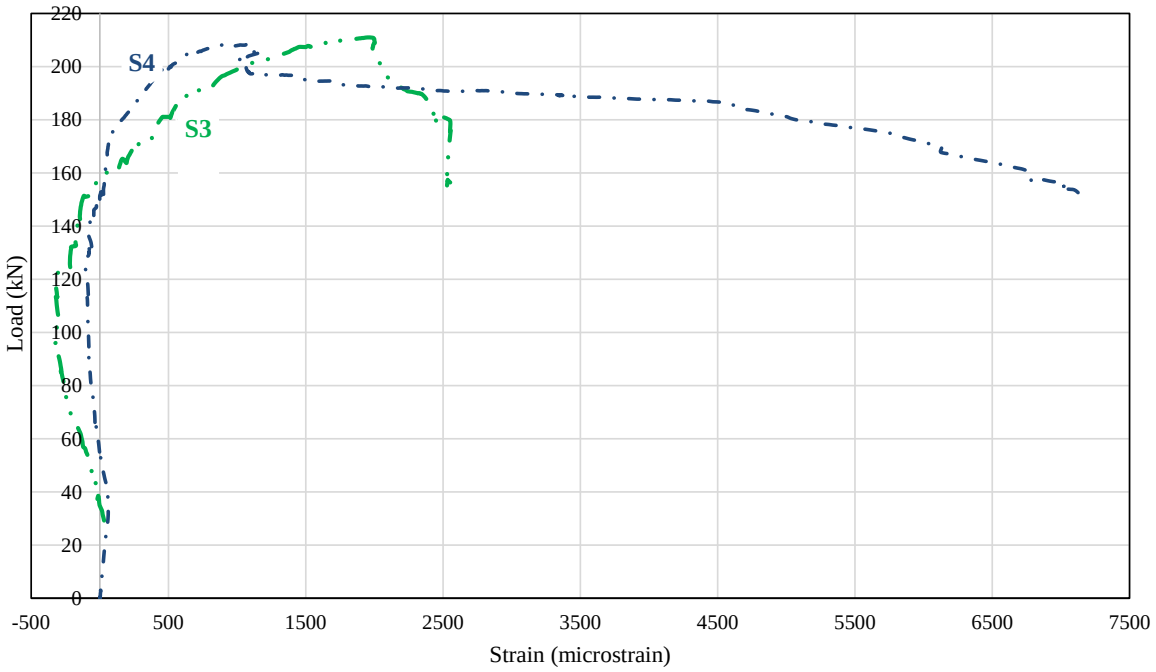

Figure 10. Load and strain relationship at the top of CRS.

4. DISCUSSION

4.1. Influence of the hollow concrete core

The influence of a hollow concrete core in a precast concrete slab reinforced with GFRP bars was evaluated by comparing the behaviour of slabs S1 and S2; the results indicated that the structural behaviour of solid and hollow core slabs was similar because both slabs failed in diagonal shear followed by the concrete crushing and the bars buckling under compression. This type of failure was expected because there was no shear reinforcement in the slabs. This was further confirmed by the maximum strain in the concrete being only 2000 microstrains. However, the failure of hollow core slab (S2) was more brittle than the solid slab (S1) because the voids collapsed. Cuenca and Serna (2013) stated that this type of failure is expected for hollow core concrete slabs because the reduced width of the web cannot resist the shear forces.

Having a hollow core did not affect the overall stiffness and capacity of the concrete slab, probably because the voids matched the outside diameter of the CRS resulting in only a 9% reduction in the gross area of slab S2 compared to slab S1. At a maximum load point, the similar behaviour of slabs S1 and S2 is because neutral axis is higher than the top of the hollow core, thus making the

uncracked concrete in compression the same for both slabs. Using the strain measured in the top concrete in Figure 7, and the strain at the bottom reinforcement in Figure 8, it can be seen that the neutral axis is 21 mm deep from the top of both slabs at an advanced loading level, which is clearly above the hollow core, as shown in Figure 11.

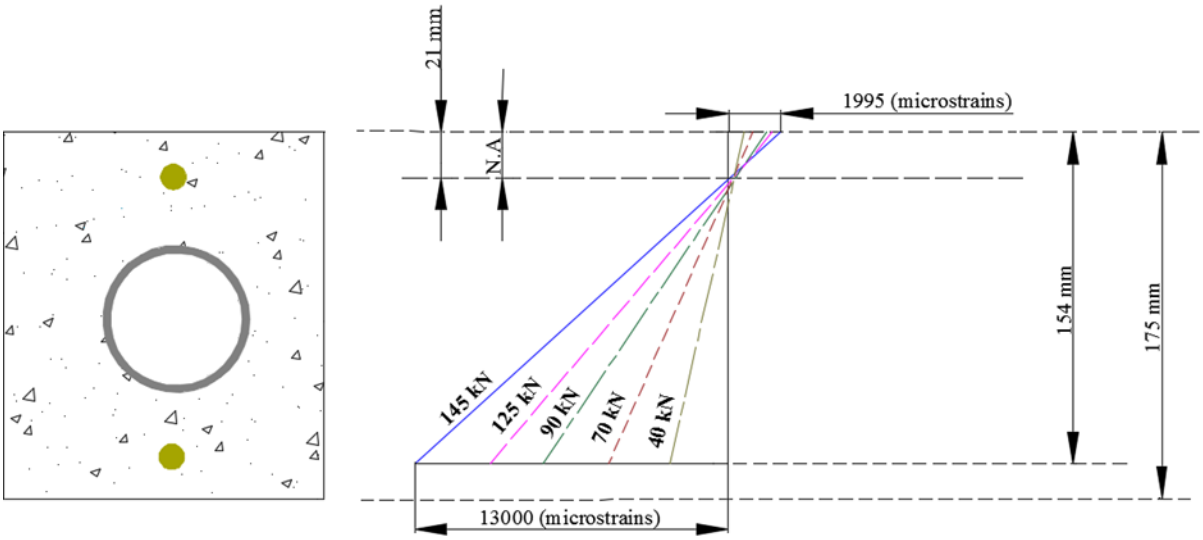

Figure 11. Strain distribution in slab S2

4.2. The effectiveness of CRS at reinforcing a concrete slab

CRS was found to be an effective way to reinforce hollow concrete slabs by comparing the behaviour of slabs S2 with S3. The provision of 3 pieces of CRS in slab S3 yielded 45% higher capacity than slab S2, indicating that CRS was acting as internal reinforcement for slab S3. This finding was supported by the load and strain of the bottom GFRP bars where the addition of CRS reduced the strain in the bottom bars in slab S3, thus showing that CRS was providing additional tensile reinforcement. CRS also increased the bending stiffness of hollow concrete slabs by 85%. Moreover, CRS changed the failure mode in slab S3 from shear failure to flexural failure observed in slab S2 because the hollow composite reinforcing stopped the vertical flexural cracks from reaching the top layer of concrete and the massive concrete crushing in the final failure. CRS controlled the direction of cracking and also made the crack path longer because they needed to pass through the CRS flanges, thereby enhancing the serviceability performance of slab S3. This enhancement in the performance of the hollow core slab due to CRS was much better than the carbon fibre reinforced polymer (CFRP) sheets implemented by (Meng, 2016) where the load

capacity only increased by 11%. This was because the latter method could not prevent the hollow core from collapsing while trying to attach CFRP to avoid the shear failure experienced beforehand, even though the increased shear failure was insignificant. However, we enhanced the flexural and shear strength until the difference between flexural failure in S3 and shear failure in S2 was 45%. There was also no debonding failure because the four flanges of the CRS interacted effectively with the concrete. On the other hand, the debonding failure seen by (Meng, 2016) on CFRP sheets occurred because the reinforcement inside the hollow slab should have been stiff enough to hold the compression and tension forces enough to resist the bending loads that have been achieved by adding thicker sheets of CRS than the thin sheets in CFRP. (Elgabbas et al., 2010) also observed improvement in the load carrying capacity of the hollow core concrete slabs after internally reinforcement with CFRP sheets but shear failure still occurred due to the CFRP sheets debonding from the concrete.

4.3. Effect of reinforcing types

The types of reinforcement had a significant effect on the overall stiffness but none on the load capacity of the hollow concrete slabs. After slab S3 & S4 first cracked, slab S4 retained almost 94% of its initial and uncracked stiffness while slab S3 retained 75%. Slab S4 was stiffer because the modulus of elasticity of steel was higher than the GFRP bars in slab S3, as many researchers observed (Ombres et al., 2000, Ali et al., 2015, Abdalla, 2002, Benmokrane et al., 1995, Bischoff, 2005, Maranan et al., 2015). However, the provision of CRS enabled the GFRP reinforced hollow concrete slab to retain most of its stiffness because it prevented wider flexural cracks from developing. For example, (El-Gamal et al., 2011) the steel reinforced slab was almost 72% stiffer than the slabs reinforced with GFRP with a similar reinforcement ratio, whereas the the steel reinforced slab (S4) was only 33% stiffer than slab S3. Moreover, the flexural capacity of slabs S3 and S4 were almost the same because the failure behaviour of these slabs was governed by CRS due to its combined bending failure and interlaminar shear. As Figure 8 shows, the addition of CRS reduced the amount of strain experienced by the GFRP bars (slab S3) thus indicating how well it utilises the tensile strength of the bars. Moreover, the GFRP bars and CRS were recorded the highest contribution in the final load. Notwithstanding this, all of the stress was transferred to the CRS when the tensile reinforcement in slab S4 yielded at a load of 140 kN. The bottom steel reinforcement stopped recording the strains (Figure 8) while the strain in the CRS increased markedly after the steel bars yielded up to their maximum load (Figure 10). Slab S4 then continued

to carry the load until the CRS failed, and then the stiffness decreased in the load-deflection curve when the steel yielded (Figure 6). This result contradicts the comparison between the stiffness at the beginning of this sections, so slab S4, which was reinforced with steel was stiffer than S3 from when cracking started until the yielding point, but after yielding this situation reversed because S3 slab showed continuous linear stiffness due to the linear elastic behaviour of GFRP bars, unlike the reduced stiffness of S4 because the steel stopped resisting. This suggests that CRS and GFRP bars are more compatible than steel bars because the stiffness of these composite materials are almost the same.

The presence of CRS prevented the concrete in slabs S3 & S4 from undergoing premature compressive failure but they still developed horizontal shear cracks at the level of the hollow reinforcing system, however, there were more horizontal cracks in slab S3 than slab S4 and they were deeper. Similar observations were made by (Chang and Seo, 2012) who indicated that the wider cracks at the same level of load in GFRP-reinforced one way slabs than the steel-reinforced one way slabs with similar dimensions and reinforcement ratios, was because the GFRP bars were not as stiff as the steel bars. The lower stiffness of GFRP bars than steel bars also explains why the deflection in slab S3 was higher than slab S4. At the maximum load, compressive crushing of the concrete began in slab S3 whereas the bottom steel in slab S4 yielded**.**

5. THEORETICAL EVALUATION

5.1. Analysis of Fibre Model

The behaviour of concrete slabs with hollow composite reinforcing system in flexure was predicted using a simple Fibre Model Analysis (FMA). This layer-by-layer approach was used successfully by (Manalo and Aravinthan, 2012, Kara and Ashour, 2012, Grothe and Park, 2000) reliably predict the flexural capacity of composite structures. In this design approach, the capacity of hollow concrete slabs was based on the cross section equilibrium, strain compatibility, and constitutive behaviour of the material. The internal force equilibrium principle was used to find the flexural capacity based on the properties of the constituent materials. It was assumed that a perfect bond exists between the reinforcement and concrete, and the strains in each layer are directly proportional to their distance from the neutral axis. The stress on each layer was calculated by multiplying the strain by the modulus of elasticity of the material. The sectional equilibrium was

maintained by balancing the net compressive and net tensile forces of the section. The flexural behaviour of the one-way slabs was analysed using an excel spreadsheet. For a hollow composite reinforcing system, the four rectangular flanges ~~are~~ considered by replacing it with an equivalent circular area and with properties that are similar to CRS. These basic assumptions are shown in Figure 12.

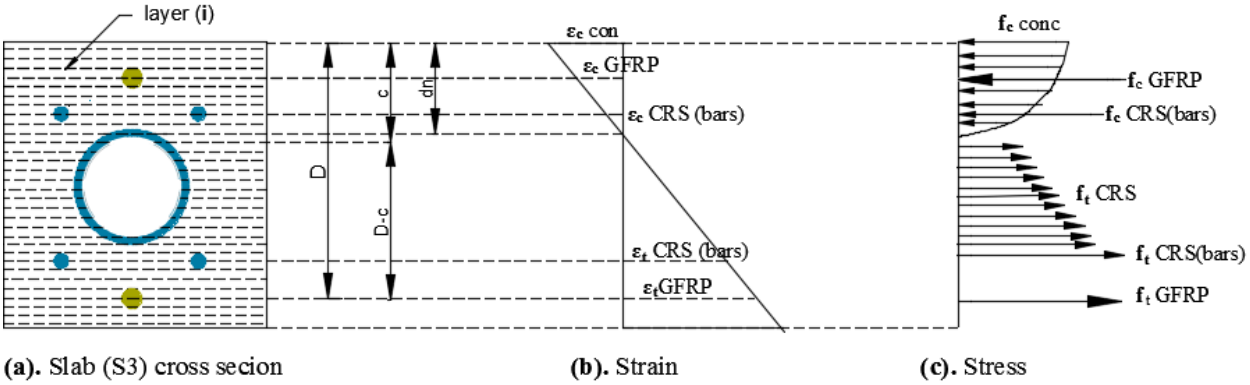

Figure 12. Basic assumptions in FMA

In Figure 12, D is the effective depth, c is depth of the layer from the extreme compression fibre, d_n is the neutral axis depth, ε_{con} is the corresponding top concrete strain, ε_{cGFRP} is the corresponding top GFRP strain, ε_{tGFRP} is the corresponding bottom GFRP strain, $f_{c,conc}$ is the compressive concrete stress, f_{cGFRP} is compressive GFRP stress, f_{cCRS} is compressive CRS stress, $f_{cCRS\,(bars)}$ is compressive CRS bars, stress f_{tCRS} is tension CRS stress, f_{cCRS} is tension CRS bars stress and f_{tGFRP} is tension GFRP stress. In the FMA, (Popovics, 1973) the stress-strain behaviour of concrete was calculated by first considering its tensile contribution and then by omitting its tensile strength. The GFRP bars and CRS were analysed as linear elastic material in both tension and compression while the steel was simplified with a bilinear behaviour (Wolanski, 2004), i.e. linear elastic before yielding and a constant stress after yield. Two cases were also considered for CRS, the first included the contribution mad by the flanges and the second was by omitting this contribution; this would show have the flange was used to help carry the load. The constitutive models for concrete, GFRP, steel, and CRS are shown in Figure 13.

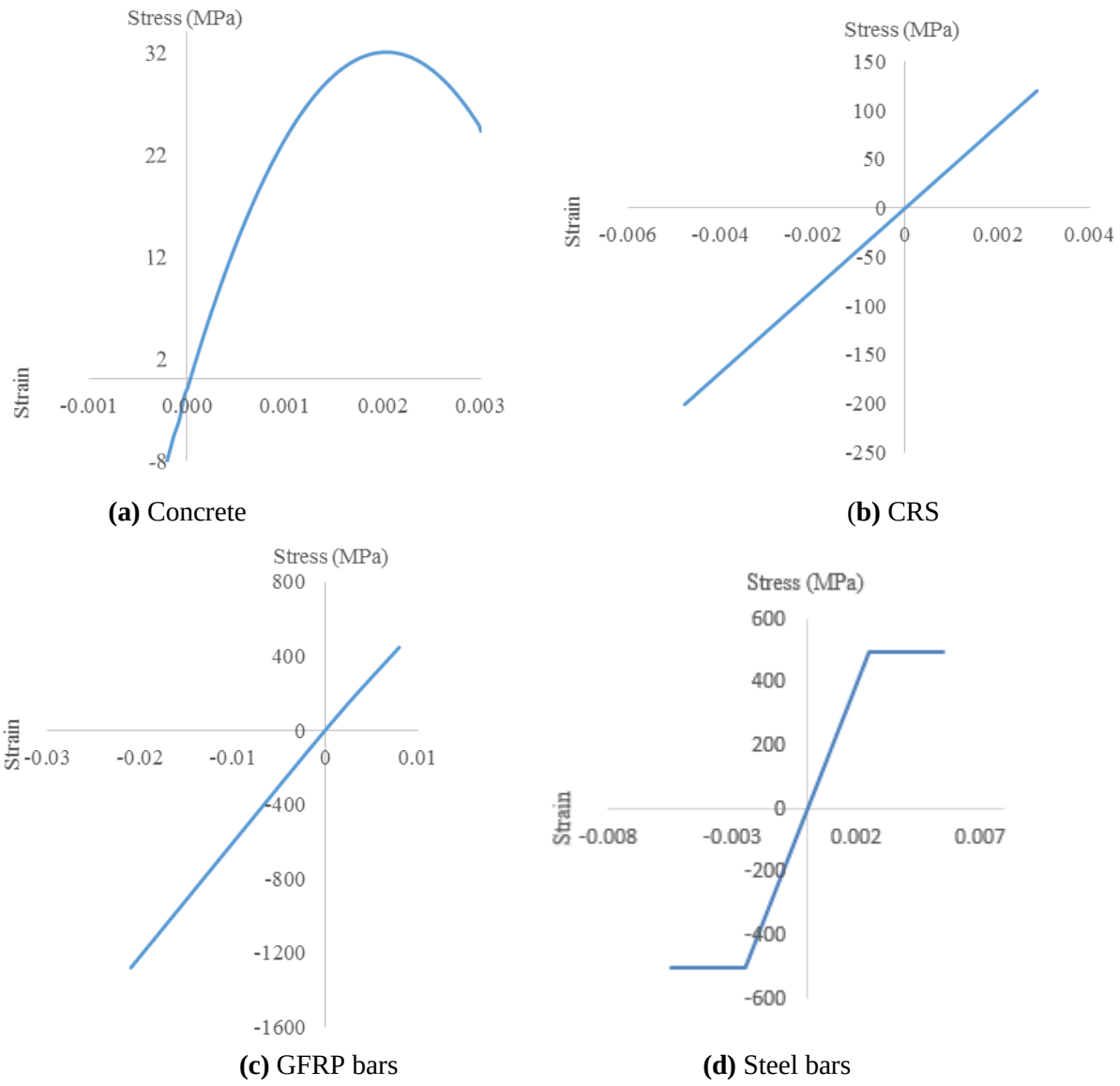

(a) Concrete **(b)** CRS

(c) GFRP bars **(d)** Steel bars

Figure 13. Constitutive materials model.

Assuming that the compressive strain at the top of the reinforced concrete slab was the first step in the FMA, the top strain is then used while the bottom strain was determined by iteration until the summation of forces became zero. While the slab remains uncracked, all the layers or element *i* contribute to the moment capacity of the section. The corresponding neutral axis depth d_n is to adjust for the strains in the top and bottom which set the force equilibrium principle calculated in the Equation 1. Moreover, the strain $\mathcal{E}_{(i)}$ at element *i* is related to the top strain (assumed 0.003 for top concrete). The stress was then calculated from the strain for each layer

multiplied by its corresponding elastic modulus. The strain equation shown below was used in the FMA.

$$\varepsilon_i = \frac{\varepsilon_{c*(dn-di)}}{dn} \quad (1)$$

Where ε_0 is the top concrete strain and ε_c is the concrete strain at depth d_i. The predicted load and moment capacities of the hollow core slabs were calculated using equations 2 and 3, respectively.

$$\sum P = \sum_{i=1}^{n} f_{i,conc}\ A_{i,conc} + \sum_{i=1}^{n=3} f_{i,CRS}\ A_{i,CRS} + \sum_{i=1}^{n=4} f_{i,GFRP}\, A_{i,GFRP} = 0 \quad (2)$$

$$\sum M = \sum_{i=1}^{n} f_{i,conc}\ A_{i,conc} di + \sum_{i=1}^{n=3} f_{i,CRS}\, A_{i,CRS}\ di + \sum_{i=1}^{n=4} f_{i,GFRP}\, A_{i,GFRP}\ di \quad (3)$$

where:

P = sum of forces,

$f_{i,conc}$ = concrete strength at layer i,

$A_{i,conc}$ = concrete area at layer i,

$f_{i,GFRP}$ = GFRP bars strength,

$A_{i,GFRP}$ = area of main reinforcement at layer i,

$f_{i,CRS}$ = CRS strength at layer i,

$A_{i,CRS}$ = CRS area at layer i,

M = bending moment capacity, and

d_i= layer depth from upper compressive layer.

5.2 Predicted failure load and comparison with the experiments

A summary of the different cases analysed using FMA are presented in Table 5. The test results indicate that slabs S3 and S4 failed when the topmost layer of concrete reached its maximum strain and failed in compression. This type of failure was used as the failure criteria to calculate the maximum capacity of the hollow concrete slabs with CRS.

Table 6 summarises the load predicted for the different cases considered and the results from the experiment. The predicted results show that the concrete contributed 2% more tensile strength to the predicted load than if it was omitted while the flanges contributed more than 8% to the predicted load when only the hollow portion of the CRS was considered. Overall, the predicted results using FMA, while considering the tensile strength of the concrete and the flanges of the

CRS, showed comparable results to the failure load measured from the experiments for slabs S3 and S4. In general, the predicted load in Case 3 was only 8% more conservative than the actual load measured from the experiment. This difference between the predicted load and the actual failure load could be due to the inherent variability of the compressive strength of concrete or because some portions of the flange not considered in the FMA may have helped to carry the load applied to the slabs during the experiment.

Table 5. The different cases considered in FMA

Cases	**Assumptions**
Case 1	Omit the tensile strength of concrete and consider CRS flanges.
Case 2	Omit the tensile strength of concrete and the CRS flanges.
Case 3	Include the tensile strength of concrete and the contribution of the CRS flanges.
Case 4	Include the tensile strength of concrete and omit the contribution made by the CRS flanges.

Table 6. Predicted and actual failure load

Slab	**Failure load (kN)**				
	Case 1	**Case 2**	**Case 3**	**Case 4**	**Experiment**
S3	167	156	182	171	211
S4	166	146	173	157	208

6. CONCLUSION

This study investigated the flexural behaviour of one-way concrete slabs reinforced with GFRP bars and hollow composite reinforcing system. Full-scale concrete slabs were tested under four-point static bending to observe the propagation of failure, load-deflection, and the load-strain behaviour. The failure load of hollow concrete slabs was also predicted using the simplified Fibre Model Analysis. Based on the results of this study, the following conclusions are drawn:

The hollow core concrete slab reinforced with GFRP bars behaved to the same as the solid slab due to only a 9% reduction in the gross area of the concrete for hollow slab than the solid slab, and the area of concrete in compression for hollow slab was located above the hollow core. Slabs S1 and S2 both failed in shear but slab S1 showed more brittle failure than slab S2 because the hollow core collapsed.

The composite reinforcing system helped to enhance the structural performance of hollow core concrete slabs. The provision of 3 pieces of composite reinforcing system increased the stiffness of the GFRP reinforced concrete hollow slab by 85% and increased the load carrying capacity by 32%. The hollow composite system also prevented vertical flexural cracks from propagating up to the top layer of concrete; this resulted in ductile flexural failure.

The hollow composite reinforcing system was more compatible to GFRP bars than steel bars due to their similar modulus of elasticity. While the slab reinforced with steel was stiffer, from the time the concrete began to crack until the steel yielded, the GFRP reinforced slab was stiffer and retained this constant stiffness until the load reached its maximum. Moreover, the GFRP bars and the CRS simultaneously resisted the load up to failure whereas all the load was transferred to CRS once the steel yielded in steel reinforced slab.

The simplified Fibre Model Analysis reliably predicted the failure load of hollow concrete slabs with composite reinforcing system. By incorporating the tensile strength of concrete and the flanges of the hollow composite reinforcing system, the predicted failure load was only 13% less than the failure load measured experimentally.

Acknowledgements

The authors would like to thank Composite Reinforcement Solutions Pty Ltd for providing the hollow composite reinforcing systems, as well as the technical staff and postgraduate students at the Centre for Future Materials (CFM) in the University of Southern Queensland for helping to prepare and testing specimens.

7. REFRENCES

ABDALLA, H. 2002. Evaluation of deflection in concrete members reinforced with fibre reinforced polymer (FRP) bars. *Composite Structures,* 56**,** 63-71.

ACI 2008. Metric specification for carbon and glass fiber–reinforced polymer bar materials for concrete reinforcement.

ADAM, M. A., SAID, M., MAHMOUD, A. A. & SHANOUR, A. S. 2015. Analytical and experimental flexural behavior of concrete beams reinforced with glass fiber reinforced polymers bars. *Construction and Building Materials,* 84**,** 354-366.

ADEL. A, S. A. 2016. NUMERICHAL ANALYSIS OF REINFORCED CONCRETE HOLLOW - CORE SLABS. *ARPN Journal of Engineering and Applied Sciences,* 11**,** -.

ALI, A. H., AFIFI, M. Z., ABDULSALAM, B., HAGGAG, H., EL HASHIMY, A., EL-SAYED, T. & MOHAMED, H. M. 2015. Performance Evaluation of One-Way Concrete Slabs Reinforced with New Developed GFRP Bars. *Materials Sciences and Applications,* 6**,** 420.

ALMUSALLAM, A. A. 2001. Effect of degree of corrosion on the properties of reinforcing steel bars. *Construction and Building Materials,* 15**,** 361-368.

ALMUSALLAM, T., ELSANADEDY, H. & AL-SALLOUM, Y. 2014. Effect of Longitudinal Steel Ratio on Behavior of RC Beams Strengthened with FRP Composites: Experimental and FE Study. *Journal of Composites for Construction,* 19**,** 04014028.

ALSAYED, S. H. & ALHOZAIMY, A. M. 1999. Ductility of concrete beams reinforced with FRP bars and steel fibers. *Journal of composite materials,* 33**,** 1792-1806.

ANDERSON, R. 1987. Web Shear Strength of Prestressed Concrete Members. *Technical Bulletin 85B1. Tacoma, WA: Concrete Technology Associates*.

APOSTOLOPOULOS, C. & PAPADAKIS, V. 2008a. Consequences of steel corrosion on the ductility properties of reinforcement bar. *Construction and Building Materials,* 22**,** 2316-2324.

APOSTOLOPOULOS, C. A. & PAPADAKIS, V. 2008b. Consequences of steel corrosion on the ductility properties of reinforcement bar. *Construction and Building Materials,* 22**,** 2316-2324.

APOSTOLOPOULOS, C. A., PAPADOPOULOS, M. & PANTELAKIS, S. G. 2006. Tensile behavior of corroded reinforcing steel bars BSt 500s. *Construction and building Materials,* 20**,** 782-789.

ARAVINTHAN, T. & MANALO, A. Field applications and case studies of FRP in civil infrastructure: the Australian experience. Proceedings of the 6th International Conference on FRP Composites in Civil Engineering (CICE 2012), 2012. International Institute for FRP in Construction (IIFC), 1-8.

ASHOUR, A. 2006. Flexural and shear capacities of concrete beams reinforced with GFRP bars. *Construction and Building Materials,* 20**,** 1005-1015.

ASSOCIATION, C. S. 2002a. CSA S806 02 Design and construction of building components with fibre reinforced polymers. Toronto, Canada: Canadian Standards Association International.

ASSOCIATION, C. S. 2002b. CSA S806 02 Design and construction of building components with fibre reinforced polymers. *Canadian Standards Association International, Toronto, Canada*.

ASSOCIATION, C. S. 2010. CAN/CSA S807-10 "Specification for fibre-reinforced polymers. *Canadian Standards Association, Rexdale, Ontario, Canada*.

ASTM 2008a. Standard test method for apparent horizontal shear strength of pultruded reinforced plastic rods by the short beam method.

ASTM 2009. Standard test method for flexural properties of fiber reinforced pultruded plastic rods.

ASTM 2011. Standard test method for tensile properties of fiber reinforced polymer matrix composite bars. *ASTM D7205-11*.

ASTM, D. 4475 (2002). *Standard Test Method for Apparent Shear Strength of Pultruded Reinforced Plastic Rods by the Short-beam Method*.

ASTM, I. 2007. Standard test methods for flexural properties of unreinforced and reinforced plastics and electrical insulating materials. *ASTM D790-07*.
ASTM, S. 2008b. Standard test method for assignment of the glass transition temperatures by differential scanning calorimetry.
AUSTRALIA, S. 2009. Concrete structures. *Standards Australia, AS*, 3600-2009.
AZAD, A. K. & HAKEEM, I. Y. 2016. Flexural behavior of hybrid hollow-core slab built with ultra high performance concrete faces. *Materials and Structures,* 49**,** 3801-3813.
BENAYOUNE, A., SAMAD, A. A., TRIKHA, D., ALI, A. A. & ELLINNA, S. 2008. Flexural behaviour of pre-cast concrete sandwich composite panel–experimental and theoretical investigations. *Construction and Building Materials,* 22**,** 580-592.
BENMOKRANE, B., CHAALLAL, O. & MASMOUDI, R. 1995. Glass fibre reinforced plastic (GFRP) rebars for concrete structures. *Construction and Building Materials,* 9**,** 353-364.
BENMOKRANE, B., MANALO, A., BOUHET, J.-C., MOHAMED, K. & ROBERT, M. 2017. Effects of Diameter on the Durability of Glass Fiber–Reinforced Polymer Bars Conditioned in Alkaline Solution. *Journal of Composites for Construction,* 21**,** 04017040.
BHAGAT, S. & PARIKH, K. 2014. Comparative Study of Voided Flat Plate Slab and Solid Flat Plate Slab. *International Journal of Innovative Research and Development*.
BISCHOFF, P. H. 2005. Reevaluation of deflection prediction for concrete beams reinforced with steel and fiber reinforced polymer bars. *Journal of Structural Engineering,* 131**,** 752-767.
BOUGUERRA, K., AHMED, E., EL-GAMAL, S. & BENMOKRANE, B. 2011. Testing of full-scale concrete bridge deck slabs reinforced with fiber-reinforced polymer (FRP) bars. *Construction and building materials,* 25**,** 3956-3965.
BRUNESI, E., BOLOGNINI, D. & NASCIMBENE, R. 2015. Evaluation of the shear capacity of precast-prestressed hollow core slabs: numerical and experimental comparisons. *Materials and Structures,* 48**,** 1503-1521.
CAIRNS, J. & MILLARD, S. Reinforcement corrosion and its effect on residual strength of concrete structures. Proc., 8th Int. Conf. on Structural Faults and Repair, 1999. Engineering Technics Press London.
CERONI, F. 2010. Experimental performances of RC beams strengthened with FRP materials. *Construction and Building Materials,* 24**,** 1547-1559.
CHANG, K. & SEO, D. 2012. Behavior of One-Way Concrete Slabs Reinforced with GFRP Bars. *Journal of Asian Architecture and Building Engineering,* 11**,** 351-358.
CHERNIN, L., VAL, D. V. & VOLOKH, K. Y. 2010. Analytical modelling of concrete cover cracking caused by corrosion of reinforcement. *Materials and Structures,* 43**,** 543-556.
CHUNG, J.-H., CHOI, H.-K., LEE, S.-C. & CHOI, C.-S. 2015. One-way shear strength of circular voided reinforced concrete floor slabs. *Proceedings of the Institution of Civil Engineers-Structures and Buildings,* 168**,** 336-350.
COMMITTEE, A., INSTITUTE, A. C. & STANDARDIZATION, I. O. F. Building code requirements for structural concrete (ACI 318-08) and commentary. 2008. American Concrete Institute.
CORONELLI, D. & GAMBAROVA, P. 2004. Structural assessment of corroded reinforced concrete beams: modeling guidelines. *Journal of structural engineering,* 130**,** 1214-1224.
CRS PERTH, A. Composite Reinforcement Solutions | CRS Perth, Australia". Composite Reinforcement Solutions | CRS Perth. N.p., 2016. . 5th International Symposium on Underwater Technology, 18 Oct. 2016 2016. Web.
CUENCA, E. & SERNA, P. 2013. Failure modes and shear design of prestressed hollow core slabs made of fiber-reinforced concrete. *Composites Part B: Engineering,* 45**,** 952-964.
DAVALOS, J. F., KODKANI, S. S., RAY, I. & LIN, C. 2008. Fracture evaluation of GFRP—concrete interfaces for freeze—thaw and wet-dry cycling. *Journal of composite materials,* 42**,** 1439-1466.
DE CASTILHO, V. C., DO CARMO NICOLETTI, M. & EL DEBS, M. K. 2005. An investigation of the use of three selection-based genetic algorithm families when minimizing the production cost of hollow core slabs. *Computer methods in applied mechanics and engineering,* 194**,** 4651-4667.

DEEPA, A., PADMANABHAN, K. & RAGHUNADH, G. 2016. Effect of Hygrothermal Loading on Laminate Composites. *Indian Journal of Science and Technology,* 9.
DITTENBER, D. B. & GANGARAO, H. V. 2012. Critical review of recent publications on use of natural composites in infrastructure. *Composites Part A: Applied Science and Manufacturing,* 43**,** 1419-1429.
DOMONE, P. & ILLSTON, J. 2010. *Construction materials: their nature and behaviour*, CRC Press.
DONOHOE, S. & KEOGH, D. Orthotropic analysis of voided slab bridges. International conference on engineering computational technology, 2000. 71-79.
DU, Y., CLARK, L. & CHAN, A. 2005. Effect of corrosion on ductility of reinforcing bars. *Magazine of Concrete Research,* 57**,** 407-419.
EL-GAMAL, S., ABDULRAHMAN, B. & BENMOKRANE, B. 2011. Deflection Behaviour of Concrete Beams Reinforced with Different Types of GFRP Bars. *Advances in FRP Composites in Civil Engineering.* Springer.
ELGABBAS, F., EL-GHANDOUR, A., ABDELRAHMAN, A. & EL-DIEB, A. 2010. Different CFRP strengthening techniques for prestressed hollow core concrete slabs: Experimental study and analytical investigation. *Composite Structures,* 92**,** 401-411.
ELLIOTT, K. S. 2016. *Precast concrete structures*, Crc Press.
ESFAHANI, M. R., KIANOUSH, M. & TAJARI, A. 2007. Flexural behaviour of reinforced concrete beams strengthened by CFRP sheets. *Engineering structures,* 29**,** 2428-2444.
FERNANDEZ, I., BAIRÁN, J. M. & MARÍ, A. R. 2015. Corrosion effects on the mechanical properties of reinforcing steel bars. Fatigue and σ–ε behavior. *Construction and Building Materials,* 101**,** 772-783.
GOLDSTON, M. W. 2016. Behaviour of concrete beams reinforced with GFRP bars under static & impact loading.
GROTHE, B. & PARK, T. J. 2000. Structure and function of the bat superior olivary complex. *Microscopy Research and Technique,* 51**,** 382-402.
GU, X., YU, B. & WU, M. 2016. Experimental study of the bond performance and mechanical response of GFRP reinforced concrete. *Construction and Building Materials,* 114**,** 407-415.
HAG-ELSAFI, O., ALAMPALLI, S. & KUNIN, J. 2001. Application of FRP laminates for strengthening of a reinforced-concrete T-beam bridge structure. *Composite structures,* 52**,** 453-466.
HALL, J. & MOTTRAM, J. 1998. Combined FRP reinforcement and permanent formwork for concrete members. *Journal of Composites for Construction,* 2**,** 78-86.
HONICKMAN, H. N. 2008a. Pultruded GFRP sections as stay-in-place structural open formwork for concrete slabs and girders.
HONICKMAN, H. N. 2008b. *Pultruded GFRP sections as stay-in-place structural open formwork for concrete slabs and girders.*
IBRAHIM, I., ELLIOTT, K., ABDULLAH, R., KUEH, A. & SARBINI, N. 2016. Experimental study on the shear behaviour of precast concrete hollow core slabs with concrete topping. *Engineering Structures,* 125**,** 80-90.
INTERNATIONAL, A. 2010. *Standard Test Method for Compressive Properties of Rigid Plastics*, ASTM International.
ISO, I. 1998. 14125: 1998 (E). *Fibre reinforced plastic composites–determination of flexural properties*.
KARA, I. F. & ASHOUR, A. F. 2012. Flexural performance of FRP reinforced concrete beams. *Composite Structures,* 94**,** 1616-1625.
KASSEM, C., FARGHALY, A. S. & BENMOKRANE, B. 2011. Evaluation of flexural behavior and serviceability performance of concrete beams reinforced with FRP bars. *Journal of Composites for Construction,* 15**,** 682-695.
LIU, S., YAN, C., WANG, G., LI, J. & WANG, Y. 2008. Experimental analysis on flexural capacity and ductility of pre-stressed RC hollow core slab strengthened by CFRP. *Journal of Building Structures,* 29**,** 125-128.

LUNDGREN, K. 2005. Bond between ribbed bars and concrete. Part 1: Modified model. *Magazine of Concrete Research,* 57**,** 371-382.
LUTZ, L. A. & GERGELY, P. Mechanics of bond and slip of deformed bars in concrete. Journal Proceedings, 1967. 711-721.
MAGNUSSON, J. 2000. *Bond and anchorage of ribbed bars in high-strength concrete*, Chalmers University of Technology.
MANALO, A., AL-FAKHER, U. & AL-RUBAYA, M. 2017. FRP Hollow Bar Characterisation. University of Southern Qeensland
MANALO, A. & ARAVINTHAN, T. 2012. Behaviour of glued fibre composite sandwich structure in flexure: experiment and fibre model analysis. *Materials & Design,* 39**,** 458-468.
MANALO, A., BENMOKRANE, B., PARK, K.-T. & LUTZE, D. 2014. Recent developments on FRP bars as internal reinforcement in concrete structures. *Concrete in Australia,* 40**,** 46-56.
MARANAN, G., MANALO, A., BENMOKRANE, B., KARUNASENA, W. & MENDIS, P. 2015. Evaluation of the flexural strength and serviceability of geopolymer concrete beams reinforced with glass-fibre-reinforced polymer (GFRP) bars. *Engineering Structures,* 101**,** 529-541.
MARANAN, G., MANALO, A., BENMOKRANE, B., KARUNASENA, W. & MENDIS, P. 2016. Behavior of concentrically loaded geopolymer-concrete circular columns reinforced longitudinally and transversely with GFRP bars. *Engineering Structures,* 117**,** 422-436.
MARANAN, G., MANALO, A., KARUNASENA, K. & BENMOKRANE, B. 2014. Bond stress-slip behavior: case of GFRP bars in geopolymer concrete. *Journal of Materials in Civil Engineering,* 27**,** 04014116.
MARANAN, G. B. 2016. *Structural behaviour of geopolymer concrete beams and columns reinforced with glass fibre reinforced polymer bars.* University of Southern Queensland.
MASMOUDI, A., OUEZDOU, M. B. & BOUAZIZ, J. 2012. New parameter design of GFRP RC beams. *Construction and Building Materials,* 29**,** 627-632.
MATOS, B., CORREIA, J. R., CASTRO, L. M. & FRANÇA, P. 2012. Structural response of hyperstatic concrete beams reinforced with GFRP bars: Effect of increasing concrete confinement. *Composite Structures,* 94**,** 1200-1210.
MEHTA, P. K. 2002. *Concrete in the marine environment*, Crc Press.
MENG, X. 2016. *Shear Strengthening of Prestressed Hollow Core Slabs Using Externally Bonded Carbon Fiber Reinforced Polymer Sheets.* University of Windsor (Canada).
MENG, X., CHENG, S. & EL RAGABY, A. 2016. STR-946: EXPERIMENTAL STUDY ON A NOVEL SHEAR STRENGTHENING TECHNIQUE FOR PRECAST PRESTRESSED HOLLOW-CORE SLABS.
MONES, R. M. & BREÑA, S. F. 2013. Hollow-core slabs with cast-in-place concrete toppings: A study of interfacial shear strength. *PCI journal,* 58**,** 124-141.
MOSALLAM, A., TAHA, M. M. R., KIM, J. J. & NASR, A. 2012. Strength and ductility of RC slabs strengthened with hybrid high-performance composite retrofit system. *Engineering Structures,* 36**,** 70-80.
NEWHOOK, J. & SVECOVA, D. 2007. Reinforcing concrete structures with fibre reinforced polymers. *ISIS Canada: Design Manual*.
NPCAA 2002. *Precast Concrete Handbook,* Australia National Precast Concrete Association Australia & Concrete Institue of Australia
OGUEJIOFOR, E. & HOSAIN, M. 1992. Behaviour of perfobond rib shear connectors in composite beams: full-size tests. *Canadian Journal of Civil Engineering,* 19**,** 224-235.
OKELO, R. & YUAN, R. L. 2005. Bond strength of fiber reinforced polymer rebars in normal strength concrete. *Journal of composites for construction,* 9**,** 203-213.
OMBRES, L., ALKHRDAJI, T. & NANNI, A. Flexural analysis of one-way concrete slabs reinforced with GFRP rebars. International meeting on composite materials, PLAST, 2000. 243-250.
PAJARI, M. 2009. Web shear failure in prestressed hollow core slabs. *Journal of Structural Engineering,* 42**,** 83-104.

PARK, R. & GAMBLE, W. L. 2000. *Reinforced concrete slabs*, John Wiley & Sons.
POPOVICS, S. 1973. A numerical approach to the complete stress-strain curve of concrete. *Cement and concrete research,* 3**,** 583-599.
ROBERT, M. & BENMOKRANE, B. 2009. Behavior of GFRP reinforcing bars subjected to extreme temperatures. *Journal of Composites for Construction,* 14**,** 353-360.
ROBERT, M. & BENMOKRANE, B. 2010. Effect of aging on bond of GFRP bars embedded in concrete. *Cement and Concrete Composites,* 32**,** 461-467.
ROBERT, M., COUSIN, P. & BENMOKRANE, B. 2009. Durability of GFRP reinforcing bars embedded in moist concrete. *Journal of Composites for Construction,* 13**,** 66-73.
SACKS, R., EASTMAN, C. M. & LEE, G. 2004. Parametric 3D modeling in building construction with examples from precast concrete. *Automation in construction,* 13**,** 291-312.
SAID, S. H., RAZAK, H. A. & OTHMAN, I. 2015. Flexural behavior of engineered cementitious composite (ECC) slabs with polyvinyl alcohol fibers. *Construction and Building Materials,* 75**,** 176-188.
SMITH, P. 2016. Design and specification of marine concrete structures. *Marine Concrete Structures: Design, Durability and Performance***,** 65.
STANDARD, A. D2344/D2344M," Standard Test Method for Short-Beam Strength of Polymer Matrix Composite Materials and Their Laminates," ASTM International, West Conshohocken, PA, 2013, DOI: 10.1520/D2344_D2344M.
STANDARD, A. 2011a. Standard test method for ignition loss of cured reinforced resin. *West Conshohocken (PA): ASTM,* 100.
STANDARD, A. A. Building Code Requirements for Structural Concrete (ACI 318-11). American Concrete Institute, 2011b.
STANDARDS AUSTRALIA 2001. Steel reinforcing materials. *4671-2001*. Australia: Standards Australia.
STANDARDS AUSTRALIA 2007. Specification and supply of concrete. *AS1379-2007* Australia SIA Global.
STANDARDS AUSTRALIA 2014. Methods of testing concrete Method 1: Sampling of concrete. *AS 1012.1-2014* Australia: Standards Australia.
TAHERSHAMSI, M. 2016. *Structural effects of reinforcement corrosion in concrete structures*, Chalmers University of Technology Gothenburg, Sweden.
TAWFIK, Q. H., KARUNASENA, W. K. & CARDONA, F. Strengthening of corroded steel angles using CFRP. Proceedings of the Composites Australia and the CRC for Advanced Composite Structures Conference 2012, 2012. Composites Australia, 1-12.
TAYLOR, R., MAHER, D. & HAYES, B. 1966. Effect of the arrangement of reinforcement on the behaviour of reinforced concrete slabs. *Magazine of concrete research,* 18**,** 85-94.
TEPFERS, R. & CONCRETE, T. G. B. M. I. F. F. S. 2000. *Bond of reinforcement in concrete: state-of-art report*, Internat. Fed. for Structural Concrete.
WARIYATNO, N. G., HARYANTO, Y. & SUDIBYO, G. H. 2017. Flexural behavior of precast hollow core slab using PVC pipe and styrofoam with different reinforcement. *Procedia Engineering,* 171**,** 909-916.
WOLANSKI, A. J. 2004. *Flexural behavior of reinforced and prestressed concrete beams using finite element analysis.*
XIANGMIN, L., FUWEN, Z. & QINGFENG, X. 2014. Experimental study and computational analysis on PC hollow core slabs strengthened with different FRP strips. *China Civil Engineering Journal,* 47.
YANG, L. 1994. Design of prestressed hollow core slabs with reference to web shear failure. *Journal of Structural Engineering,* 120**,** 2675-2696.
YARDIM, Y., WALEED, A., JAAFAR, M. S. & LASEIMA, S. 2013. AAC-concrete light weight precast composite floor slab. *Construction and Building materials,* 40**,** 405-410.

YEE, A. A. & ENG, P. H. D. 2001. Structural and economic benefits of precast/prestressed concrete construction. *PCI journal,* 46**,** 34-43.